VOYAGER

SPACECRAFT Phase B, Task D

FINAL REPORT

OCTOBER 1967

Prepared for

GEORGE C. MARSHALL SPACE FLIGHT CENTER

Huntsville, Alabama

Voyager Operations
Space Vehicles Division

TRW SYSTEMS GROUP

One Space Park, Redondo Beach, California

MODEL OF TRW RECOMMENDED VOYAGER SPACECRAFT

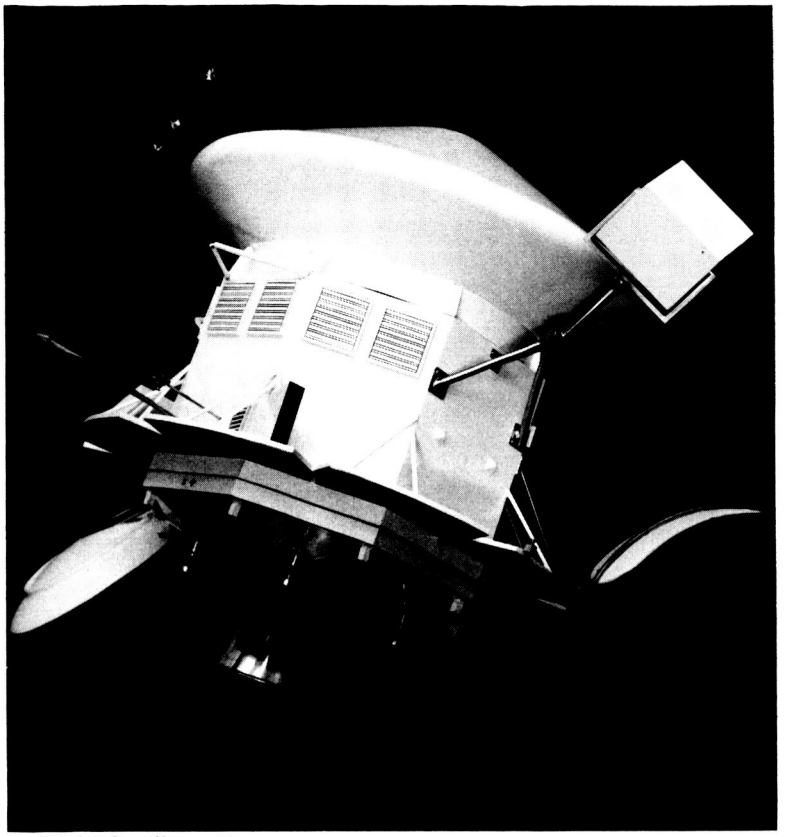

In-Flight Configuration

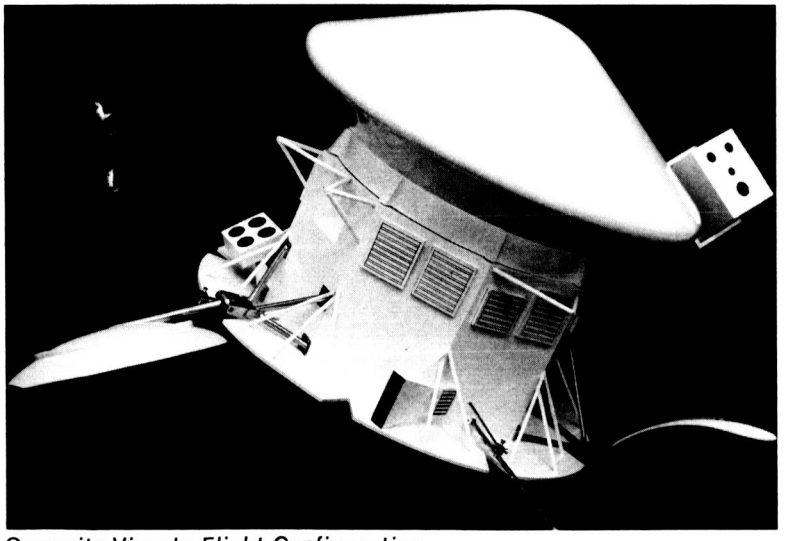

Opposite View In-Flight Configuration

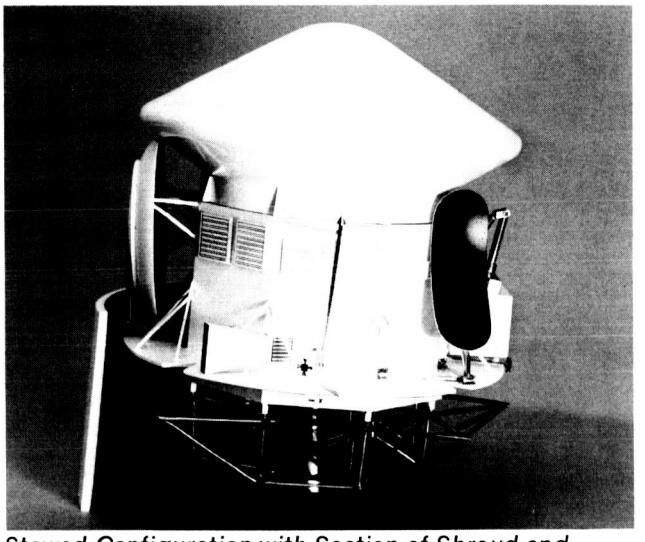

Stowed Configuration with Section of Shroud and Planetary Vehicle Adapter

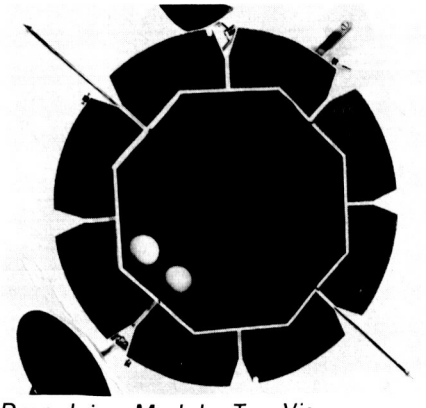

Propulsion Module, Top View

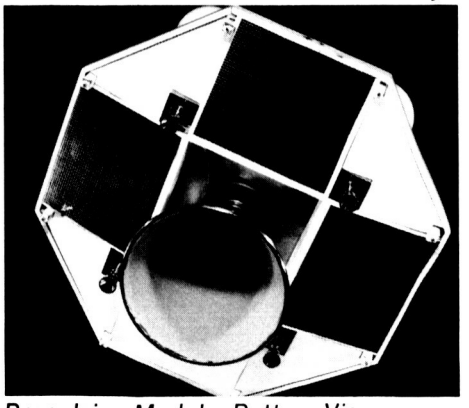

Propulsion Module, Bottom View

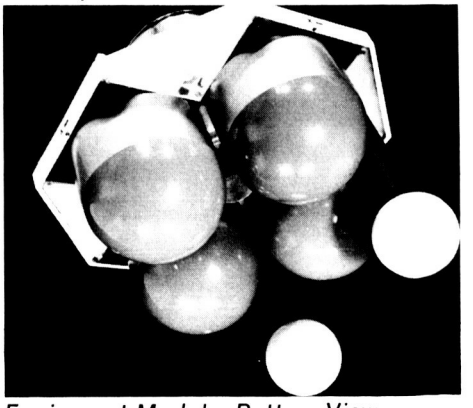

Equipment Module, Bottom View

Copy 4

VOYAGER

SPACECRAFT Phase B, Task D

FINAL REPORT

Volume 10. Engineering Study Tasks: Shroud, Temperature Control, Plume Heating

OCTOBER 1967

Prepared for
GEORGE C. MARSHALL SPACE FLIGHT CENTER
Huntsville, Alabama

TRW
SYSTEMS GROUP

Voyager Operations
Space Vehicles Division

One Space Park, Redondo Beach, California

CONTENTS

1. INTRODUCTION

This volume describes three engineering tasks, associated with the Voyager spacecraft, which were performed as part of the Task D efforts. These include shroud venting and separation, temperature control schemes, and engine plume heating.

Vents for the configuration are described and separation and release mechanisms for shroud sections and the planetary vehicles are discussed in the shroud venting and separation study. A set of separation velocities is suggested for each of the separating bodies, which will yield probabilities of collision less than 10^{-6}.

The investigation of temperature control schemes includes 1) evaluation of the predominant parameters affecting temperature excursions of the spacecraft and its components; 2) the various possible temperature control schemes that can be used on the Voyager spacecraft; 3) application of OGO, Pioneer, Mariner, Pegasus, and Nimbus louver systems for Voyager; and 4) design and fabrication parameters for insulations to assure repeatable insulation thermal characteristics. The results of the engineering task recommend a preferred temperature control subsystem and a preferred type of insulation with suggested design and fabrication parameters.

The third engineering task, engine plume heating, concerns LM Descent Engine plume heating and areas of impingement, and the effect on critical spacecraft components of radiation from the nozzle extension. The results of this task give the temperatures for critical spacecraft components due to engine plume heating and nozzle radiation.

2. SHROUD VENTING AND SEPARATION

2.1 SUMMARY

The Voyager shroud supports and protects two identical planetary vehicles during the launch and boost phases of the mission and isolates them from surface contaminants until there is no further sensible earth atmosphere (Figure 2-1). During ascent, the contained atmosphere in the shroud elements and planetary vehicle compartments must be vented, and the planetary vehicles must each be separated from the launch vehicle early in their interplanetary trajectories. Thus the shroud venting and separation study task becomes one of investigating a system of vents for the configuration, defining a design concept capable of performing the required separation events, and finally performing a separation and collision probability analysis of the individual separated elements.

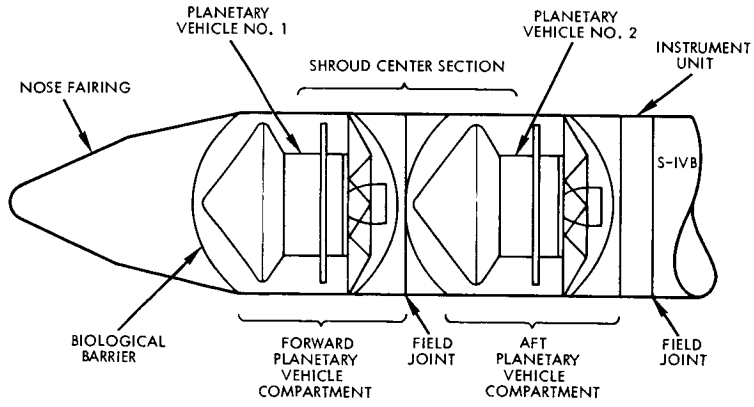

Figure 2-1

SHROUD CONFIGURATION illustrates interchangeability of planetary vehicles and corresponding shroud sections. Each module extends from forward biological barrier to field joint aft of each planetary vehicle compartment.

Figure 2-2 shows the recommended set of vent areas for the different elements of the configuration, based on allowable pressure differentials determined by strength and contamination considerations and using an assumed Saturn V ascent trajectory. These vents will allow gradual decompression of the spacecraft, meet the contamination guideline, and eliminate residual atmosphere within the shroud compartment and spacecraft by the time parking orbit is attained.

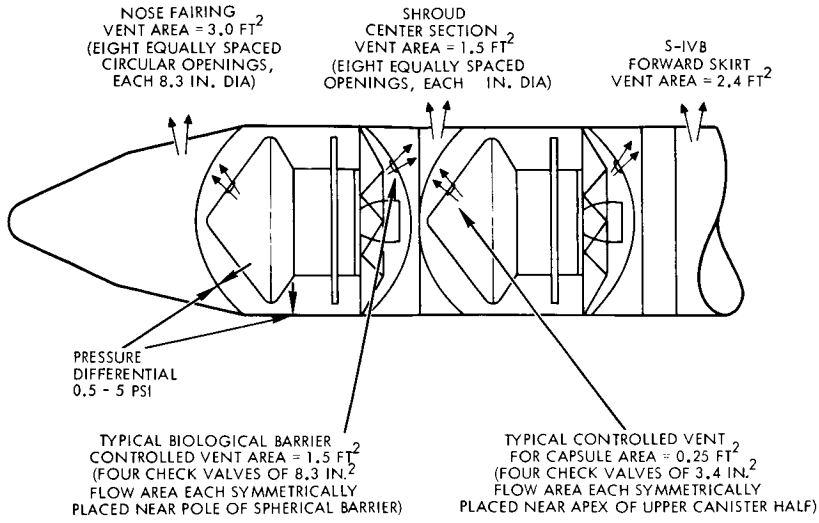

Figure 2-2

AFT VENTING is recommended. Vent areas are based on maximum allowable pressure differentials plus minimum overpressure required to prevent contamination during ascent. The atmosphere within the shroud at liftoff is dry, sterile nitrogen.

The sequence of separation events and the use of an over-the-nose separating mode are dictated by the study guideline[1]. Based on the dynamic analysis described in Section 2.4, shroud separation planes have been selected for the nose fairing and the shroud mid-section. In the spacecraft configuration described in Volumes 2, 3, and 4, stowed appendages and solar array are located well aft of the selected shroud separation plane. This requires the planetary vehicle to be guided "out of the hole" during separation. A simple scheme for imparting a separation impulse and guiding the planetary vehicle until it is clear of its shroud is described in Section 2.3.

Using the recommended separation design concept and separation velocity for each of the elements, probabilities of collision of the shroud elements with the planetary vehicles during all separation events are less than 1×10^{-6}; the analysis is described in Section 2.4.

2.2 SHROUD VENTING

During the launch trajectory, the ambient atmospheric pressure drops rapidly to a negligible value. In order to prevent large pressure differentials across shroud components and planetary vehicle elements, a system of vents is required. This system must allow gradual outflow of the atmosphere, contained within the planetary vehicles and shroud

elements, while retaining minimum positive differential pressures within the sterile capsule and decontaminated spacecraft until the stage is above the sensible atmosphere.

The vents for the capsule and the planetary vehicle compartment must be controlled, i.e., each has the capability of automatically restricting outflow to retain a given pressure differential, with the further capability of being fully opened upon receipt of a signal to completely vent down to external ambient. These controlled vents may be simple spring-loaded check valves, with an over-riding solenoid to open them fully on command. The nose fairing, shroud, and SIV-B forward vents are uncontrolled, i.e., they are merely openings in the structure to provide the required flow areas without the capability of being regulated in any way.

The recommended vent configuration is shown in Figure 2-2. Efflux from the controlled vents is directed into adjacent shroud compartments rather than directly overboard to give greater reliability, allow more flexibility in vent location, present simpler sealing demands, and incur less risk of contamination than if these vents were directly exposed to the turbulent boundary layer. Only the uncontrolled vents go directly overboard.

In this configuration the sterile nitrogen atmosphere within each planetary vehicle compartment vents aft. The required nose fairing vent areas are small enough to minimize influx of hot boundary layer air and consequent heating of the forward bulkhead during portions of the ascent. Local shields over each opening can be used to restrict the inflow of hot air further without restricting the flow areas.

Forward venting of each planetary vehicle compartment has also been examined. The openings required in the nose fairing are considerably larger than for aft venting; these would increase boundary layer inflow and require more structural reinforcement. For these reasons aft venting is the preferred approach.

Figure 2-3 shows some of the Voyager trajectory parameters used in this analysis. Pressures within each compartment will decay rapidly with time after liftoff since the external ambient decays to essentially zero within 140 seconds, as shown in Figure 2-4. The controlled vents

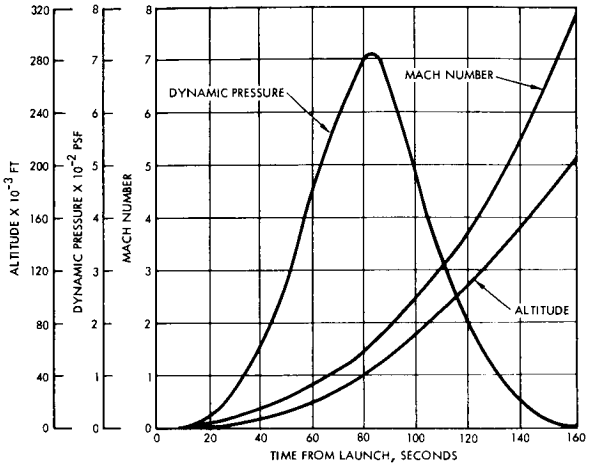

FIGURE 2-3
TRAJECTORY PARAMETERS used in venting analysis for Voyager

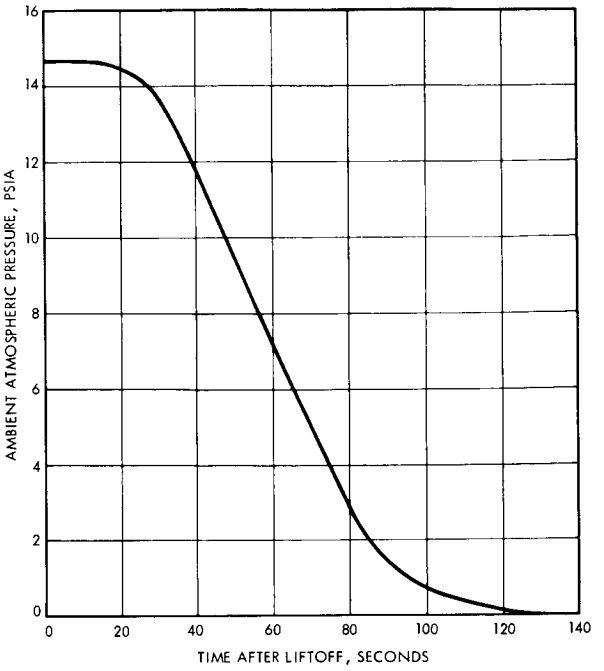

Figure 2-4
PRESSURE DECAY AFTER LIFT-OFF.

for the capsule and compartment have been fully closed long before that point, maintaining the required positive pressures within the capsule and planetary vehicle compartment. The stage altitude at that time is about 150,000 feet. When the SIV-B begins its burn to attain parking orbit, at about 200 seconds, the stage is at 300,000 feet; the controlled vents will be opened at that point in the trajectory with the same signal that initiates the SIV-B ignition. Well before parking orbit is achieved, at about 630 seconds, all portions of the capsule and spacecraft are fully vented so that there will be no thrusting of the spacecraft and no gas impingement on shroud components due to residual venting of entrapped gases during subsequent separation events. Details of the venting analysis are given in Appendix A.

Each electronic assembly will have sufficient vent area in its own cover to minimize any pressure differential across it. This is required to purge the assemblies during their initial decontamination cycles and to assure that no pressure differentials will be present during flight which might damage the components or create thrusting gas streams.

Only if a particular component requires the presence of a unique atmosphere, will it be sealed. The multilayer thermal insulation blankets use perforated materials (1/8-inch holes, six inches on center) to allow them also to vent down. It is estimated that the blankets on the recommended spacecraft will vent their approximately 4.5 pounds of contained nitrogen within two minutes. Any transient pressure differentials will be small enough to avoid structural damage to the blankets.

Thus the whole spacecraft will vent down gradually as the atmosphere is traversed. No condensation from the dry nitrogen is anticipated because of the low flow rates.

2.3 SEPARATION DESIGN CONCEPT

The separation design concept includes sequence and timing of separation events, mode of separation, selection of separation planes, and the means of separating the various elements with respect to each other. A basic constraint is that each planetary vehicle and its separation mechanism, when installed in its compartment (Figure 2-5), be completely interchangeable. Thus each encapsulated planetary vehicle can serve in either the forward or aft position in the shroud. This simplifies the sparing requirement: The spare encapsulated planetary vehicle can take the place of either vehicle in the event of a malfunction after planetary vehicle encapsulation.

The sequence of separation events during the mission has been defined in the Reference 1 guidelines for this study: The nose fairing is released as soon as possible after attainment of the parking orbit. The last SIV-B burn injects the stage into the Mars trajectory. The first planetary vehicle is then separated, followed by the shroud center section. The second planetary vehicle is released last. These events are illustrated in Figure 2-6. Before each separation event the stage is restabilized by the SIV-B attitude control system.

Each of these separation events is performed in an over-the-nose mode, i.e., each separated element moves axially with respect to the portion of the stage left behind, again in accordance with the guideline requirement.

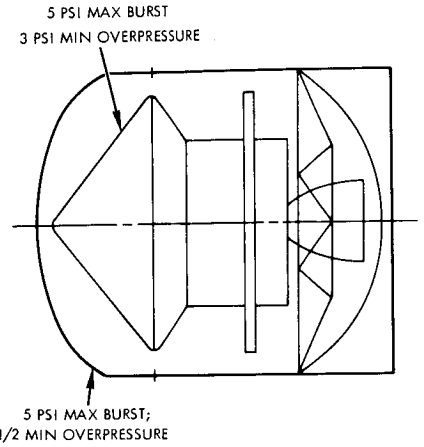

Figure 2-5

CONSTRAINTS ON PERMISSIBLE PRESSURE DIFFERENTIAL across the shroud elements and capsule determine requirements for the vent areas and controlled vent valves.

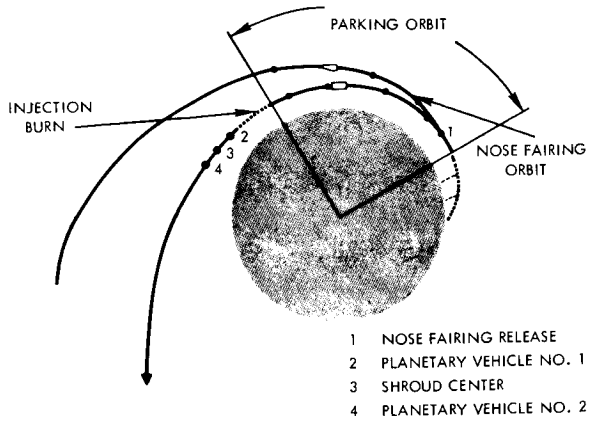

Figure 2-6

SEPARATION EVENTS separation velocity imparted to nose fairing during parking orbit puts into an eccentric orbit so that it gains altitude with respect to the SIVB stage. Following injection, the final three separation events are preformed as soon as real-time communications are re-established for command override capability.

2.3.1. Timing of Separation Events

Nose-fairing separation occurs as soon as possible after establishment of parking orbit to minimize the probability of collision between the fairing and the stage. With the constraint of minimum times in parking orbit and the dynamics of the separating fairing, these probabilities are very small (see Section 2.4).

The remaining separation events occur after injection. They should begin as soon as possible after the SIV-B is shut down (including engine tail-off), provided adequate real-time communication with the planetary vehicles and stage is established for command over-ride capability. This approach minimizes the demands on the SIV-B control system. It permits all spacecraft appendages to be deployed and the solar array to start recharging its batteries as soon as the vehicles leave the earth's shadow.

2.3.2 Selection of Separation Planes

The selection of separation planes depends on the spacecraft configuration. The maximum diameter of the recommended spacecraft at the fixed solar array is about 12 feet aft of the maximum flight capsule diameter. Deployable elements are stowed within the limits of the spacecraft dynamic envelope. With a single cut in the shroud for each vehicle, considerable relative motion is required to free the planetary

vehicle from the shroud. If the plane is near the capsule maximum diameter, the spacecraft has to travel 12 feet before it is free of the shroud. For this reason, it is desirable to separate as much of the shroud as possible during the nose fairing separation event in parking orbit to minimize the weight to be injected into the Mars trajectory. A separation plane was therefore chosen 4.6 feet aft of the assumed maximum capsule diameter. This allows the nose fairing separation to include a considerable portion of the shroud. Yet it can separate without any guidance mechanism. Appendix B contains the analysis on which this selection of separation plane is based.

2.3.3 Shroud Separation System Design

A means of breaking the shroud circumferentially and imparting a ΔV to the separated parts is required. In this process, the following constraints are present:

a) The process should be contamination-free, both for the release of gases or other combustion products, and for the fragmentation of structural connections.

b) Shock to the structure and equipment must be minimized to prevent damage or malfunction.

c) Joint weight must be low.

d) Separation reliability must be high.

e) There must be sufficient static clearances to prevent hang-up.

The characteristics applicable to the Voyager shroud, from Reference 1, are:

1) Diameter of joint: 260 inches

2) Aerodynamic shroud loads (maximum shear = 156,000 pounds; moment = 74,000,000 inch-pounds)

3) Maintain maximum internal pressure of 5 psia

4) Withstand temperature range of -100 to 250°F.

In addition to the particular characteristics outlined above, the separation technique should consider the following characteristics:

1) Ability of separation system to impart ΔV to separated parts of joints

2) Shock forces generated and their effects on the system

3) Capability of joint to be opened and closed nondestructively

4) Ability to provide a pressure-tight structure

5) Any particular hazards associated with the technique

6) Estimate of capability to be manufactured reproducibly within design tolerances.

The recommended separation system for the shroud section consists of two independent elements: a means of fracturing the shroud, and a means of imparting a ΔV to the separated parts. Selecting a nonthrusting type of separation joint permits the ΔV mechanism alone to control the impulse imparted to the separating part. Such control is desirable for the Voyager shroud because of its large size. A design concept for a nonthrusting shroud separation joint is described in Section 2.5.

The recommended scheme of imparting a ΔV to the separating shroud parts consists of four preloaded compression springs, equally spaced around the separation plane. These springs are sized to provide the required impulse and can be matched before installation in a manner similar to that used on other spacecraft projects by TRW Systems, such as OGO. The matched set of springs limits tip-off velocities of the separating parts to values well below limiting values. These have been used in the selection of the separation plane station as described in Appendix B.

Advantages of springs are:

a) Reliability: automatically actuated when joint is separated

b) Analytically predictable

c) Can be tested.

For the current design, each of the four springs has a rate of 9.2 pounds/inch with a 12-inch working stroke. This provides the impulse required to achieve the 2-feet/second selected nose-fairing separation velocity, as described in Section 2.4, and also the shroud center section separation velocity.

2.3.4 Planetary Vehicle Separation Mechanism

As described in Section 2.3.2, a separation plane for the planetary vehicle compartment has been selected that is 4.6 feet below the capsule maximum diameter. The planetary vehicle must then move some 7.4 feet before the danger of impacting the shroud is past. A scheme has been selected to separate, impart an impulse, and provide sufficient guidance to the planetary vehicle as it comes out of the hole.

The planetary vehicle is supported in the shroud by the planetary vehicle adapter which is described in Volume 3. There are 12 points of attachment between the vehicle and its adapter, with a dual redundant release device (Figure 2-7) at each. The device uses two explosive bolts to retain a split collar around an interface bolt; actuation of either explosive bolt will release the collar to initiate separation. The device and its reliability are discussed in Volume 3.

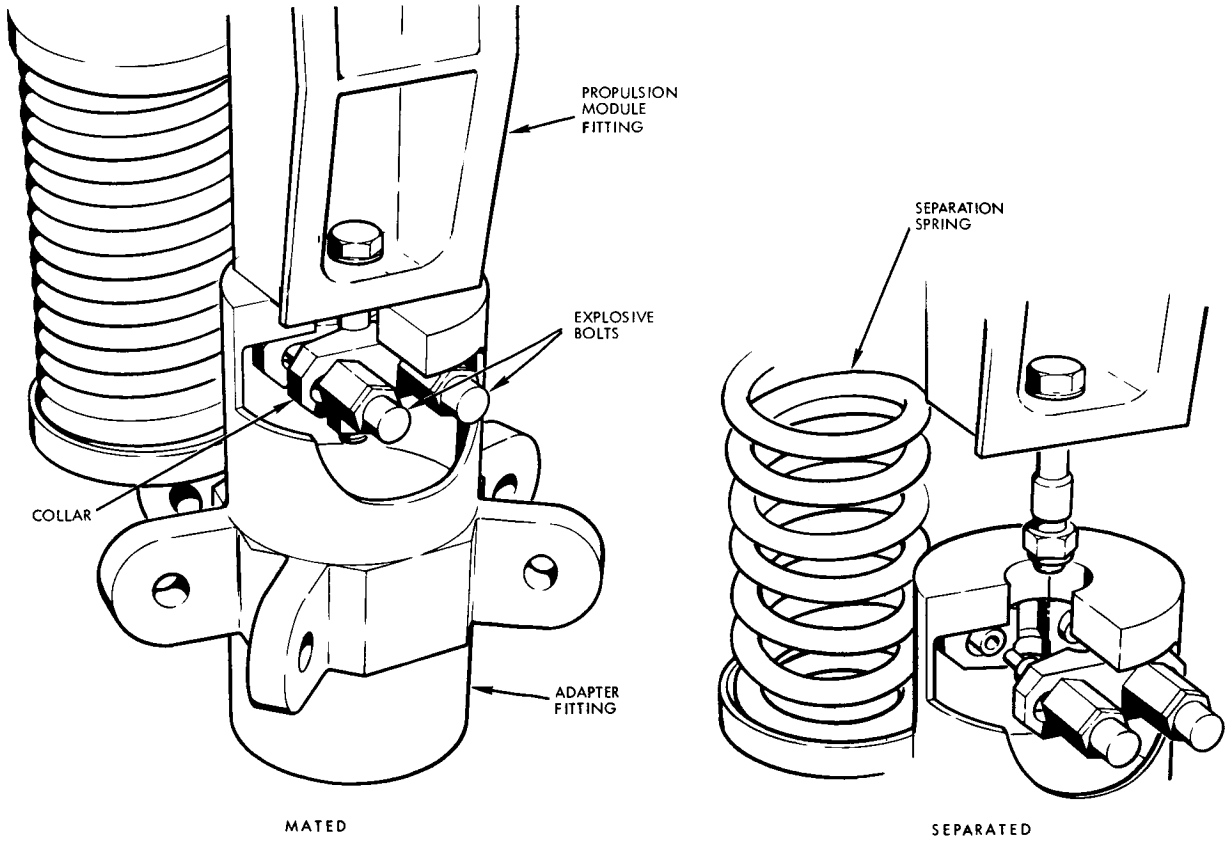

Figure 2-7
PLANETARY VEHICLE/ADAPTER RELEASE MECHANISM firing either explosive bolt releases the planetary vehicle and allows it to separate by the action of the springs.

A preloaded compression spring near each of the release devices is used to impart a separation impulse to the planetary vehicle. With 12 springs, the perturbation impulse, due to errors in the spring which tends to impart lateral and rotational motions to the spacecraft, will be statistically small. Each of these springs has a spring constant of 16.6 pounds/inch with a working stroke of 12 inches. This provides the recommended separation velocity for a 22,000-pound planetary vehicle.

Expected spacecraft center-of-mass offsets will not produce unacceptable rotations of the spacecraft. Full advantage is taken of the available spacecraft dynamic envelope to maximize the solar array diameter, which is the largest diametric dimension. Since clearance between the array diameter and dynamic envelope is nominally one inch on the radius, it is necessary to provide lateral restraint for the spacecraft within the shroud to ensure a margin of safety for the separation event.

A concept for this restraint is shown in Figure 2-8. Four equally spaced channels, attached to the shroud between the solar array and the separation plane, act as rails. A roller is attached to the solar array opposite each channel. Its function is to react any spacecraft lateral motion against the sides of the channel. Clearance is provided for each roller when the spacecraft is attached to its adapter, to allow the shroud to deflect during the high dynamic pressure portions of the trajectory without inducing loads in the solar array. Once the spacecraft is released, the rollers move within the confines of the channels, with only enough clearance to take up spacecraft and shroud assembly tolerances without loading the array.

Any contact between rollers and channel sides will induce loads only in the plane of the solar array. Such loads are expected to be small, less than 100 pounds, because of the flexibility of the channel and array and the small component of the separation force that induces such contact.

This scheme is relatively simple and, since the center-of-mass offsets will be known with reasonable accuracy, will be very reliable. For example, with one-half-inch unknown offset, and a planetary vehicle ΔV of 2 feet/second, the planetary vehicle will rotate at a rate of 0.0023 radian/second with a total rotation of 0.50 degree when it clears the shroud. The lateral excursion will be about 0.75 inch at that time.

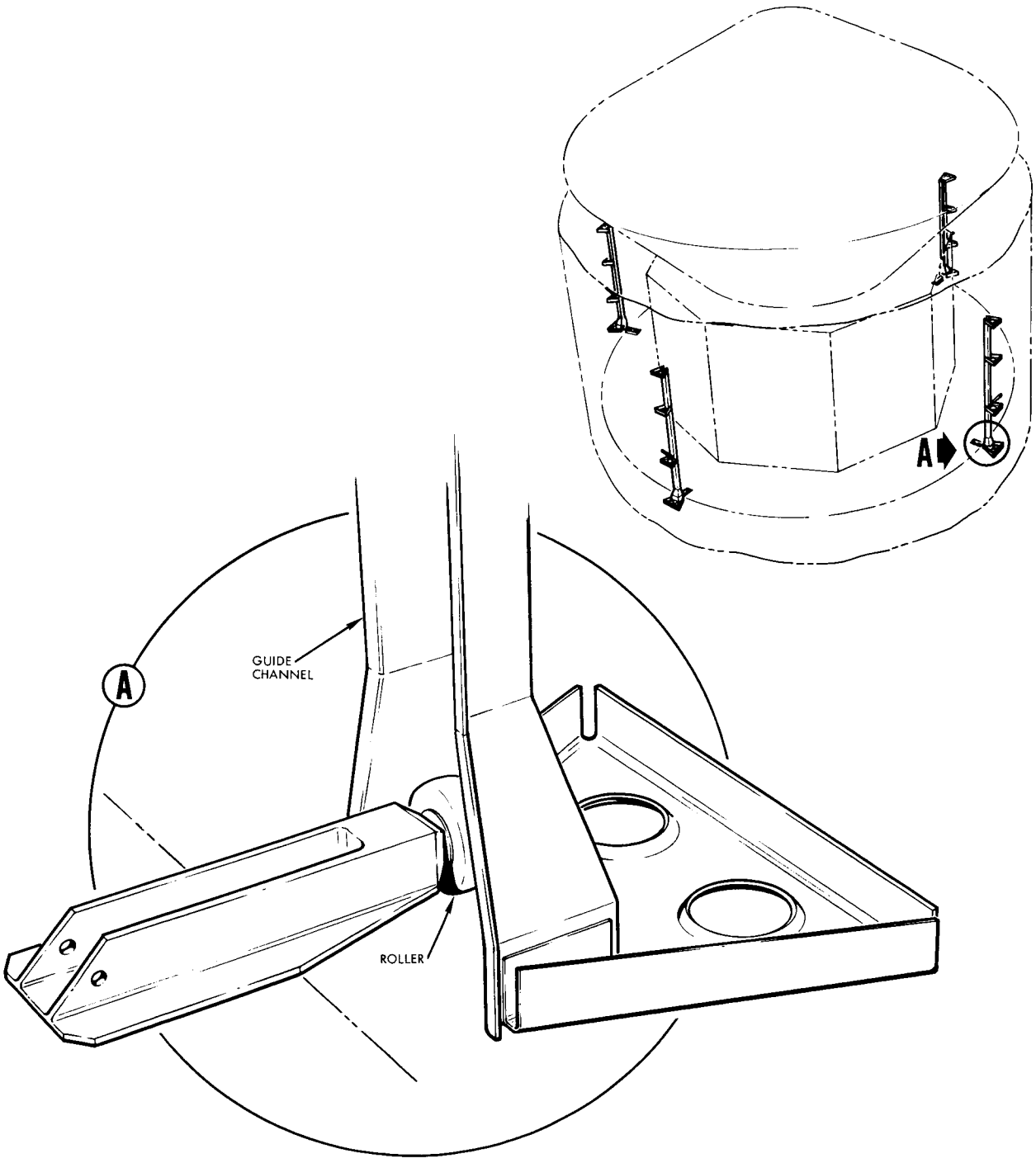

Figure 2-8

PLANETARY VEHICLE SEPARATION. Twelve explosive bolts release planetary vehicle from adapter and twelve springs impart required separation velocity. Planetary vehicle is guided out of shroud by rollers mounted on annular solar array and running in rails attached to shroud.

An alternative scheme involves slowly elevating the planetary vehicle until the solar array is near the plane of the shroud opening; then a set of springs, imparting a separation impulse, is released. This is described in Reference 2. It is a relatively complex scheme compared to the recommended design.

2.4 SEPARATION DYNAMICS AND COLLISION ANALYSIS

This section describes the analysis of the separation dynamics of the shroud elements and planetary vehicles, and the collision probabilities of the separating parts. The effects of shock loads generated by the pyrotechnic separation devices on the spacecraft design are also discussed.

The sequence and timing of separation events has been discussed in Section 2.3.

2.4.1 Nose Fairing Separation

The over-the-nose method of nose-fairing separation was discussed in Section 2.3. Of interest here is what happens following the nose-fairing separation event.

Once pyrotechnic severance has been completed, an impulse is imparted to the nose fairing by the shroud separation springs, injecting it into an eccentric orbit from the circular parking orbit so that it gains altitude with respect to the stage. The nose fairing continues to move forward and higher with respect to the stage and reaches its maximum distance ahead of the stage in about 10 minutes. At approximately 18 minutes (an interval that is essentially independent of separation velocity), the stage has caught up with and is passing below the fairing. The distance between them is approximately 1200 feet for each foot per second of initial separation velocity (Figure 2-6).

The stage will continue to move ahead of and below the nose fairing until re-ignition of the SIV-B propulsion system for the injection burn. Then the stage's orbital path becomes increasingly eccentric as the stage gains altitude climbing above the nose-fairing orbit. The nose fairing at this time is far behind.

The time-span of interest then is from 15 minutes to 18 minutes after earth parking orbit acquisition or, if stabilization requires as long

as one minute, from 14 to 18 minutes. Collision probabilities for this period were calculated with the aid of equations and data extracted from Reference 3. Table 2-1 gives the probability of impact between the fairing and the vehicle as a function of time after nose-fairing separation (T_c) and its separation velocity.

Table 2-1. Nose-Fairing Collision Probability

T_c (minutes)	ΔV=1 (feet/second)	$\Delta V = 2$	$\Delta V = 4$
14	2.06×10^{-4}	7.38×10^{-10}	1.79×10^{-18}
15	9.16×10^{-6}	4.82×10^{-14}	4.22×10^{-29}
16	2.01×10^{-6}	2.91×10^{-22}	5.57×10^{-52}
17	5.11×10^{-8}	4.30×10^{-43}	--
18	2.31×10^{-10}	--	--

Since the nose fairing is separated as soon as possible after earth parking orbit is achieved, if the time in parking orbit is greater than 18 minutes, the likelihood of the stage colliding with the nose fairing becomes extremely small. In reviewing trajectory data, launch opportunities, etc., for the 1973-1979 missions, it was found that the shortest time in parking orbit may be as low as 15 minutes. As shown in Table 2-1, the collision probabilities increase rapidly as time between nose-fairing separation and termination of parking orbit decreases; therefore, the fairing separation event must occur as soon as possible after orbit acquisition. Following the S-IVB burn, only stage stabilization should be performed before the separation.

Details of this analysis are in Appendix C.

On the basis of these results, a nose-fairing separation velocity of 2 feet/second is selected to provide sufficiently small collision probabilities. The shroud separation springs of Section 2.3.3 are sized for this ΔV.

Because the two planetary vehicle compartments are interchangeable, the shroud center section separation velocity will be determined

by these same springs. It will be seen in the next section that planetary vehicle separation velocities are also uniquely determined once the nose-fairing separation velocity is selected.

2.4.2 Post-Injection Separations

The timing of post-injection separation events is discussed in Section 2.3.1.

To minimize collision probabilities with the over-the-nose separating mode, it is desirable to have the value of the nominal velocity of the center section midway between the nominal velocities of the two planetary vehicles. Then the probabilities of collision between the shroud center section and each of the separating vehicles will be equal.

A post-injection collision probability analysis is shown in Appendix D, including a calculation of the velocities of each of the separating bodies. These are interdependent and, as stated in Section 2.4.1, are uniquely determined once the nose-fairing separation velocity is selected.

With a nose-fairing separation velocity of 2 feet/second, the velocities of Table 2-2 follow. The planetary vehicle separation springs described in Section 2.3.4 are sized on this basis. For nose-fairing separation velocities other than 2 feet/second, these velocities will change proportionately.

Table 2-2. Separation Velocities of Separating Bodies (Based on Nose-Fairing Separation Velocity of 2 feet/second)

	Note 1	Note 2
Forward planetary vehicle	17.2 in./sec	24.0 in./sec
Shroud Center Section	12.0 in./sec	20.6 in./sec
Aft planetary vehicle	7.0 in./sec	27.0 in./sec

Note 1. Velocities relative to the center of mass of the injected configuration; differences between these velocities are true relative velocities between separating elements.

Note 2. Velocities relative to the portion of the configuration from which the element separates.

With these velocities, collision probabilities will all be less than 10^{-6} (Appendix D).

As an alternate separating configuration, it is feasible to bias the attitude control system of the SIV-B to separate the shroud center section in a direction away from the stage velocity vector. This would eliminate the interdependence of the nose-fairing separation velocity from the planetary vehicle separation velocities. However, since the collision probabilities, without requiring additional SIV-B steering, are acceptably low, no further consideration is given to this alternate.

2.4.3 Separation Shock Environment

In addition to collision hazards during shroud and planetary vehicle separation, the pyrotechnic devices themselves induce shock loads which will affect the design of many spacecraft components.

Pyrotechnic separation, both for the shroud elements and the planetary vehicles, as well as spacecraft appendage release devices as described in Volumes 3 and 4, will induce shocks throughout the spacecraft. The magnitude of these shocks and their effect on the spacecraft are discussed in Appendix E.

Estimates of such shock levels are stated. It is concluded, however, that although in a qualitative sense the configuration design with its particular locations of separation planes and other devices will not cause serious shock problems, additional analysis is required to determine realistic design and test criteria for critical equipment elements.

2.5 SHROUD DESIGN AND CONTAMINATION CONSIDERATIONS

2.5.1 Shroud Design

The guideline document, Reference 1, includes most of the detail design concepts of the shroud structure and a candidate shroud fracturing scheme. This separation scheme is described in some detail along with some further considerations of it.

Some contamination considerations of the shroud and the shroud separation process are also mentioned.

The recommended shroud fracturing system, shown in Figure 2-9 as extracted from Reference 1, employs pyrotechnics in a noncontaminating, stressed-skin system. The system consists of a conventional mild detonating fuse (MDF) completely contained within an expansible jacket which imparts the full pressure pulse generated by the detonating MDF

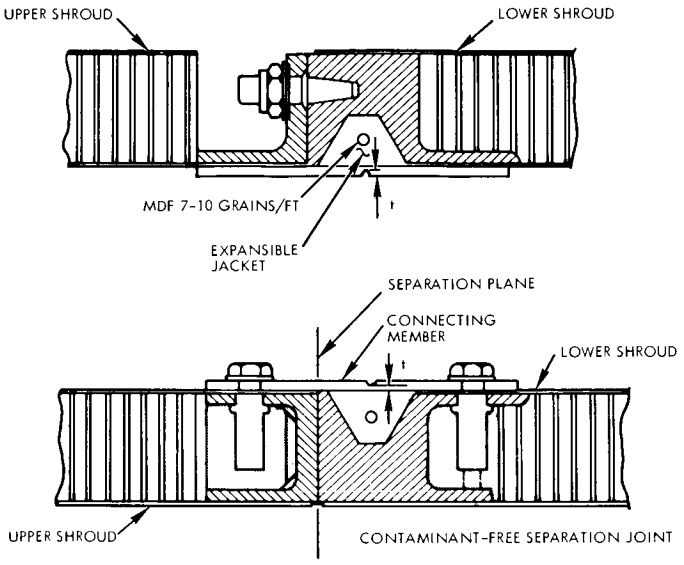

Figure 2-9

SHROUD SEPARATION JOINT Non-thrusting, contamination-free design uses MDF in an expansible jacket to fracture a groove in the connecting member. Upper drawings shows alignment pins used to take out lateral loads at several circumferential locations. Lower drawings shows tension-compression tie.

core to the surrounding structure and then to the designed failure point (i.e., "V" groove) without permitting escape of the explosive products. The expansible jacket is captured between a backup structure and a doubler strip which is designed to fail the length of a carefully machined V notch the entire length of the strip.

The operation of the system consists of initiating the MDF at its ends with an encapsulated initiator. As the explosive shock progresses through the expansible jacket, it causes the doubler strip to sever at the groove due to the expansion of the gases within the expansible jacket. Since the expansible jacket is wholly on one side of the joint, there is no appreciable thrusting of the separated elements. After the doubler strips have severed, the jacket continues to expand and pushes on the two severed halves of the broken doubler; due to their permanent deflection

after fracturing, i.e., the slope of the local meridian is no longer zero at the fracture, and a small thrust component results.

System reliability and noncontamination are the over-riding selection criteria. Other considerations which make this selected concept favorable are:

- Improved efficiency by using the maximum energy available in MDF
- Reduced pyrotechnic shock impulse level
- Improved safety and reliability of linear separation applications
- Ability to maintain a seal against an internal pressure
- Capability of joint to be opened nondestructively
- Access capability from the exterior of the vehicle
- Simplicity of the design indicates that the parts can be manufactured reproducibly within the design tolerances
- Separation joint may also serve as a field joint.

While this concept appears to have considerable merit, flight experience with this system does not exist, and evaluation testing will be required to develop the confidence required for application of this device to the Voyager program. The means of sealing a joint like this must be included in its further development.

The encapsulating jacket must retain its elastomeric strength to function properly. Testing is required to establish its permissible temperature ranges.

Shock pulses are generated in the structure due to the breaking of the doubler strip and the explosive shock. These pulses must be measured and factored into the design random and acoustical vibration environments described in Volume 3.

This type of joint is similar to one currently being developed by Lockheed Missiles and Space Corporation for TRW Systems Group for a

shroud whose application is classified. Verification tests on this joint are currently in progress.

Other types of joints were examined briefly. Explosive bolts or nuts are generally used for smaller shrouds, but the sealing problem plus the large size of the Voyager shroud would make the reliability of a system using a discrete number of electroexplosive elements very poor. Thrusting joints such as the one developed by Douglas (Reference 4) are undesirable since their impulse is difficult to control; they are more suited to clam-shell shroud separations.

2.5.2 Contamination Considerations

The shroud design described in Reference 1 can meet the following cleanliness standards:

- Surface is smooth to facilitate physical cleaning and is free of cracks, crevices, protuberances, etc., that would entrap particles.
- Able to maintain a positive overpressure within compartment so that all leakage will be from within.
- Has controlled vent system
- Shroud separation system contains all debris
- Shroud compartments are hermetically sealed and free of leaks.

The shroud can be decontaminated according to procedures outlined in Volume 9. As Reference 1 points out, the major concern is the effect of antibiological agents on shroud materials, particularly the honeycomb bond adhesives. Volume 9 describes materials compatible with ethylene oxide.

It is possible, with a fracturing joint, that fragments or particles will be ejected at rupture. With the planned trajectory, velocities of these particles of about 100 feet/second (relative to the planetary vehicle) are required for the particles to have any probability of independently impacting Mars. These particles can be considered to emanate from two general areas around the rupturing notch of Figure 2-9: either they will include a portion of machined surface, on either side of the notch,

or they will be from the virgin portion from within the notched element which has not been exposed to the atmosphere since doubler strip was rolled and machined.

Virgin metals are contamination-free below the first few thousandths of an inch of depth from their surfaces. Metals more than several thousandths of an inch thick are impervious, and are subjected to melting temperatures above 1300°F during alloying.

Small particles containing surface elements, which are presumed to be contaminated, will be heated by sunlight during transit to Mars. With black paint on one surface, temperatures will attain values above 260°F, which is sufficient to eliminate any viable organisms well before entering the Martian atmosphere.

Thus it is concluded that there is no reasonable probability that a particle released at any shroud separation joint will contaminate the planet surface.

REFERENCES

1. "Voyager Spacecraft – Phase B, Task D Guidelines," MSFC, 14 July 1967, reprinted by TRW as VVV-353, 17 July 1967.

2. TRW Interoffice Memo 67-35212-216, "Voyager Planetary Vehicle Separation Mechanism (Elevator)," 21 September 1967.

3. "Description of Design Considerations for the Voyager 1971 Spacecraft Utilizing the Saturn V Launch Vehicle Configuration," JPL Report No. PD-86, June 1966.

4. Space-Aeronautics, July 1966, p. 86.

system using a discrete number of electroexplosive elements very poor. Thrusting joints such as the one developed by Douglas (Reference 4) are undesirable since their impulse is difficult to control; they are more suited to clam-shell shroud separations.

2.5.2 Contamination Considerations

The shroud design described in Reference 1 can meet the following cleanliness standards:

- Surface is smooth to facilitate physical cleaning and is free of cracks, crevices, protuberances, etc., that would entrap particles.
- Able to maintain a positive overpressure within compartment so that all leakage will be from within.
- Has controlled vent system
- Shroud separation system contains all debris
- Shroud compartments are hermetically sealed and free of leaks.

It can be sterilized and decontaminated according to procedures outlined in Volume 9. As Reference 1 points out, the major concern is the effect of antibiological agents on shroud materials, particularly the honeycomb bond adhesives. Volume 9 describes materials compatible with ethylene oxide and other decontaminating agents.

It is possible, with a fracturing joint, that fragments or particles will be ejected at rupture. With the planned trajectory, velocities of these particles of about 100 feet/second (relative to the planetary vehicle) are required for the particles to have any probability of independently impacting Mars. These particles can be considered to emanate from two general areas around the rupturing notch of Figure 2-12: either they will include a portion of machined surface, on either side of the notch, or they will be from the virgin portion, i.e., from wholly within the notched element never having been directly exposed to atmosphere since being formed into the plate from which the doubler strip was rolled and machined.

Virgin metals are contamination-free below the first few thousandths of an inch of depth from their surfaces. Metals more than several thousandths of an inch thick are impervious, and are subjected to melting temperatures above 1300°F during alloying.

Small particles containing surface elements, which are presumed to be contaminated, will be heated by sunlight during transit to Mars. With black paint on one surface, temperatures will attain values above 260°F, which is sufficient to eliminate any viable organisms well before entering the Martian atmosphere.

Thus it is concluded that there is no reasonable probability that a particle released at any shroud separation joint will contaminate the planet surface.

REFERENCES

1. "Voyager Spacecraft – Phase B, Task D Guidelines," MSFC, 14 July 1967, reprinted by TRW as VVV-353, 17 July 1967.

2. TRW Interoffice Memo 67-35212-216, "Voyager Planetary Vehicle Separation Mechanism (Elevator)," 21 September 1967.

3. "Description of Design Considerations for the Voyager 1971 Spacecraft Utilizing the Saturn V Launch Vehicle Configuration," JPL Report No. PD-86, June 1966.

4. Space-Aeronautics, July 1966, p. 86.

3. TEMPERATURE CONTROL

3.1 INTRODUCTION AND SUMMARY

This engineering task investigated: 1) predominant parameters affecting spacecraft and component temperature excursions; 2) various possible temperature control schemes; 3) OGO, Pioneer, Mariner, Pegasus, and Nimbus louver systems for Voyager use; and 4) design and fabrication parameters for insulation to assure repeatable thermal characteristics.

The predominant parameters affecting temperature excursions of the spacecraft are environment, orientation, internal heat dissipation, and engine firing. Methods of minimizing and/or controlling these temperature excursions have also been summarized, based on information from TRW studies. For Voyager an insulated enclosure with variable heat dissipation devices (louvers) is required.

Numerous temperature control concepts were investigated during tradeoff studies made in Reference 3-1 through 3-4. A careful review was made of all the concepts investigated during the previous TRW studies of Voyager. A summary of the various temperature control schemes and their effectiveness in the Voyager application is presented in Section 3. 3. From the review of these possible concepts, an optimized temperature control subsystem for the Voyager application was selected. The optimum scheme is a combination passive-active system using the totally insulated enclosure concept, thermal louvers, thermostatically controlled heaters, thermal finishes, and varying degrees of structural thermal coupling.

OGO, Pioneer, Mariner, Pegasus, and Nimbus louver systems were compared for Voyager use. OGO, Pioneer, Mariner, and Pegasus use bimetallic actuated louvers. Nimbus uses two-phase fluid actuated louvers. Bimetallic actuated louvers were selected as the preferred louver system because of their reliability, lower weight per square foot, simplicity, and proven flight performance. The design and operating characteristics are presented in Section 3. 4 along with a summary of the louver study.

Various types of insulation were considered for Voyager applications. The effect on uncertainties in insulation thermal properties, due to repeatability considerations generated by fabrication and installation procedures, has been evaluated analytically and empirically. Additional work should be done to evaluate this factor on the basis of test and statistical analysis. The design factors considered were type of insulation, number of layers, blanket size, attachment, perforations, overlapping, interleaving, and blanket contour. Various seams and joint designs were studied for manufacturing feasibility and design integrity. The thermal performance for the insulation was based on existing test data. A summary of the insulation design and fabrication study and the selected insulation technique is presented in Section 3.5. Multilayer crinkled aluminized Mylar was selected as the preferred insulation because it provides the best thermal performance with minimum weight. The preferred method of attachment is Velcro tape since it provides ease of removal with minimum weight.

3.2 DEFINITION OF THERMAL CONTROL PARAMETERS

3.2.1 Introduction

During this engineering task, it was required that predominant parameters which cause large temperature excursions during all phases of the mission be identified. These include environment, orientation, engine firing, and internal heat dissipation. The methods of controlling or minimizing the temperature excursions are the thermal control techniques used. The sum total of the thermal control techniques is the temperature control subsystem. Overall temperature control is sensitive to the requirements of each piece of equipment within the spacecraft, to the varying environmental extremes, and to the spacecraft orientations.

3.2.2 Environmental

During the Voyager mission (Figure 3-1) the spacecraft will be subjected to such environmental conditions as:

1) Launch. Heating from the shroud during launch and boost

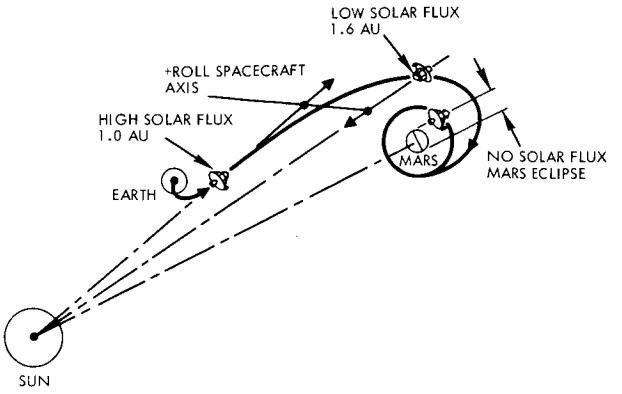

Figure 3-1

HOT AND COLD CONDITIONS DURING MISSION dictate design requirements for temperature control subsystem. Solar input varies from 442 BTU/HR FT^2 near earth to 159 near Mars and zero during Mars eclipse.

2) Near-earth. Solar heating on the solar array, base of spacecraft, and the engine at a near-earth solar flux of 442 Btu/hr-ft^2. Spacecraft subject to earth albedo and emission.

3) Near-Mars. Solar heating on the solar array, base of spacecraft, and engine at a near-Mars solar flux of 159 Btu/hr-ft^2. Spacecraft subject to Mars albedo and emission.

4) Eclipse. No solar heating on spacecraft.

3.2.3 Orientation

The temperature control subsystem is required to provide the desired thermal environment for all spacecraft orientations. The Voyager spacecraft is normally fully attitude-stabilized utilizing celestial references (sun and Canopus). Solar radiation is normally colinear with the axis of the engine (Figure 3-1). For this orientation, only the solar arrays, the insulation on the base of the spacecraft, the engine, and some of the appendages see the sun. There are, however, periods when the spacecraft is not attitude-stabilized. These occur during earth eclipse, initial stabilization, first interplanetary trajectory correction, Mars orbit insertion, capsule release, and Mars eclipse. During these periods, any portion of the spacecraft may see the sun. During eclipse periods, however, there is no solar heat input to the spacecraft.

3.2.4 Engine Firing

During engine firings, the spacecraft is subjected to plume heating and nozzle radiation, particularly during:

1) First Interplanetary Trajectory Correction Transient. An upper bound hot condition associated with the first interplanetary trajectory correction. The engine firing is 380 seconds (1700-pound thrust, insulated nozzle). Soakback effects upon the solar array, engine components, feed lines, and spacecraft structure can cause excessive temperatures.

2) Mars Orbit Insertion Transients. The low temperature prior to firing, thermal shock, and soakback effects. The engine firing is 380 seconds (9850-pound thrust, insulated nozzle).

3.2.5 Internal Heat Dissipation

Wide variation in internal heat dissipation (150 watts prelaunch to 700 watts orbital operation) requires a temperature control subsystem that is capable of dissipating varying amounts of waste heat. During eclipse, it is desirable to have a minimum amount of heat radiated to space. But during near-Mars insolation, it is desirable to radiate to space all the heat dissipated by the equipment.

3.3 COMPARISON OF TEMPERATURE CONTROL SCHEMES

3.3.1 Introduction

Temperature control of a spacecraft and its components is accomplished by maintaining a thermal balance between internally generated heat, external heat sources, and external radiant emission, at temperature levels within the temperature limits of the components. The system must conform to these limits for all phases of the mission, must provide repeatable thermal performance, and must be reliable. The basic tradeoffs are between an insulated and an uninsulated spacecraft and between passive and active temperature control or a combination of the two.

3.3.2 Insulated Versus Uninsulated

In the insulated concept, a closed, insulated envelope minimizes the effects of environmental extremes, orientation, and engine firing. It also eliminates a complex radiation analysis and permits predictable control of component temperatures by means of appropriate radiation areas.

An uninsulated spacecraft would require thermal shielding of spacecraft components. This imposes higher heat dissipation requirements on the temperature control subsystem during hot conditions and higher heater power requirements on the system during the cold conditions. The uninsulated concept would be more complicated and less predictable.

For the Voyager application the insulated concept has been selected to minimize the effects of the thermal control parameters defined in Section 3.2. External surfaces are covered with insulation except for the radiating areas. Possible insulations for Voyager application are presented in Section 3.5 with a preferred insulation selected. Possible control techniques for the radiating areas are discussed in Section 3.3.3.

3.3.3 Passive Versus Active

Passive temperature control employs the inherent thermal properties of the spacecraft structure and its materials, the spacecraft geometry, motion, and orientation to maintain the temperature of the spacecraft. This type of system is extremely reliable and simple. The weight associated with this system is minimized since there are no moving parts. The types of thermal control techniques that are considered to be passive are:

1) Surface coatings

2) Structural thermal coupling

3) Insulation

4) Radiation panels.

External surface temperature can be controlled by proper selection of the solar absorptivity (α) to emissivity (ϵ) ratio. Figure 3-2 indicates that, for $\alpha/\epsilon = 0.3$, the equilibrium surface temperatures at 1.0 and 1.6 AU are 75 and $-50^{\circ}F$, respectively. A wide variety of surface finishes (thermal coatings) or combinations thereof can be used to achieve this or almost any other desired ratio.

In many cases, thermal coatings alone are inadequate to control heat flow in and out of the vehicle. Insulation is therefore used to provide additional control of heat flux and local temperature

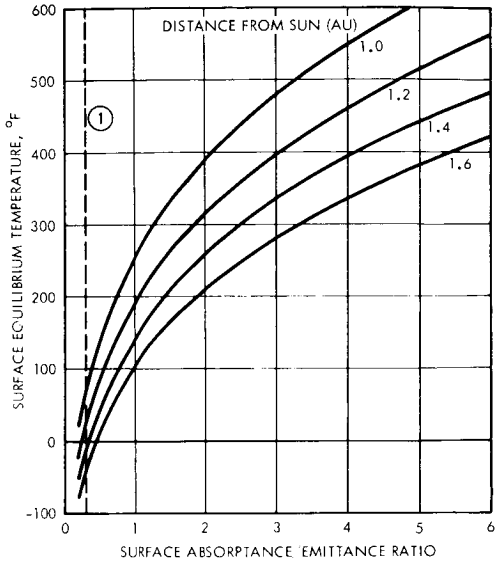

① TYPICAL FOR ALUMINIZED MYLAR WITH MYLAR SIDE OUT $\alpha/\epsilon = 0.3$
TYPICAL FOR WHITE PAINT $\alpha/\epsilon = 0.3$

Figure 3-2
EQUILIBRIUM TEMPERATURES are dependent on the ratio of absorptance to emittance for external surface and distance from the sun.

levels. This is further supplemented by the choice of thermal coupling (i.e., low or high conductivity joints) and of thermal control of structural materials. Geometry and orientation are utilized to shade radiating surfaces. Thermal control of equipment is implemented by choice of equipment surface emissivities and limitation of baseplate power density (i.e., heat dissipation per unit of baseplate area).

A fully passive system, sized to accommodate the hot condition, would require a large radiating area. The large radiating area represents a large heat loss during eclipse. The heat loss from the radiator would be greater than the heat dissipation from the components. Thus the components would drop below their lower temperature limits. Conversely, sizing the radiators passively for cold conditions causes high spacecraft component temperatures during hot conditions.

A fully passive temperature control system is unable to satisfy the Voyager requirements. The addition of a few relatively simple active thermal control elements can, however, create an acceptable temperature control subsystem. In general, these elements are actuated by on-board temperature levels or differences at or near the point of control.

Thermostatically controlled heaters can be used to hold components within narrow temperature limits. The simplest of such heaters (TRW

Specification PT4-13004) is the on-off type, operating within some design bandwidth of temperatures. Either thermostats (TRW Specification PT2-2004) or proportional controllers (TRW Specification PT4-10) can be used to control the heating rate. The proportional controller gives finer temperature control but at the cost of increased weight and complexity. Figure 3-3 shows a comparison of the two control methods. For the Voyager application, where most of the components have wide temperature bands, the thermostat provides adequate control.

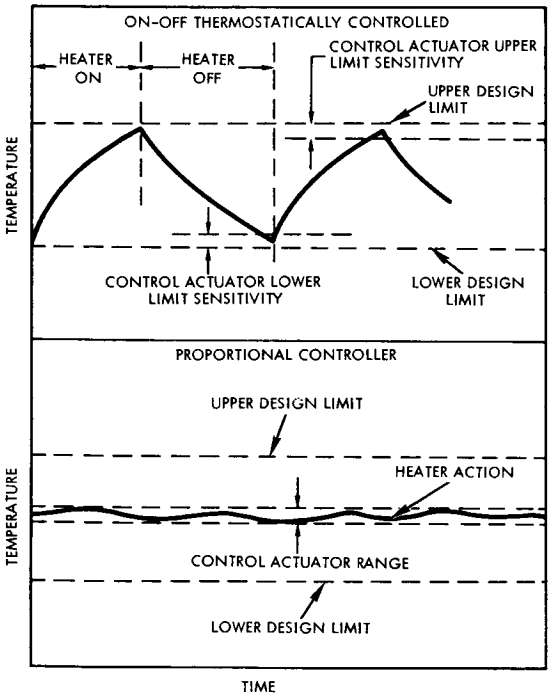

Figure 3-3
HEATERS - Thermostatic control compared with proportional control.

Temperature-responsive radiation louvers have been used successfully in the OGO, Pioneer, Mariner, Pegasus, and Nimbus spacecraft. The function of these louvers is to vary the effective emissivity of a radiating surface in response to temperature. There are numerous methods of actuation for the louvers. Mariner, OGO, Pioneer, and Pegasus make use of bimetallic actuators. Nimbus uses two-phase fluid-actuated louvers. A comparison of these louver systems is made in Section 3.4.

A thermal switch has been investigated recently by TRW Systems on a study and research basis. The switch is a device whose thermal conductivity varies from zero or nearly zero to relatively high values in response

to changes in temperature levels. A laboratory model (References 3-5) that achieved a 38:1 control range has been built and tested. A study was made (Reference 3-6) of another switch which is somewhat similar and, though simpler, was less efficient in operation. Thermal switches are still in a development stage. They are more complex and less reliable than louvers. In the Voyager application, when relatively high heat rates are encountered, the thermal switch is inappropriate as the closed resistance to heat transfer is high compared to louvers requiring many switches. for the batteries or TWT's for example.

Heat pipes have been investigated in the laboratory at TRW. In physical appearance, they consist of several internal capillary layers, enclosed with a small amount of working fluid in a tube that is sealed at both ends. Heat transport is accomplished by vaporization of the contained fluid at the heated end of the tube and its condensation at the cool end. Vapor transport is brought about by small pressure differences within the system and liquid return by capillary action of the material lining the tube interior. The heat pipe will transfer heat at a high rate unless the cut-off temperature of the working fluid is reached. This is the temperature at which the fluid freezes. Below this temperature any heat transport is by conduction through the materials alone. Theoretically, the heat pipe may have an unlimited number of geometries. Actual limitations are due to engineering considerations, and the most useful shape yet to arise is that of a long, thin cylinder connecting a heat source to a heat sink. The most suitable capillary wick is annular and fits snugly against the central core of the pipe; returning condensate flows through the annular wick. For Voyager, it is desirable to develop a two-dimensional heat pipe. This could be used to distribute the heat from components with excessively high power density (i.e., TWT) and with concentrated heat sources (sequential shunts).

On a major system level, active thermal control design may be described as composed of numerous interrelated thermal control subsystems, most of which employ active elements such as radiators, pumps, valves, louvers, heaters, evaporators, and switches. Generally, the system is designed to handle not only large heat fluxes, but also

large changes in total load. Operational mode may be varied automatically or manually. Fluid loops are used extensively to transport heat from point of origin to point of rejection, since normal passive measures are incapable of sustaining required heat fluxes across the temperature gradients which are the result of design temperature levels.

With high and variable heat rejection from electronic components, a fluid loop can be used to transport heat from the electronics to a point of ejection. The heat can be dissipated to space by use of a radiator, boiler, or sublimator. The typical radiator (Figure 3-4) is a closed-loop system in which the fluid or transport medium is pumped through a cold plate under the electronics, then pumped to radiator surfaces which have a good view of space and are isolated from solar heat input. This type of system could be used in the Voyager spacecraft, but it is heavy, not too reliable, and quite complicated. In order for this system to be redundant, it is necessary to provide dual lines and pumps. The Apollo program uses a recirculating glycol/water loop with a water boiler (Figure 3-5). Dual pumps and valves are required for failure mode reliability. This open-loop-tube system would not be desirable for the Voyager program because of the penalty required to carry sufficient water for the boiler to meet the requirement for six months in Mars orbit.

Sublimators are also undesirable because, although they weigh less than boilers, they are still too heavy to be practical for space applications.

Active thermal systems, capable of meeting the heat-load, life, and reliability requirements of spacecraft, are inherently too complex and bulky to be practical. Adequate redundancy in an active system can only be provided by duplication of components. Protection from micrometeoroid damage has to be provided for each of the components in an active system and, in particular, for the fluid lines. The fluids used in an active system would have to provide the following items:

1) High specific heat
2) Low viscosity
3) Lightweight
4) Low freezing temperature.

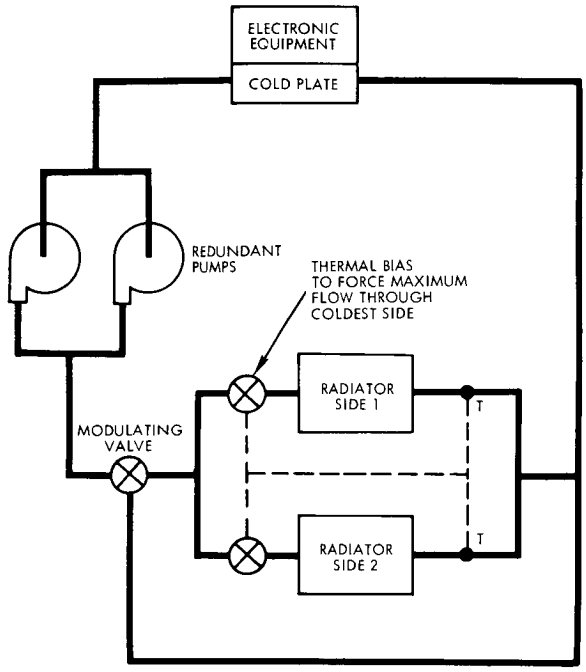

Figure 3-4
COOLING SYSTEM - Closed loop.

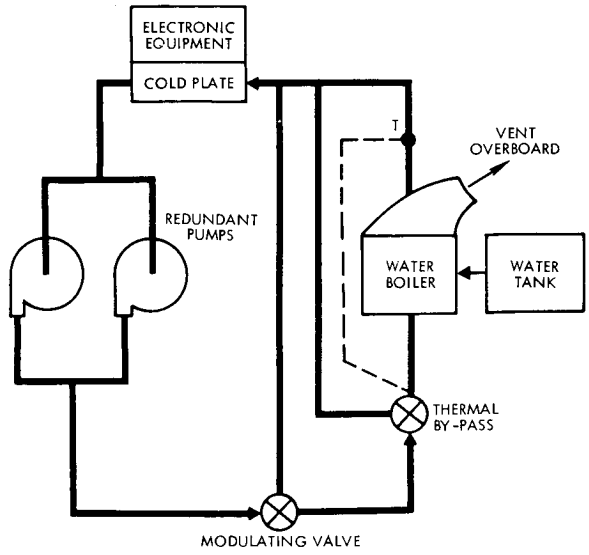

Figure 3-5
COOLING SYSTEM - Open loop.

In most present spacecraft applications of active fluid systems, potential freezing problems have been encountered. Normally a glycol/water medium has been used. It is possible, however, to use a commercial fluid such as Dowtherm, which has a lower freezing point than glycol/water but is still not adequate for space applications.

The best active system from a Voyager application standpoint appears to be a mechanically active system which uses louver blades covering a radiator panel. Section 3.4 presents a comparison of various possible louver systems for Voyager application.

3.3.4 Conclusions and Recommendations

From the standpoint of the varying natural and induced environments in which the Voyager spacecraft must operate, the most desirable temperature control subsystem consists of a combination active-passive system. The passive components of the system are:

1) Surface finishes to obtain desired thermal radiation properties

2) Appropriate location and mounting of electronic equipment

3) Structural design to achieve various degrees of thermal coupling

4) Multilayer aluminized Mylar insulation.

The active components of the system are:

1) Louvers

2) Thermostatically controlled heaters.

Temperature control of the basic spacecraft is achieved by covering the entire outside of the spacecraft with multilayer insulation, except for radiation areas on the equipment panels which are covered by the louver assemblies. This type of system is highly reliable and will provide maximum redundancy.

3.4 LOUVER COMPARISON

3.4.1 Bimetallic Actuated Louvers

3.4.1.1 Description

Mariner, OGO, Pioneer, and Pegasus make use of bimetallic actuated louvers. Figure 3-6 presents an OGO louver assembly panel. Table 3-1 shows a comparison of bimetallic actuated louvers and two-phase, fluid-actuated louvers. The louver shafts are coupled to coiled bimetallic elements (Figure 3-7) which contract or expand in response to temperature. The louver blades are thus rotated from fully closed to fully open over a relatively narrow temperature range. The range of the Pioneer louvers is 40 to 85°F. OGO louvers go from closed to open over a 27°F temperature range.

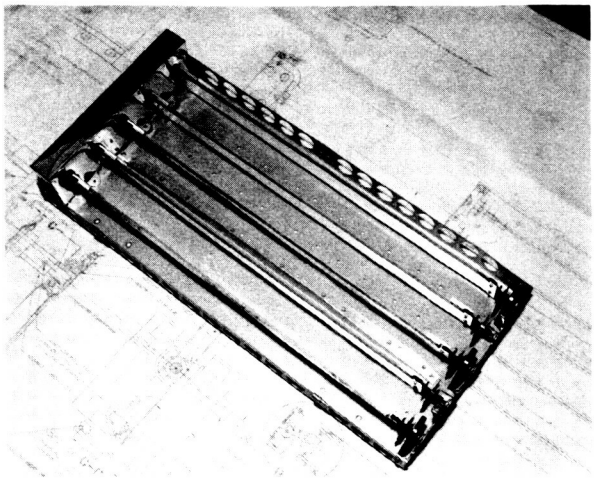

Figure 3-6
PREFERRED LOUVER ASSEMBLY has been space-qualified on the OGO series of scientific satellites and has been in trouble-free operation during more than two years in earth orbit.

Table 3-1. Comparison of Louvers

	Two-Phase Fluid	Bimetallic
Service (at a given temperature change)	Moderate force range at large deflections	Small force at small deflections
Structural effects (launch loads)	Not serious	Critical: Subject to hysteresis and spring unwinding
Louver operation	Gang operation	Individual blade operation
Louver closure	Tight closure seal	Closure sealing difficult
Ground operation	Pressure-compensated bellows functionally independent of ambient pressure	As is
Redundancy technique	Twin actuators	Not possible (adjacent blades assume control)
Failsafe accommodate	Not difficult	Difficult; limited return spring force capability if at all
Space irradiation	May be a problem	None
Development	Moderate: Test experience validates fluid selection, filling procedures, sensor tube location, and bellows design	Moderate: Trial/error design, structural design critical
Potential problem	1. Space irradiation effects	1. Structural degradation from vibration, temperature, and cycling
	2. Filling procedure critical	2. Heat flow to sensor may not be predictable or repeatable

Table 3-1. Comparison of Louvers (Continued)

	Two-Phase Fluid	Bimetallic
	3. Superheat control	3. Failsafe difficult to accommodate
	4. Micrometeoroid puncture/leakage	4. Blade full close heat leak may be excessive
		5. Temperature response slow
Advantages	1. Moderate forces available	1. Simple, compact
	2. GE-MSD past design/ test data	2. Built-in redundancy unless many fail
	3. Redundancy incorporation not difficult	3. Unaffected by irradiation
	4. Fast response to temperature changes	
	5. Failsafe in closed position easy to accomplish	
	6. Tight blade closure	

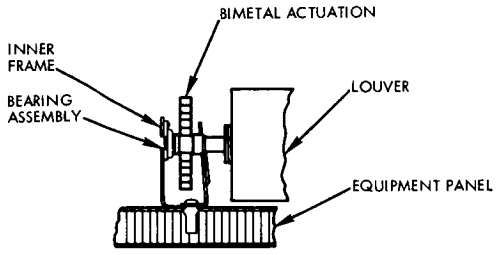

Figure 3-7
SPIRAL BIMETAL ACTUATION

On Mariner, the louvers are fully closed at 55°F and fully open at 85°F. The OGO bimetal spring is highly magnetic (2000 γ at 6 inches), but it can be demagnetized to 42 γ at 6 inches.

The weight of the bimetal is 0.9 pound per square foot. It is flight proven and is highly reliable. Individual blade actuation makes this louver assembly multiredundant. The only disadvantage of a bimetallic actuated louver is that the bimetal provides a very small force for opening or closing the louver. This mechanism develops a torque of about 0.01 inch pound. As a result of this small force, the blade size is limited. The maximum blade width is approximately 2 inches and the maximum blade length is approximately 15 inches. Lubrication requirements for bimetals can be met by use of molybdenum disulfide-impregnated, sintered silver bearings. These bearings are used on both OGO and Pioneer.

3.4.1.2 Application

The OGO type louver shown in Figure 3-6 is proposed for Voyager application. Each louver unit consists of the louver blade, support bearings at each end, plastic end fittings, a bimetallic spring, and stops to limit the fully closed and open positions. The louver blades are lightweight, center-rotating members constructed of two 0.005-inch aluminum sheets spotwelded together along the two edges. The surfaces are bare, highly reflecting and specular. The bimetallic actuators serve dual purposes of sensing the local mounting panel temperature and providing the driving torque necessary to rotate the louver blades. The actuators are placed alternately at opposite ends of the louvers, thereby providing a more even distribution of the sensing elements over the equipment mounting panel. The complete louver system, including all hardware, weighs 0.9 pounds per square foot.

Selection of the bimetal is based on a requirement of the maximum temperature sensitivity and high temperature-torque characteristics consistent with minimum size and weight. The coil has a free length of 38 inches and a torque constant of 0.0016 in-pounds per degree Fahrenheit. A 14°C change in temperature rotates the louvers 90 degrees

from fully closed to fully open. The nominal operating range of the louvers is 17°C to 32°C (63°F to 90°F).

Thermally coupling the bimetal springs to the mounting panel is accomplished by anchoring the fixed end to the panel, oxidizing the bimetal to obtain a high infrared emittance, and insulating the free end from the louver by means of a low thermal conductivity plastic end fitting. In addition, further isolation from the varying external thermal environment is accomplished by means of an insulated housing.

Louver blades rotate in one-eighth-inch inside-diameter sleeve bearings which are housed in a bearing support bracket at each end of the louver assembly. Selection of reliable bearing and shaft materials and lubricants was recognized early as a problem area in the OGO program. A test program was developed and an extensive series of bearing tests was conducted in high vacuum. A series of sintered silver alloys containing various percentages of molybdenum disulfide and molybdenum disulfide and graphite were tested along with two different shaft lubricants and coatings.

The tests were run continuously for periods up to 90 days in a vacuum between 1×10^{-7} and 5×10^{-7} mm Hg. Up to 360,000 cycles were obtained in addition to cycling interrupted by dwell periods of 24 hours and one week. On the basis of these test results, a bearing composed of 80 percent silver and 20 percent molybdenum disulfide sintered material was selected for OGO and appears to be applicable to the Voyager along with a shaft coating consisting of a molybdenum disulfide in a sodium silicate binder. For this combination of materials, the highest starting torques experienced were 0.033 inch-pounds. This corresponds to a temperature increase of the bimetallic actuator of about 1.5°F to overcome worst-case static friction torques.

Tests of bimetallic actuated louver assemblies have been conducted as a part of the OGO and Pioneer program to determine their performance after repeated cycling of the louver position as well as vibration tests to ensure mechanical integrity under anticipated launch conditions. The OGO cycling tests were performed in air with a side assembly

containing 51 louvers by placing it in a cold environment where the louvers were closed and then heating the actuators with heat lamps to drive the louvers open. At the completion of the test, no out-of-tolerance performance or other damage was detected. Vibration tests were run with a smaller 4-louver unit. These initial tests revealed structural weaknesses at the ends of the louvers as well as failure of some of the spot welds. Redesign improved the structural integrity until the development models passed unit mechanical qualification vibration levels. The vibration levels are given below:

Sinusoidal, One Sweep per Axis

5-250 cps	250-400 cps	400-3000 cps
3.5 g rms	6.5 g rms	12 g rms
20-2000 cps	0.1 g^2/cps	12 minutes per axis

Thermal characteristics of the louver system of OGO and Pioneer have been examined experimentally and analytically for selected conditions. The test consisted of an assembly of louvers, whose position could be mechanically controlled, mounted over a radiation panel having a hemispherical infrared emittance of $\epsilon = 0.86$. Electrical power was supplied to heaters mounted to the back of the panel to simulate either uniform or concentrated, non-uniform heat distribution. The backside was insulated to keep the heat losses small; the losses also were evaluated by first running a test with a similar insulated cover in place of the louvers, determining the total heat transfer and then apportioning the loss through the back from the ratio of surface areas. The test was conducted in vacuum with the chamber wall maintained at liquid nitrogen temperature. From these tests it was learned that neither transient temperature lag of the actuators when the panel was suddenly cooled, nor the louvers, nor a concentrated heat source under the actuator housing can cause the temperature of the mounting panel to exceed the acceptable temperature levels. It was also learned that the average actuator temperature was about 4°C colder than the local radiating plate temperature, requiring a correction in the calibration to offset this temperature difference.

The effective surface emissivity of a radiating panel with a surface emissivity $\epsilon = 0.8$ is decreased with the presence of the louvers. A substantial portion of the loss in efficiency is attributed to the thickness of the louver blades, since they occupy 11 percent of the panel area in the open position. Because of the space between the louver blades and the actuator housing and a narrow gap between the louvers themselves, an uncertainty range exists in a region where the louvers are fully closed. When evaluating the louver performance this uncertainty was always included in the analysis by assuming two values, each value conservative for a given situation. Thus, the larger value is taken in the cold condition and smaller in the hot.

3.4.1.3 Reliability

Test data on the similar projects are used in the reliability calculations. Test results are given in Reference 3-7.

In these tests there were 510,000 individual louver cycles with no failures. The mechanism failure rate can be calculated:

$$Q = 1 - R,$$

where

Q = the mechanism failure rate/cycle

R = the mechanism reliability/cycle

Reliability (R) can be calculated:

$$R^n = 1 - \gamma,$$

where

n = the number of test cycles = 510,000

γ = the desired confidence level (50 percent confidence level is used here)

Thus

$$R^n = 1 - \gamma$$

$$R^n = 0.5$$

$$\ln R = \frac{\ln 0.5}{n} = \frac{-0.693}{0.51 \times 10^6} = -1.36 \times 10^{-6}$$

$$R = e^{-1.36 \times 10^{-6}} = e^{-\lambda c}$$

where

λ = failure rate in cycles

c = 1 cycle

Since

$$Q = 1 - R$$

$$Q = 1 - e^{-1.36 \times 10^{-6}} = 1 - e^{-\lambda}$$

but for small exponents $Q = \lambda$

Thus

$$Q = \lambda = 1.36 \times 10^{-6} = 1.4 \times 10^{-6}$$

The failure rate is thus calculated to be 1.4×10^{-6} Failures/cycle.

It is estimated that the louver system will be subjected to 500 operative cycles during the mission. For the purposes of this analysis, it is assumed that the mission phase cyclic louver operation will be proportional to the mission phase duration. Thus the operative cycles assigned for each phase are as follows:

Phase	Operative Louver Cycles
1	0
2	247
3	3
4	42
5	208

Using $\lambda = 1.4 \times 10^{-6}$ failures/cycle and $R = e^{-\lambda c}$ where c = cycles/phase as above, mechanical mission phase reliability is calculated to be

$$R_1 > 0.9^6$$

$$R_2 = 0.9^3 6542$$

$$R_3 = 0.9^5 58$$

$$R_4 = 0.9^4 412$$

$$R_5 = 0.9^3 7088$$

$$R_m = 0.9^3 3$$

System mission phase reliability calculations:

$$R_{s1} > 0.9^6$$

$$R_{s2} = 0.9^4 88$$

$$R_{s3} = 0.9^6$$

$$R_{s4} = 0.9^6$$

$$R_{s5} = 0.9^6$$

$$R_s = 0.9^4 84$$

3.4.2 Two-Phase Fluid Actuated Louvers

3.4.2.1 Description

The Nimbus (Reference 3-8) two-phase, fluid-actuated louvers make use of fluid-filled bellows driving a piston which then actuates the louvers. Figure 3-8 presents a schematic of the Nimbus louver system. The panel surface temperature is sensed by a tube soldered to the panel and containing a liquid-vapor mixture. One end of the tube is sealed; the other end is connected to a bellows actuator with a spring-loaded return. Motion of the bellows actuates the louvers by means of a rack and pinion linkage. As the temperature of the panel rises, the temperature of the liquid also rises and increases the vapor pressure within the tube and bellows. The increase in vapor pressure causes an increase in vapor volume which displaces the bellows by an equivalent volume. The bellows is forced out against the load of the spring return until a balanced position is reached causing the louver to pivot to a new position. The Nimbus louvers are designed to be fully closed at 77°F and fully open at 95°F panel surface temperature.

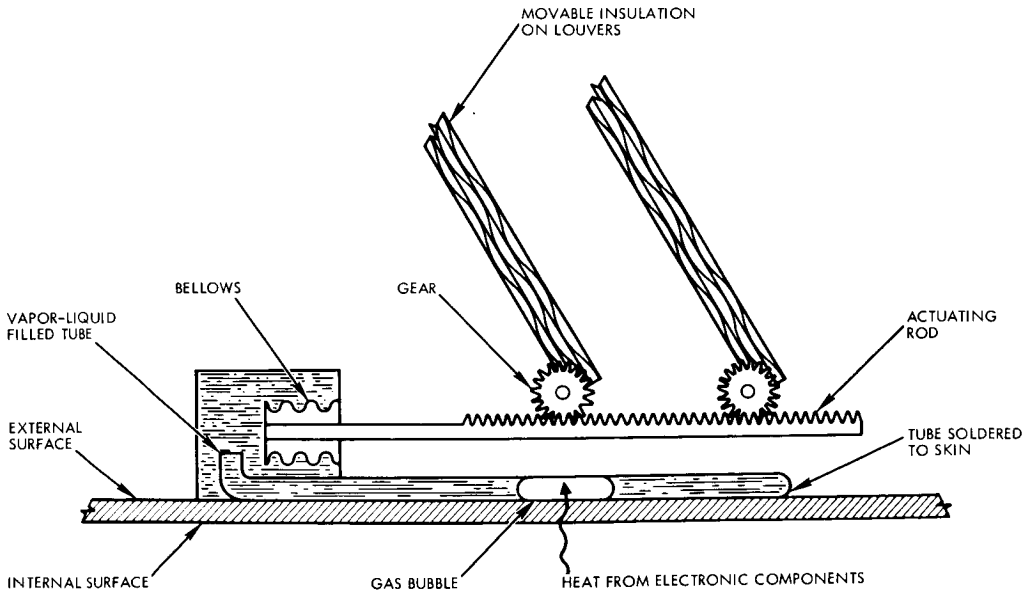

Figure 3-8
NIMBUS LOUVERS ACTUATION

In the event of a failure caused by loss of actuating fluid, a positive fail-safe feature is used by Nimbus to open the shutters to a predetermined angle best suited to maintain operating temperature. In the Voyager application, this would not be desirable because of the long Mars eclipse. Redundancy could be built into the system by using two fluid-filled bellows driving two pistons. Each of the actuators would be sufficient to drive all of the louvers in that assembly so that failure of one actuator could be tolerated with no loss in temperature control performance.

3.4.2.2 Application

A proposed two-phase fluid-actuated louver system (Reference 3-9) for Voyager application is shown in Figure 3-9. This system makes use of two fluid-filled bellows driving two pistons which actuate the louvers. The bellows actuator is of two-phase fluid design which operates under limited vapor superheating. The control fluid is ethyl chloride, and its normal operating pressure ranges from 10.8 psia at $40^{\circ}F$ to 20 psia at $70^{\circ}F$ (saturation conditions). The fluid is contained in a beryllium copper bellows that is silver soldered to the housing and to the piston inner stop. The actuator is a pressure-compensated design in which actuator motion is independent of ambient pressure. This is accomplished by a secondary bellows soldered to the reverse side of the piston face. The space between the housing and the bellows and within the secondary bellows is evacuated.

The louver assembly is shown in Figure 3-9. Each louver is suspended on the in-board face by support adapters from either end and modulates as the individual drive drum rotates. This method of suspension minimizes louver heat leak and maximizes the panel radiating area for a given louver assembly envelope. The use of individual drive drums permits the remaining louvers to operate if a louver fails. The basic drive linkage is an aluminum cross-link bar which runs the height of the panel traveling beneath the column of drive drums. It is joined to the drums by twin beryllium copper tapes connected both for clockwise and counter-clockwise rotation. Two actuators are used per assembly for redundancy. The actuators are offset from the crosslink by individual

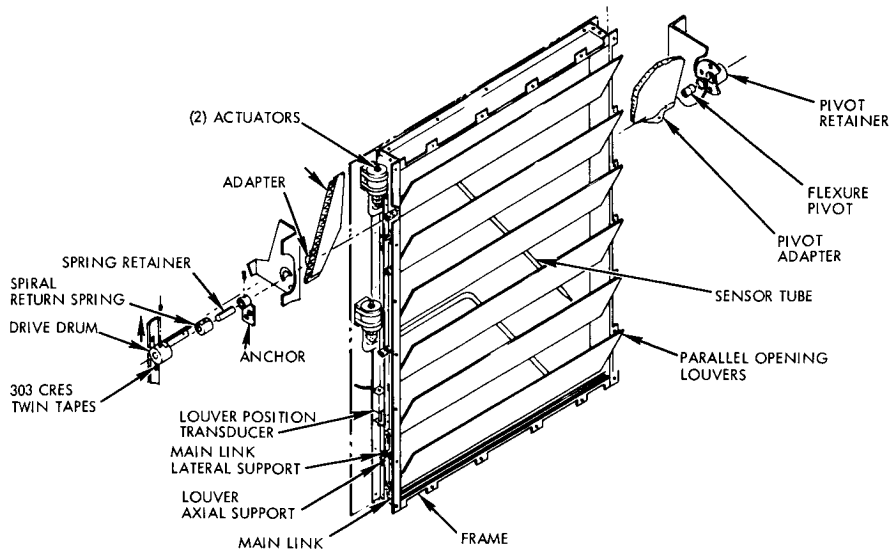

Figure 3-9
PROPOSED TWO-PHASE LOUVER ASSEMBLY

side links which are joined to the actuator piston end through a spherical, seated connector that permits limited angular misalignment between the two. A calibration nut at the connector is provided for temperature bias control or adjustment and, in addition, to permit disassembly of the louver frame without removing the bellows actuator from the thermal control/shear panel.

In order to avoid potential lubrication problems under extreme vacuum-temperature conditions and long-term wear effects, conventional bearings are not employed. Self-lubricating coatings are used for link sliding supports (to limit lateral or axial motion) since material loss under long-term vacuum exposure is not critical there. Flexure pivot bearings have been selected for the louver mounts (at the undriven end) since they do not require lubrication and do not produce static friction or have any significant hysteresis effect. Spiral coil springs, integral with each drive drum, support each louver at the driven end.

The 90-degree flexure pivot has a restraining ring overhang to prevent lateral deflection. The spiral coil spring serves as a restraining force (acting against the actuator force) for positioning the louver in a closed (counter-clock-wise) position. The closed position, therefore, is maintained if the actuator fails.

All materials employed are nonmagnetic. Support bracketry is fiberglas with hard-anodized aluminum fittings. Linkages and lateral supports are anodized aluminum. The actuator housing is nonmagnetic stainless steel, and the bellows material is beryllium copper. Louver material consists of phenolic honeycomb, faced on the external and internal surfaces with aluminum sheets.

Two-phase fluid actuation has been successfully space-flight proven and successfully thermal-vacuum tested in conjunction with the Nimbus program. The system characteristics are compared to bimetallic actuated louvers in Table 3-1.

3.4.2.3 Reliability

Test data on similar projects are used in the reliability calculations. Test results are given in Reference 3-10. The reliability formulas for the mechanism and the system are the same as in Section 3.4.1.3

Calculation results are:

$$R_1 = 0.9^4 64$$

$$R_2 = 0.9^3 475$$

$$R_3 = 0.9^5 1$$

$$R_4 = 0.9^4 13$$

$$R_5 = 0.9^3 564'$$

$$R_m = 0.9^2 8907$$

$$R_{s1} = 0.9^6$$

$$R_{s2} = 0.9^5 7$$

$$R_{s3} = 0.9^6$$

$$R_{s4} = 0.9^5 8$$

$$R_{s5} = 0.9^5 7$$

$$R_s = 0.9^4 8$$

3.5 INSULATION DESIGN PARAMETERS

3.5.1 Introduction and Summary

The purpose of this study is to select the preferred insulation and to establish design and fabrication parameters.

The temperature control subsystem for Voyager is based on the insulated enclosure concept (Section 3.3). Voyager requires insulation that operates under steady-state vacuum with a thermal conductance of 0.001 Btu/hr-ft^2-$^\circ$F when the interior and exterior layers of the insulation are +85 and -315°F, respectively.

Various insulations were investigated. The lowest thermal conductances for each type and their associated weights are tabulated in Table 3-2. Only multilayer insulations meet the requirements. It generally consists of a series of separated, highly reflective, opaque, radiation shields.

Table 3-2. Comparison of Various Types of Insulation

Insulation	Thermal Conductance (Btu-in/hr-ft^2-$^\circ$F)	Weight (lb/ft^2)
Foam plastics	0.141	0.167
Glass fiber	0.012	0.306
Powders	0.0036	0.584
Multilayer	0.00045	0.13

In determining design parameters a number of insulations were considered (i.e., Dimplar, crinkled aluminized Mylar, aluminized Mylar with separators). For Voyager, crinkled aluminized Mylar is preferred. It has an optimum layer density of 70 layers/inch and an optimum aluminum deposit thickness of 500 angstroms. The blankets are 1 inch thick and consist of 70 layers of 1/4 mil crinkled aluminized Mylar with a 3 mil aluminized Mylar face sheet on each side. They are large, covering one side of the spacecraft, and flat. Velcro tape is the preferred method of attachment since it allows the insulation to be removed without damage.

However, some additional attachment is required to sustain the insulation during boost (Section 3.5.2). The blankets are perforated to prevent ballooning during launch and to provide access for the decontamination gases.

Fabrication requires extreme care in handling, assembly and installation. Details of the fabrication parameters are presented in Section 3.5.3.

3.5.2 Design Parameters for Multilayer Insulation

The basic design parameters are: required thermal characteristics, weight, and compatibility with the natural and induced environment for the Voyager spacecraft. Table 3-3 presents a summary of the design parameters.

Table 3-3. Summary, Design Parameters

Parameter	Effect on Ideal* Thermal Conductance	Cost
A. Induced Environment		
1. Decontamination		
a) Decontamination gas (ethylene oxide) at 122°F	No effect on conductance	
1) 3 cycles		
2) 6 cycles		
b) Decontamination gas (ethylene oxide), 35 to 50 percent relative humidity, 122°F		
1) Gas and water vapor pre-mixed – adequate gas circulation	Water condensate removes aluminum deposit; if have good gas circulation, will minimize condensation and consequently negligible conductance degradation	Costlier than if no gas circulation
b.1.1 3 cycles		
b.1.2 6 cycles		
2) Gas and water vapor pre-mixed – insufficient gas circulation	Will significantly increase thermal conductance	
b.2.1 3 cycles		
b.2.2 6 cycles		
c) Decontamination gas (ethylene oxide) at 250°F	Will affect the structural integrity of the Mylar and thus may degrade conductance	
1) 3 cycles		
2) 6 cycles		
d) Effect of condensation	Will remove aluminum deposit from Mylar film; degrade design conductance	
2. Blanket depressurization	May cause tearing of blanket if blankets are insufficiently vented; therefore, degrade conductance; also conductance will increase if have trapped gas within blanket	
3. Air conditioning 40 to 60°F	If have good circulation, will not affect conductance	

*Ideal thermal conductance does not incorporate effects of insulation design and mission parameters

Table 3-3. Summary, Design Parameters (Continued)

Parameter	Effect on Ideal* Thermal Conductance	Cost
4. Blanket vibration, 5 g maximum	No effect on conductance if have good adhesion of aluminum deposit to Mylar film	
5. Blanket quasistatic acceleration and steady acceleration	May increase conductance only during period of application; increase is a 20 percent maximum	
6. Blanket boost acceleration	May cause detachment of blanket from Velcro tape; degrade conductance severely; may require Dacron thread and button attachments in addition to Velcro.	
7. Blanket acoustic excitation	No effect on conductance for Mylar film greater than 1/4 mil	
8. Shock load on blanket	No effect on conductance	
9. Aerodynamic heating during boost	Shroud takes the load; therefore, no conductance degradation	
10. Engine firing - plume and hot engine	Must expose only to insulated engine; if so, no increase in conductance	
11. Dry nitrogen purge	No effect if purge gas velocity is 50 ft/min or less	
12. Dry air environment	No effect on conductance	
B. Natural Environment		
1. Micrometeoroid impingement	Will increase conductance 10 percent maximum	
2. Ambient air 40 to 90°F	If relatively dry then no effect	
3. Proton bombardment	No significant effect on conductance	
4. Earth albedo and emission	No significant effect on conductance	
5. Mars albedo and emission	No effect	
6. Asteroids and solar particles	Will degrade insulation conductance similar to micrometeoroids	
7. Ultraviolet exposure	Will increase exterior face sheet surface absorptivity; no effect on conductance	
8. Environment temperature variation and extremes	-400°F will make Mylar stiff; exposure to +250°F and then cool down will cause Mylar shrinkage; however, there is no significant increase in design conductance. Changes in boundary temperatures will alter thermal conductance values.	

*Ideal thermal conductance does not incorporate effects of insulation design and mission parameters

3.5.2.1 Preferred Insulation Selection

The following multilayer insulation constructions were investigated:

1. Metal-coated Mylar
2. Aluminized fiberglas
3. Aluminized Teflon
4. Aluminum foil
5. Metal-coated Kapton (H-film)
6. Metal-coated dimpled Mylar
7. Uncoated Mylar film.

A metallic coating, usually gold or aluminum because of their low emissivity, applied to one surface of each sheet of Mylar or Kapton provides sufficient insulating capability. Aluminum oxidizes: the thin layer does not appreciably affect the thermal properties of the insulation as it is transparent to IR radiation. There is no significant oxidation of the gold.

In selecting insulation, the compatibility with the natural and induced environments of Voyager must be examined. During decontamination of the spacecraft, the insulation is subjected to ETO gas. Mylar 65 H.S. Dupont becomes brittle (Reference 3-11) when exposed. Teflon reacts with the freon in the gas. Kapton reacts with ETO. These materials are unsuitable. All of the materials are compatible with the temperature extremes experienced by Voyager. Aluminum-foil insulation is undesirable because it is sensitive to the acoustic excitation loads (Reference 3-12) and it is difficult to fabricate and handle.

Both aluminized fiberglas and aluminized teflon are heavy compared to Mylar or Kapton. Aluminum foil or aluminized Mylar can be used with separators. Typical separators (i.e., net or posts) are fiberglas, nylon, dacron, glass and paper. These are heavier than crinkled metal-coated Mylar or Kapton.

Dimplar blankets are composed of 1/4 mil (minimum thickness) reflector sheets separated by 1/2 mil (minimum thickness) dimpled sheets. The dimpled sheets are generally aluminized on both faces in order to obtain low thermal conductance. This makes Dimplar considerably heavier than crinkled Mylar.

Elimination of the spacers between aluminized Mylar sheets results in maximum point contact thermal conductance between the sheets. This negates the resistance capability of the insulation to radiant heat transfer between inner and outer sheets. This type of multilayer insulation is not acceptable.

Flat or crinkled, uncoated Mylar film is eliminated as an insulation candidate because the emissivity of Mylar does not provide sufficient thermal resistance to heat leakage by radiation through the insulation.

Based on preliminary comparisons, the following multilayer insulations were selected for further investigation:

- Crinkled gold-coated Mylar
- Crinkled aluminized Mylar
- Aluminum foil with glass separators
- Aluminized Mylar with paper, dacron net, or dexiglass separators
- Dimplar.

The preferred insulation is the insulation with the required thermal conductance and lowest weight. The required conductance is based on the Voyager application where the insulation is required to have its maximum performance. This condition occurs during Mars eclipse. The thermal conductivity (0.001 Btu/hr-ft^2-$^\circ$F) is based on an interior insulation temperature of +85°F and exterior insulation layer temperature of -315°F. For lower temperature differentials across the insulation or for higher levels of insulation temperatures, the thermal conductance will be increased.

Thermal conductance and associated weight of 1-inch-thick multilayer insulations are presented in Figures 3-10 through 3-15.

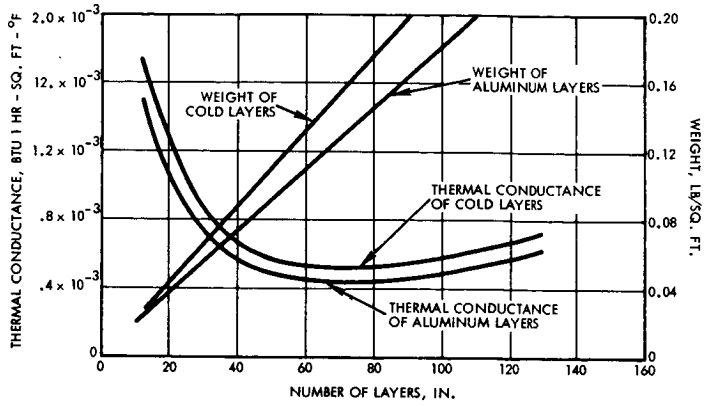

CONDITIONS:
1) IDEAL THERMAL CONDUCTANCE: EFFECTS OF FABRICATION, ATTACHMENT AND MISSION PARAMETERS NOT INCLUDED
2) 1/4 MIL MYLAR, ALUMINIZED ONE SIDE
3) HOT BOUNDARY TEMPERATURE: 85°F
4) COLD BOUNDARY TEMPERATURE: -315°F
5) STEADY STATE VACUUM
6) 1 INCH THICK INSULATION BLANKET

Figure 3-10
CRINKLED MYLAR INSULATION - Thermal conductance and weight.

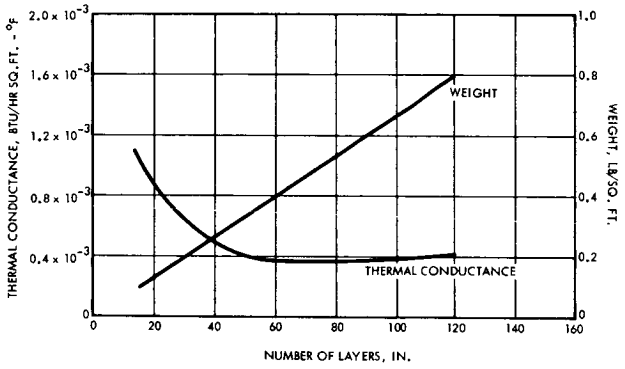

CONDITIONS:
1) IDEAL THERMAL CONDUCTANCE: EFFECTS OF FABRICATION, ATTACHMENT AND MISSION PARAMETERS NOT INCLUDED
2) 1/4 MIL FLAT ALUMINUM SHEETS
3) HOT SIDE TEMPERATURE: 85°F
4) COLD SIDE TEMPERATURE: -315°F
5) STEADY STATE VACUUM
6) 1 INCH THICK INSULATION BLANKET

Figure 3-11
ALUMINUM FOIL WITH FIBERGLAS SPACER - Thermal conductance and weight.

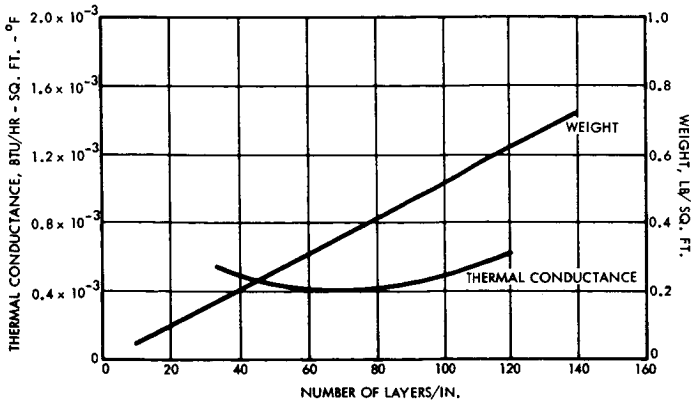

CONDITIONS:
1) IDEAL THERMAL CONDUCTANCE: EFFECTS OF FABRICATION, ATTACHMENT AND MISSION PARAMETERS NOT INCLUDED
2) 1/4 MIL FLAT MYLAR SHEETS, ALUMINIZED ONE SIDE
3) HOT BOUNDARY TEMPERATURE:85°F
4) COLD BOUNDARY TEMPERATURE:-315°F
5) STEADY STATE VACUUM
6) 1 INCH THICK INSULATION BLANKET

Figure 3-12
ALUMINIZED MYLAR WITH PAPER SPACERS - Thermal conductance and weight.

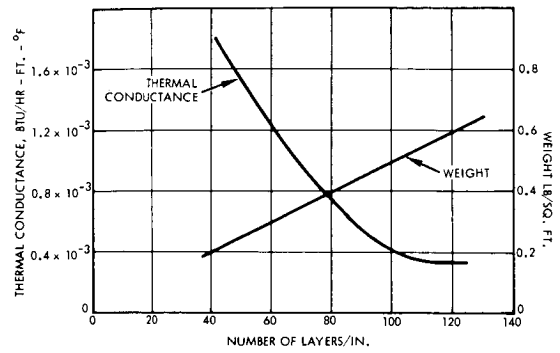

CONDITIONS:
1) IDEAL THERMAL CONDUCTANCE: EFFECTS OF FABRICATION, ATTACHMENT AND MISSION PARAMETERS NOT INCLUDED
2) 1/4 MIL FLAT MYLAR LAYERS, ALUMINIZED ONE SIDE
3) HOT SIDE TEMPERATURE:85°F
4) COLD SIDE TEMPERATURE:-315°F
5) STEADY STATE VACUUM
6) 1 INCH THICK BLANKET INSULATION

Figure 3-13
ALUMINIZED MYLAR WITH DACRON NET SPACERS - Thermal conductance and weight.

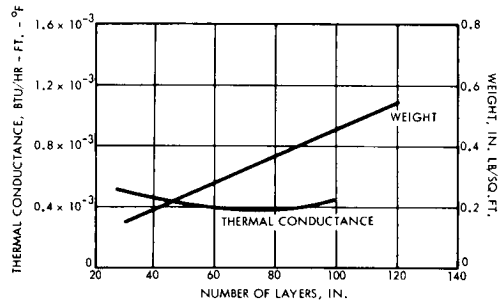

CONDITIONS:
1) IDEAL THERMAL CONDUCTANCE: EFFECTS OF FABRICATION, ATTACHMENT AND MISSION PARAMETERS NOT INCLUDED
2) 1/4 MIL FLAT MYLAR LAYERS ALUMINIZED ON BOTH SIDES
3) HOT BOUNDARY TEMPERATURE: 85°F
4) COLD BOUNDARY TEMPERATURE:-315°F
5) STEADY STATE VACUUM
6) 1 INCH THICK INSULATION BLANKET

Figure 3-14
ALUMINIZED MYLAR WITH DEXIGLAS SPACERS - Thermal conductance and weight.

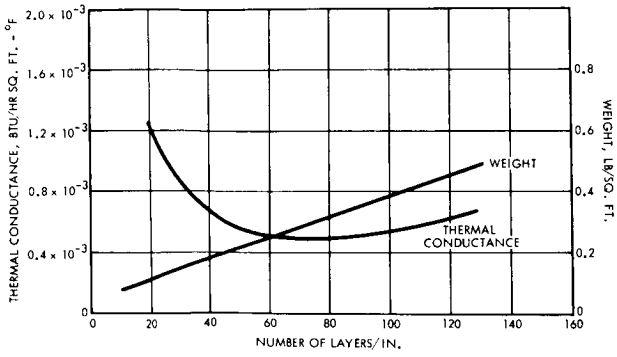

CONDITIONS:
1) IDEAL THERMAL CONDUCTANCE: EFFECTS OF FABRICATION, ATTACHMENT AND MISSION PARAMETERS NOT INCLUDED
2) 1/2 MIL FLAT MYLAR DEFLECTORS AND 1/2 MIL MYLAR DIMPLED SPACERS ALUMINIZED ONE SIDE
3) HOT BOUNDARY TEMPERATURE: 85°F
4) COLD BOUNDARY TEMPERATURE:-315°F
5) STEADY STATE VACUUM
6) 1 INCH THICK INSULATED BLANKET

Figure 3-15
DIMPLAR - Thermal conductance and weight.

These thermal conductance curves are best-fit curves obtained from TRW tests and references 3-12, 3-13, and 3-14. A comparison of the curves in the figures indicates that crinkled aluminized Mylar gives the best thermal conductance for minimum weight. Table 3-4 presents a comparison of the seven insulations for a thermal conductance of 0.0052 Btu/in./hr-ft^2-^{o}F. Crinkled aluminized Mylar requires 45 layers/inch and weighs 0.084 lb/ft^2. It weighs 45 percent less than the next best insulation (crinkled gold-coated Mylar).

Table 3-4. Comparison of Multilayer Insulation

Thermal Conductance 0.0052 Btu-in./hr-ft^2-^{o}F	Layers/Inch	Weight (lb/ft^2)
Crinkled aluminized Mylar	45	0.084
Crinkled gold-coated Mylar	70	0.154
Aluminum foil and glass	38	0.25
Aluminized Mylar and paper	35	0.18
Aluminized Mylar and dacron net	91	0.45
Mylar aluminized two sides and dexiglass	40	0.19
Dimplar	55	0.23

In addition, TRW experience with aluminized Mylar indicates that it is more desirable. Aluminized Mylar is easier and less expensive to fabricate. Gold adheres poorly to Mylar film. As indicated in Figure 3-10, gold-coated crinkled Mylar has a thermal conductance 12 percent higher than aluminum at the optimum layer density. Although aluminum has a higher emissivity than gold by a factor of 1.3, the thermal conductivity of gold exceeds that of aluminum by a greater factor. The higher lateral heat leakage becomes more significant than the increased thermal radiation resistance, and the result is an increased overall thermal conductance for the gold-coated Mylar. Gold-coated Mylar was considered as an alternative candidate

only because there was concern that water condensation during ETO decontamination might cause removal of aluminum deposit from its Mylar film. TRW tests (Reference 3-15) indicate that aluminized Mylar is not sensitive to humidity in the range required for decontamination.

The crinkled aluminized Mylar has a maximum insulating capability for a specified weight. Based on the thermal conductances and weight comparison, crinkled multilayer insulation is the insulation for Voyager preferred by TRW.

3.5.2.2 Crinkled Aluminized Mylar

The crinkled aluminized Mylar consists of a number of 1/4 mil Mylar sheets, aluminized on one side, crinkled, either mechanically or by hand, and sandwiched between 3-mil one side aluminized Mylar face sheets.

Crinkling acts as a separator and minimizes contact area. From Figure 3-10, the optimum layer density for crinkled aluminized Mylar is 70 layers/inch. At higher layer densities, contact conductance between sheets increases and thus provides shorts to the thermal radiation insulating capability of the individual layers. This explains the rise in thermal conductance (Figure 3-10) for layer densities higher than 70 layers/inch. A comparison of the thermal energy transferred by conduction and radiation through a typical multilayer insulation is indicated in Figure 3-16. For 70 layers/inch or less the radiation predominates, and above 70 layers/inch conduction is the primary heat transfer mode.

Thermal conductance as a function of various insulation temperatures is presented in Figure 3-17 for 70 layers of 1/4 mil aluminized crinkled Mylar. Analysis to date indicates that during near-earth steady-state conditions, the insulation on the base of the spacecraft reaches temperatures of 246 and 90°F (Volume 3, Section 5) on exterior and interior surfaces, respectively. For this condition (Figure 3-17) the thermal conductance is 0.007 Btu/hr-ft^2-°F. This provides the desired temperature control (as presented in Volume 3, Section 5) of the spacecraft for this phase of the Voyager mission.

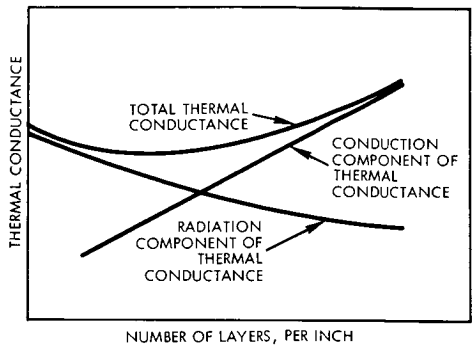

Figure 3-16
MULTILAYER INSULATION - Thermal radiation and conduction, typical.

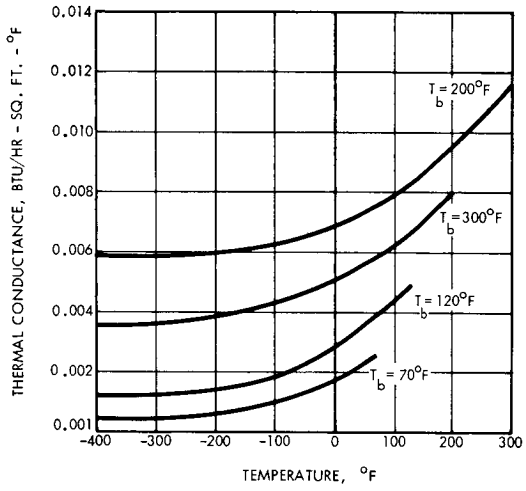

CONDITIONS:
1) IDEAL THERMAL CONDUCTANCE: EFFECTS OF FABRICATION, ATTACHMENT AND MISSION PARAMETERS NOT INCLUDED
2) 1/4 MIL MYLAR, ALUMINIZED ONE SIDE
3) STEADY STATE VACUUM
4) 1 INCH THICK BLANKET INSULATION
5) 70 LAYERS/INCH

Figure 3-17
CRINKLED ALUMINIZED MYLAR - Thermal conductance for various interior and exterior surface temperatures.

The insulation is designed to vent trapped gas during launch in accordance with depressurization schedules for Voyager (Figure 3-18). The increase in thermal conductance for various interstitial gas pressures is illustrated in Figure 3-19. To reduce the time lag in reaching the final value of thermal conductance after boost, the insulation includes vent holes.

Before the layers of insulation are formed into blankets, they are perforated to provide venting during launch and to allow decontamination gases to penetrate the insulation. An analysis of the venting requirements indicates that 1/8-inch-diameter perforations at 6-inch centers satisfy the design requirements. Each blanket layer is perforated separately, and the hole patterns are staggered when the blanket is layed up.

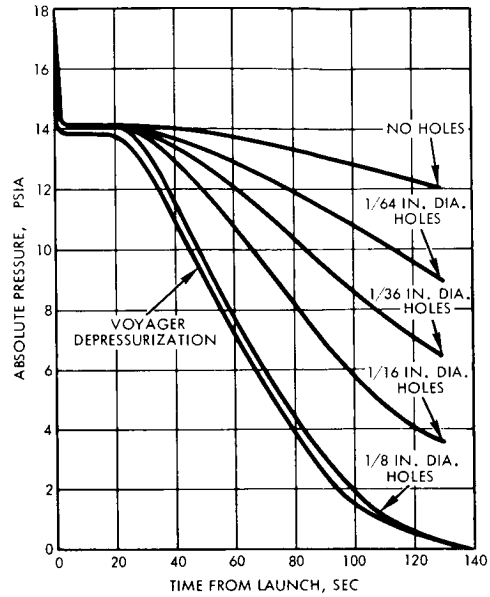

CONDITIONS:

1) PERFORATIONS ON 6 INCH CENTERS.
2) HOLES ARE STAGGERED.
3) 1 INCH THICK, 70 LAYERS/INCH
4) AVERAGE TEMPERATURE: 70°F.

Figure 3-18
DEPRESSURIZATION OF INSULATION BLANKETS WITH VARIOUS SIZE VENT HOLES.

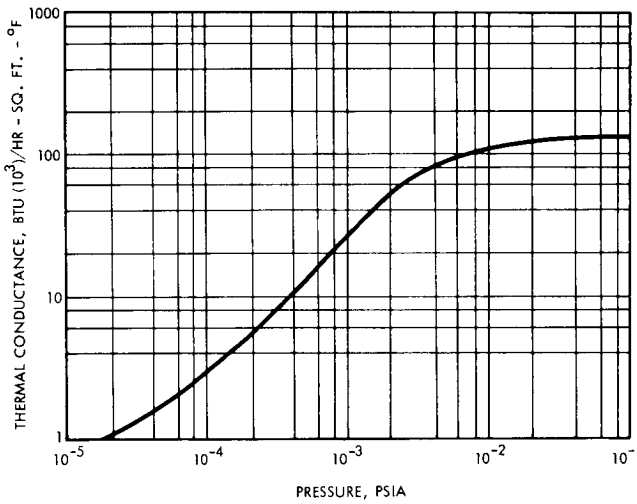

CONDITIONS:

1) IDEAL THERMAL CONDUCTANCE: EFFECTS OF FABRICATION, ATTACHMENT AND MISSION PARAMETERS NOT INCLUDED
2) 1/4 MIL FLAT MYLAR LAYERS ALUMINIZED ON ONE SIDE
3) STEADY STATE VACUUM
4) 1 INCH THICK INSULATION BLANKET
5) 70 LAYERS 1 INCH
6) HOT BOUNDARY TEMPERATURE:85°F
7) COLD BOUNDARY TEMPERATURE:-315°F

Figure 3-19
CRINKLED ALUMINIZED MYLAR - Thermal conductance vs. interstitial gas pressure.

After the sheets are perforated, the blankets are layed up and the sheets of blanket are fastened together at the edges by tape caps and ultrasonic welds (see Section 3.5.2.5). The blanket layers are so arranged that the aluminum side faces the spacecraft. This provides exposure of the warm interior to a low-emissivity surface. The welding

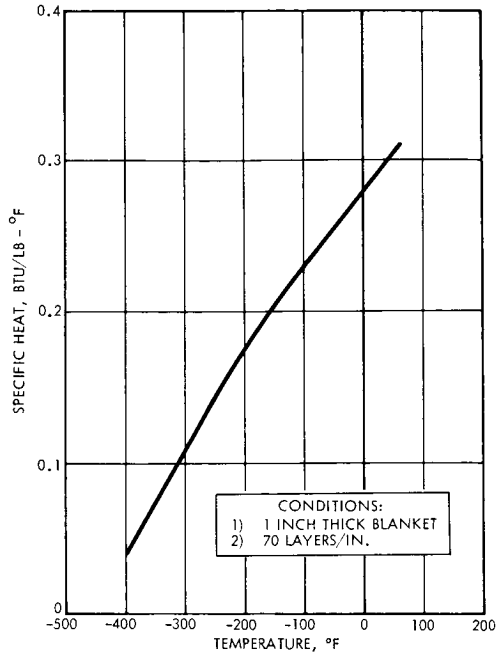

Figure 3-20
CRINKLED ALUMINIZED MYLAR - Specific heat vs temperature.

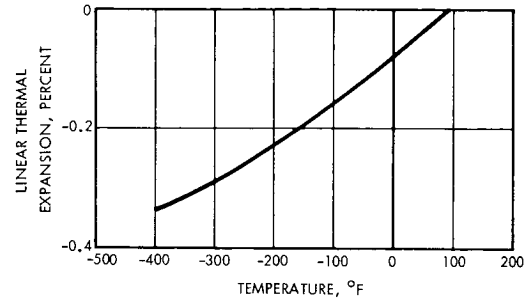

Figure 3-21
LINEAR THERMAL EXPANSION

provides good contact between layers in point-sized areas only. The tape caps help to contain the 70 layers within the desired 1-inch thickness. The additional conductance path provided by the tape caps between the face sheets does not significantly degrade blanket performance. Ultrasonic welding fuses the Mylar sheets locally, but the effect on blanket performance is not significant.

Figure 3-20 indicates the variation of the specific heat of crinkled aluminized Mylar with temperature. The specific heat of crinkled aluminized Mylar does not differ significantly from that of other multilyaer insulation. Linear thermal expansion or contraction of aluminized Mylar is shown in Figure 3-21. No significant thermal expansion or contraction will occur in the blanket layer over the operating temperature range.

The thermal conductance curve for aluminized crinkled Mylar represents ideal conditions and therefore does not incorporate such effects as attachment, packing, and handling that exist during the Voyager application. A typical thermal conductance curve that includes these effects is presented in Figure 3-22. For 70 layer/inch Mylar, thermal conductance is increased more than 100 percent. This is considered a typical degradation for multilayer radiation shields applied to an actual spacecraft. The curve indicates that, even with this

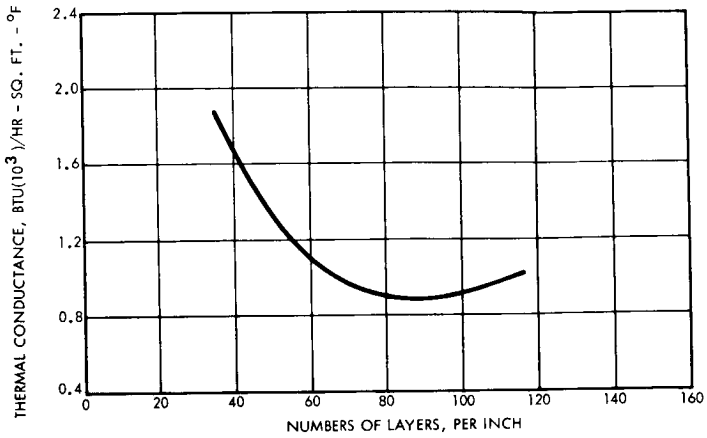

Figure 3-22
CRINKLED ALUMINIZED MYLAR - Thermal conductance with velcro tape attachment.

degradation, the 70 layer/inch design satisfies the requirement for a thermal conductance of 0.001 Btu/hr-ft^2-^{o}F.

It is felt that a 1-inch-thick layer aluminized Mylar blanket with a density of 70 layers per inch is a conservative selection. If thermal analysis and tests indicate that a higher thermal conductance than 0.001 Btu/hr-ft^2-^{o}F is allowed, then blanket thickness can be reduced accordingly to save weight.

3.5.2.3 Methods of Attachment

The ground rules for selecting an attachment method are that it be simple and removable. Degradation of thermal performance should be minimized. Table 3-5 presents a summary of attachment parameters.

Attachment methods (References 3-11, 3-16 and 3-17) which are commonly used are:

a) Permanent type attachments

- Welding
- Bonding with epoxy cement.

b) Attachments where limited access is required include:

- 3M 830 tape
- EE 6600 tape

Table 3-5. Summary of Attachment Parameters

Parameter	Effect on Ideal* Thermal Conductance	Cost	Availability of Equipment, Tools, and Materials	Insulation Weight
Insulation Blanket Attachment				
1. At structure corners or bends interleafing	Will minimize degradation of design conductance due to edge or seam loss	Very costly		May save some insulation weight because of no closeouts
a) Interleafing distance				
2. Design adjacent insulation blankets such	Will minimize conductance degradation because closeout in blanket form reduces loss through gap and the whole seam	Not costly	Strips available	Will add to insulation weight
a) Two adjacent design size blankets				
b) Staggered smaller size blankets whose total thickness equals design size	Will minimize bending at corners; therefore, less degradation of design conductance	Costly because have to work with a large quantity of blankets		
c) Size of blanket strip	A minimum 4-inch-wide strip will be optimum from weight-conductance standpoint			
3. Overlap adjacent blankets at corner bend				
a) Two adjacent blankets	Will degrade conductance because of bending of thick blankets at corner; will have compression load			
b) Staggered smaller size blankets whose total thickness equals design size	Will preserve design conductance because compression loading at corners is reduced	Very costly, have to work with large quantity of blankets		
4. Velcro tape spacing	12-inch spacing will minimize attachment heat loss and will maintain structural integrity in dynamic environment. Conductance degradation is 5 percent maximum	Tape is not costly	Tape is available	Will add to overall insulation weight
5. Velcro tape size	0.6 x 3 inches, 0.15 inch thick, is sufficient size and will not degrade conductance significantly			
6. Allowance for struts or cabling protruding through insulation				
a) Cutout for strut only	Will degrade design conductance significantly			
b) Cutout for strut or cable and wrap multilayer insulation around strut or cable	Improved conductance but will still have gap loss	More costly than a)		Adds to insulation weight

*Ideal thermal conductance does not incorporate insulation design and mission parameters

Table 3-5. Summary of Attachment Parameters (Continued)

Parameter	Effect on Ideal* Thermal Conductance	Cost	Availability of Equipment, Tools, and Materials	Insulation Weight
c) Cutout for strut or cable and wrap multilayer insulation around strut or cable; then additional insulation to cover small gap between blanket insulation and strut or cable	Will preserve design conductance	More costly than b)		Adds to insulation weight more than situation b)
d) 3M 850 tape for penetration insulation attachment	Will not provide significant heat shorts; has favorable removal force requirement	Not costly		Will not add significant weight
e) EE 6600 tape for penetration insulation attachment	Will not provide significant heat shorts; has unfavorable removal force requirement	Not costly	Available	Will not add significantly to overall weight
f) Epoxy	Will not provide significant heat shorts; has unfavorable removal force requirement	Not costly	Available	Will not add significantly to overall weight
g) Repeated blanket removals for access	Usually must destroy special penetration insulation; will have to reconstruct to maintain design conductance	Will be costly		
7. Gaps or uncovered discontinuities in insulation	Avoid this; if exists, then use closeout strips	Closeout strips will add to cost	Strips are available	Strips will add to overall insulation weight
8. Blanket packing during attachment				
a) Pack a specified amount in areas close to attachment	Packing here is unfavorable; will degrade conductance; degradation in conductance is 35 percent maximum			
b) Pack a specified amount in areas far removed from attachment point	Minimize packing in these areas to prevent additional conductance degradation			
9. Degradation of face sheet aluminum film by Velcro tape in area of attachment because of repeated blanket removals	Will have localized degradation on face sheet only; therefore insignificant effect on overall insulation conductance			
10. Allowance for vehicle deployment	Deployment mechanism located exterior to blanket; no allowance required; no conductance degradation			

*Ideal thermal conductance does not incorporate insulation design and mission parameters

- Silver tape
- Mechanical stitching
- Mechanical stapling
- Nylon stud with buttons
- Dacron rod and button
- Glass or dacron fiber threads and buttons.

c) Attachments, where repeated access is required, include:

- Piano hinge (developed at TRW)
- Metallic snaps
- American Velcro tape.

TRW has employed many of these materials and techniques in spacecraft applications and has developed a piano hinge which can be used for joining adjacent blankets. This is formed by overlapping the face sheets, cutting flaps in the overlapped area, and wrapping the flaps around a thin, solid Mylar rod. The rod is taped to the spacecraft at numerous points. The Mylar rod and tape provide a significant increase in thermal conductance.

Ultrasonic welding can be used in fabrication of the blanket and also to attach the blanket to the spacecraft. If the blanket is welded to the spacecraft, it is naturally damaged by removal. Epoxy bonding is another possible attachment method but it is also permanent. For this reason, neither of these methods is feasible for the Voyager application.

Aluminized tape such as 3M 850 or EE 6600 provides a simple, light-weight method of attachment. The tapes, once applied, adhere to both the insulation and the spacecraft surface through a wide range of temperatures. However, if the tapes are allowed to remain attached for over 24 hours, it is very difficult to remove them. Removal in most cases would result in damage to the insulation blanket.

Mechanical stitching or stapling requires a special machine and is limited to areas where access is readily available. In this concept, the blanket would be stapled or stitched directly to the spacecraft.

Use of a nylon rod with a button on the end provides a firm attachment. However, the heat leak through the rod would significantly degrade the overall thermal performance of the insulation. Glass or dacron thread has often been used with buttons to attach insulation blankets. The system consists of passing the thread through the insulation blanket and securing a button on the outside of the insulation. The heat leak is greatly reduced by using the thread instead of the nylon rod. This procedure, however, does not provide for easy removal of the insulation blankets.

Metallic snaps and Velcro tape are simple designs and do not appreciably increase thermal conductance. Both of these fastening techniques provide contact only between the innermost blanket layer and the structure. Metallic snaps tend to tear crinkled Mylar blankets, however, during removal of the blankets.

Velcro tape consists of two mating sections. One section consists of a thin nap attached to a backing tape which can be applied to a surface by activating the mastic on the tape with a solvent. The mating section is composed of many small plastic filaments so formed as to make hooks. These hooks are set in a backing material similar to the backing for the nap. The hooks attach to the nap by pressing the mating sections together. Separation is not attained unless a force of 0.5 pounds/inch is applied in shear as well as in tension. Two disadvantages of Velcro tape should be noted. One, it has a density of 0.191 pound/foot which is relatively heavier than other attachment materials. Two, it tends to cause removal of the metal coat on the Mylar film in the local area of the attachment if tape contact is on the metal side. In spite of these minor liabilities, however, Velcro tape is selected as the preferred attachment for Voyager.

3.5.2.4 Insulation Closeouts

The multilayer blankets must be joined to minimize heat leak at the corners of the spacecraft. Three closeout procedures are presented.

- Blanket Overlap - Two Blankets. Two blankets are overlapped at a corner or bend as indicated in Figure 3-23. Overlap distance is set at a 2-inch minimum. The advantage in this attachment is that it permits maximum edge venting during depressurization. Fewer layer perforations are required. Bending of the blankets, however, causes significant blanket compression and degradation of thermal performance.

- Blanket Overlap - Staggered Buildup. Several thinner blankets are stacked 1 inch thick and overlapped at the corner or bend as shown in Figure 3-24. No specific overlap distance is set. The advantage of this attachment is that the compression effect is minimized. The disadvantages are: minimal edge venting and increased number of blankets.

- Two Blankets and a Blanket Strip. Two blankets are attached as close to each other as possible at a corner and a 1-inch-thick strip of 2-inch minimum width is attached over the two blankets to form the corner (Figure 3-25). The advantages are: no bending of the blankets, simplicity, and no degradation of thermal performance. Disadvantages are: impaired edge venting and increase in number of components (closeout strips).

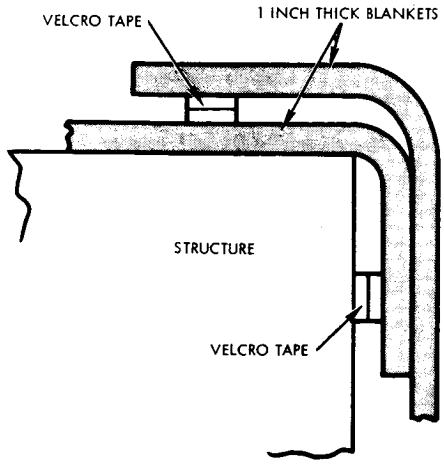

Figure 3-23
INSULATION CORNER CLOSEOUT - Overlapped blankets

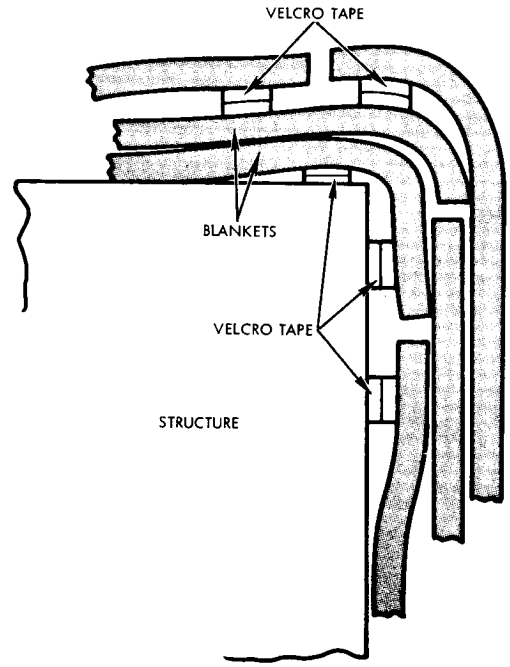

Figure 3-24
INSULATION CORNER CLOSEOUT - Staggered blankets

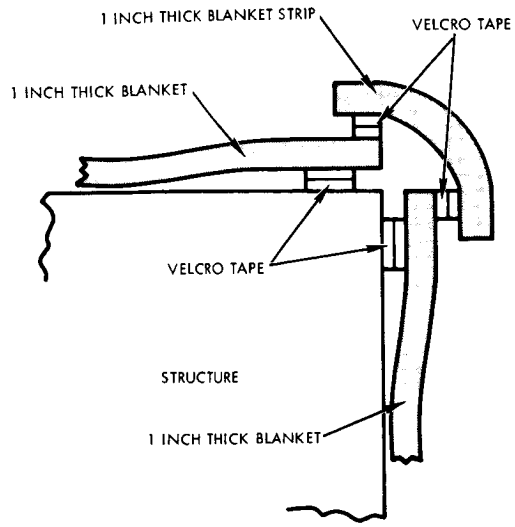

Figure 3-25
INSULATION CORNER CLOSEOUT - Closeout strips

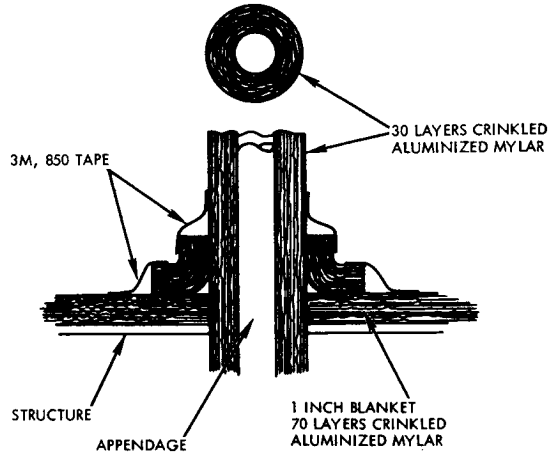

Figure 3-26
APPENDAGE INSULATION.

The last of these three techniques is selected as the preferred attachment procedure for Voyager insulation. This procedure satisfies the design requirements of minimum heat leaks at blanket joints as well as design simplicity.

Thermal coupling by conduction from the spacecraft interior through a strut or cable and subsequent radiation to the cold space environment negates the effectiveness of the Voyager insulation. Essentially, a bare strut or cable acts as a radiating fin. Therefore, insulation is provided at each strut or cable protruding from the spacecraft through the 1-inch insulation blanket. A design for such a penetration is shown in Figure 3-26.

3.5.2.5 Application to Recommended Spacecraft

The preferred insulation design as applied to the recommended spacecraft is indicated in Figures 3-27 and 3-28. Multilayer crinkled aluminized Mylar blankets are attached to the spacecraft exterior surfaces covering the sides, top, and bottom. One blanket is provided for each side. It covers from the top of the equipment module to the bottom of the propulsion module. Cutouts are to be provided for louvers, appendages, and the engine nozzle assembly. In addition, the insulation

A. INSULATION ATTACHED TO TOP AND SIDE SURFACES

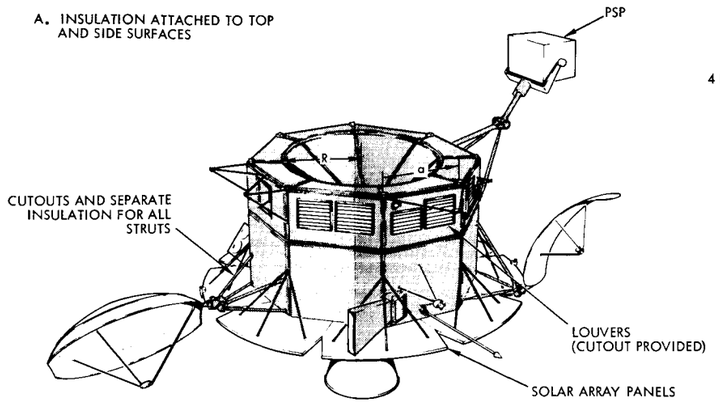

B. INSULATION ATTACHED TO BOTTOM SURFACE

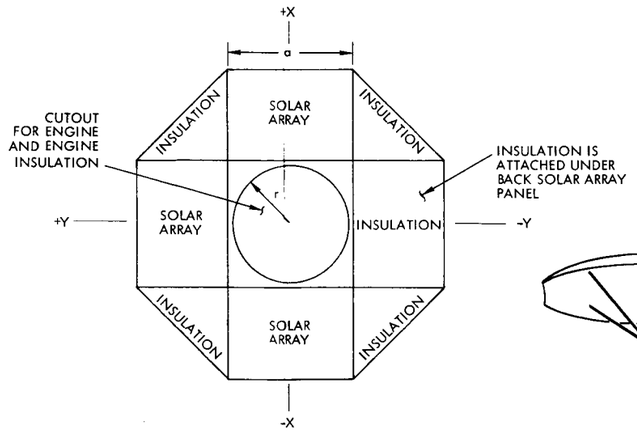

C. INSULATION ATTACHED TO SIDES (TOP VIEW)

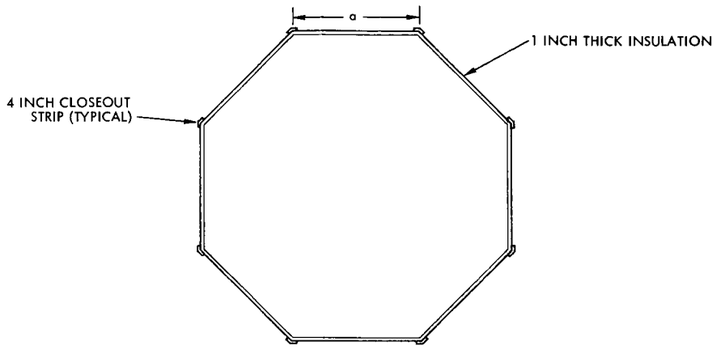

D. INSULATION ATTACHED TO SIDES (COMPLETE VIEW)

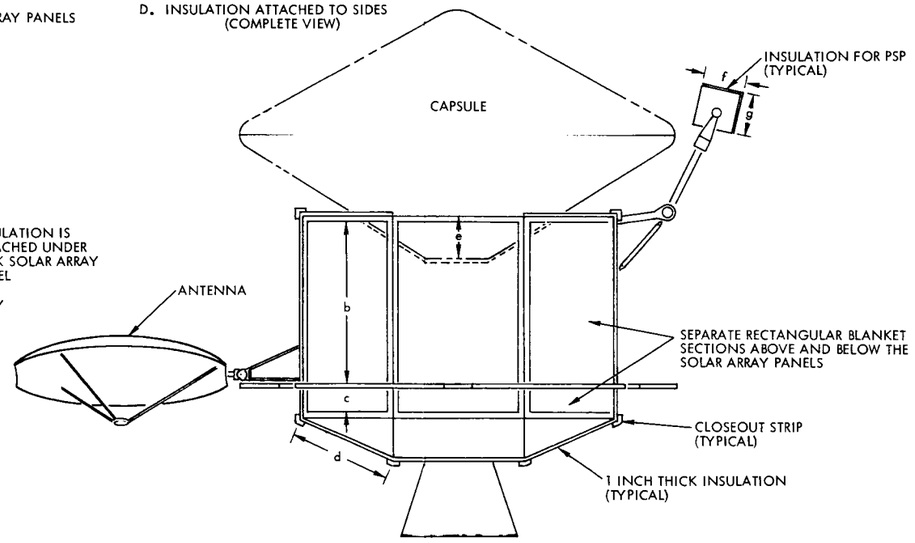

Figure 3-27
INSULATION DESIGN

1) THE INSULATION IS APPLIED TO THE RECOMMENDED CONFIGURATION
2) THERE ARE 8 SPACECRAFT SIDES. SEPARATE BLANKETS ARE REQUIRED FOR EACH SIDE
3) A TOTAL OF 8 BLANKET SECTIONS WILL BE REQUIRED TO INSULATE THE SIDES

A. BLANKET SECTIONS COVERING AREAS FROM SPACECRAFT TOP PLANE TO SOLAR ARRAY PLANE - 8 REQUIRED

BASE
b = DISTANCE FROM TOP PLANE TO SOLAR ARRAY
Δ= DISTANCE FROM SOLAR ARRAY TO BASE

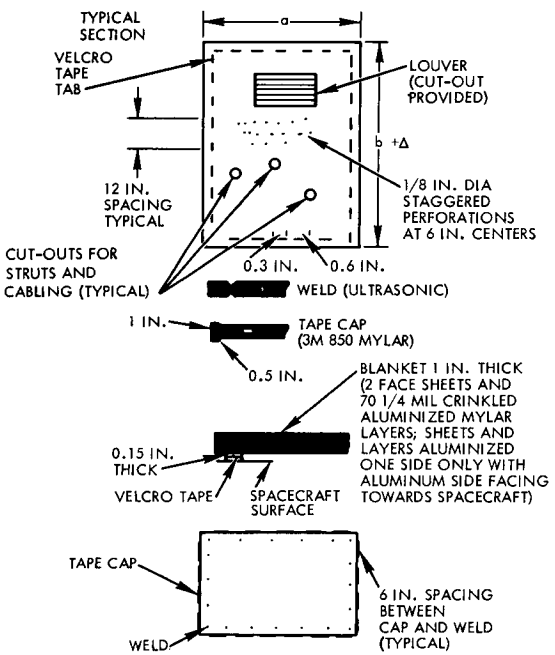

B. BLANKET SECTIONS COVERING SPACECRAFT BOTTOM SURFACE - 2 REQUIRED

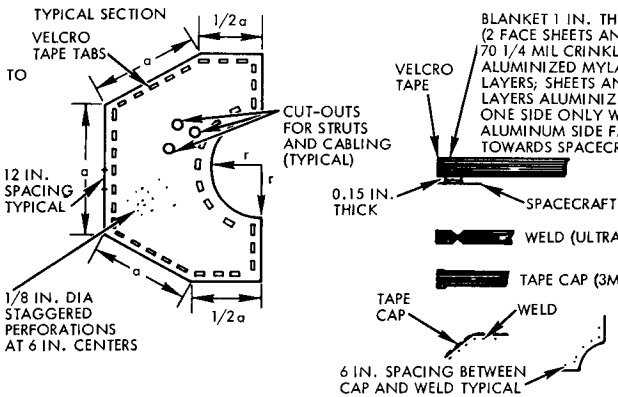

C. BLANKET SECTIONS COVERING SPACECRAFT TOP FLAT SURFACES - 2 REQUIRED

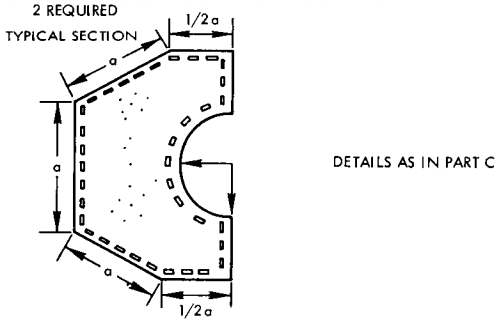

D. BLANKET SECTIONS COVERING SPACECRAFT TOP CURVED SURFACES - 2 REQUIRED

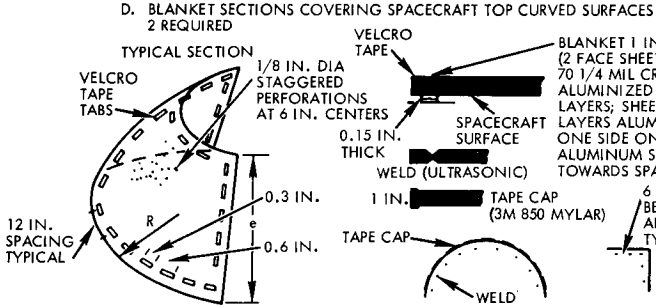

E BLANKET SECTION COVERING SPACECRAFT TOP FLAT DISC AREA - 1 REQUIRED

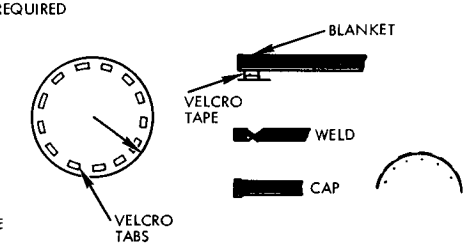

F. BLANKET SECTIONS FOR THE PSP - 3 REQUIRED

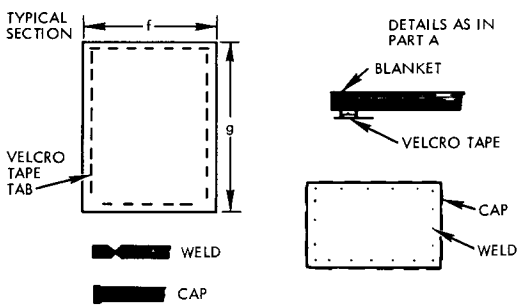

G. CLOSE OUT STRIPS - REQUIRED TO COVER GAP BETWEEN ANY BLANKET SECTION PAIR

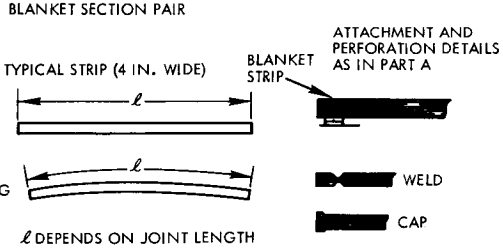

I. SEPARATE INSULATION LAYERS TO BE PROVIDED FOR PROTRUDING STRUTS AND CABLING AS REQUIRED

Figure 3-28
MULTILAYER BLANKET - Details for recommended configuration.

design must accommodate protruding struts that support exterior equipment, solar array support structure, and cabling. With the present design, at least 40 struts are used to support exterior equipment and 23 support struts as associated with the solar array. Also, a conical insulation contour is used on the top where the capsule is inserted. In addition to the main spacecraft insulation, at least six multilayer insulation blankets will be required for the interior of the planetary scan platform. The proposed blankets and their typical sizes and contours are presented in Figures 3-27 and 3-28.

The design procedure for insulating struts or cables is that a cutout in the main blanket is allowed for the strut or cable. Thirty crinkled metallized Mylar layers are interleaved around the cable or strut. 3M 850 tape, which provides a strong tape bond but is removable, is used for attachment. This insulation scheme must be reconstructed around each protrusion after each removal. It has been shown in thermal tests that thermal performance with this protrusion insulation is not significantly different from that for a blanket with no protrusions.

Damage caused by micrometeoroids of high kinetic energy can reduce the effectiveness of crinkled aluminized Mylar insulation. The damage to the crinkled aluminized Mylar blankets will be as extensive for other multilayer radiation shields. The insulation is generally punctured or torn at particle impact. A laboratory simulation of micrometeoroid bombardment was conducted at TRW utilizing the 2-million-volt Van de Graaff accelerator. Particles were charged by electronic techniques for measurement of particle velocity and mass. It was determined that two percent of an exposed surface would be damaged by micrometeoroid impact per year, assuming a density of 8 gms/cc. It is estimated that a blanket thermal conductance degradation not in excess of 10 percent would result. If it is found in later development tests that the damage is more extensive, then the blankets will have to be attached behind a micrometeoroid bumper. A micrometeoroid would sublime after impact with the bumper. The insulation would be attached at sufficient distances from the bumper so that the vaporized

debris would lose sufficient momentum by expansion to cause insignificant damage to the insulation. If a bumper is required, then care must be taken that the bumper does not reduce insulation effectiveness.

Voyager insulation will be subjected to accelerations as high as 5.6 g at SI-C stage burnout. Since the insulation is a lightweight type, the inertial load produced by an acceleration of 5.6 g represents a mild environment for the insulation blanket and the Velcro attachments. Therefore, the crinkled Mylar insulation blanket will maintain its structural integrity during quasi-static acceleration. Also, the insulation will not be damaged by constant accelerations of 20 g maximum for 5 minutes. However, the insulation thermal conductance increases during acceleration periods. This effect is indicated in Figure 3-29. The degradation in thermal conductance at a 16 g axial acceleration is 25 percent. This is explained by the fact that acceleration changes tend to cause compacting of some of the insulation blankets.

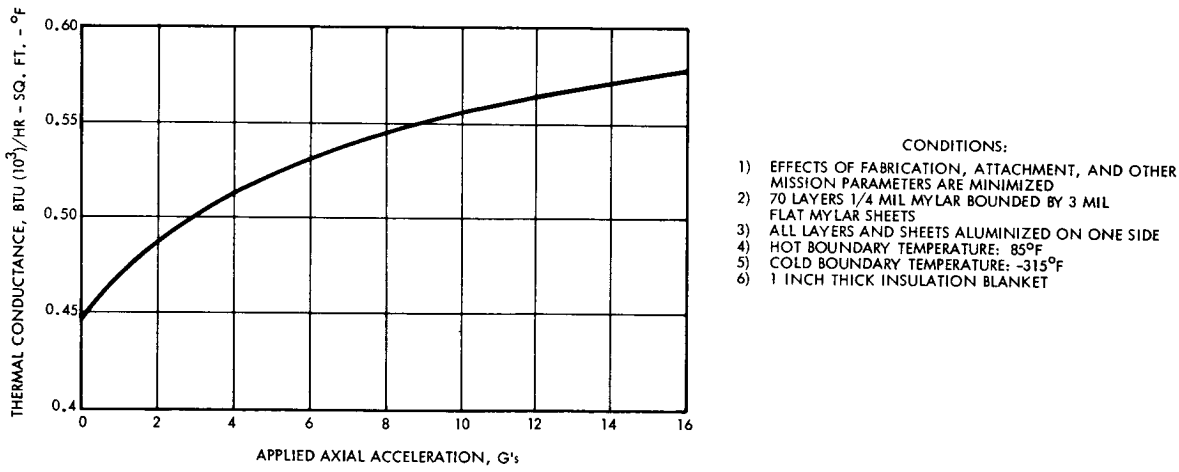

Figure 3-29
EFFECT OF ACCELERATION LOADING ON THERMAL CONDUCTANCE - Aluminized Mylar.

The crinkled aluminized Mylar blanket is not affected by vibration loads at 150 Hz, 3 g amplitude maximum. Acoustic excitation at 155 db maximum for 3 minutes does not damage a crinkled aluminized Mylar blanket as long as there is good adhesion between the aluminum deposit and its Mylar film. It has been noted that acoustic excitation damages an aluminized Mylar sheet less than 1/4 mil thick. However, the

blanket is provided with 3 mil aluminized Mylar face sheets and thus no problems are anticipated. For the expected vibration and acoustic loading, a theoretical analysis of these effects on insulation blanket thermal conductance is difficult to conduct.

Shock loading will be imposed on the insulation during fairing removal and spacecraft separation. These loads occur at very high frequencies where an insulation of the multilayer type does not respond. Therefore, no damage to the crinkled aluminized Mylar blanket is expected.

Crinkled aluminized Mylar insulation is sensitive to aerodynamic heating during the boost phase, because the maximum operating temperature of Mylar is 300°F. Shielding of the insulation is provided by the fairing which is subjected to aerodynamic heating load.

Aluminized Mylar cannot maintain its structural integrity if heat inputs from the hot engine and plume result in blanket temperatures in excess of +300°F. The area of particular concern is the aft end of the spacecraft. Therefore, the engine nozzle is provided with high-temperature insulation consisting of blankets of alternate layers of aluminum foil and fiberglas paper. Analysis of the effects of engine firing in combination with solar loading indicate that, with the present insulation, the aluminized Mylar insulation blankets will not exceed 250°F. Application and subsequent decrease of such a temperature level will result in some shrinkage of the Mylar film.

Exposure of aluminized Mylar to ambient air for extended periods will cause oxidation of the aluminum deposit. Tests indicate that even for oxygen concentration as high as 2.55 percent by volume, the resultant increase in emissivity is negligible.

Proton bombardment, in densities of 10^{16} protons/cm^2 blanket will cause insignificant damage. The solar absorptivity of the aluminum will be increased five percent upon direct exposure.

Ultraviolet exposure of the aluminum side of the insulation layer will cause an increase of solar absorptivity from 0.24 to 0.32 after

1000 hours of exposure. Only the outer layer is affected, and thus overall insulation thermal conductance is not altered significantly.

The analysis indicated that the insulation maximum and minimum temperatures for the Voyager mission will be +250 and -300°F, respectively. The insulation is designed to operate between such temperature extremes as -400 to +300°F. At the lower extreme the Mylar becomes slightly stiff, but structural integrity is not impaired. As low temperatures are attained, contraction differences between the aluminum deposit and Mylar substrate are not significant.

The selection of insulation design and attachment as well as effects of insulation design parameters must be substantiated by additional development tests. In assessing effects of parameters it must be noted that the thermal conductance in a crinkled aluminized Mylar insulation blanket is highly anisotropic. This is illustrated in Figure 3-30 where it shows that large temperature differences exist for lateral points on the individual layers. Therefore, the thermal conductance is based on average insulation boundary temperatures, and differences between average and maximum or between average and minimum should be noted.

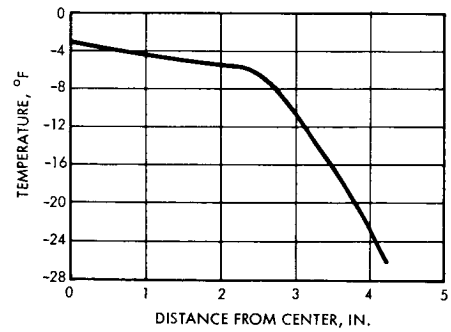

5TH LAYER OF A 14 LAYER BLANKET
AVERAGE HOT BOUNDRY TEMPERATURE : 30°F
AVERAGE COLD BOUNDARY TEMPERATURE : -45°F

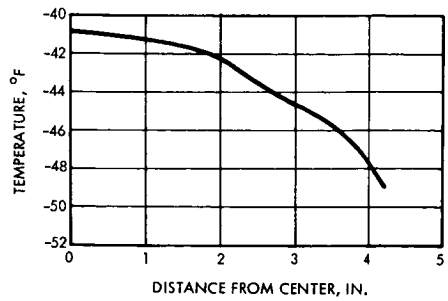

EXTERIOR LAYER OF A 14 LAYER BLANKET
AVERAGE HOT BOUNDARY TEMPERATURE : 30°F
AVERAGE COLD BOUNDARY TEMPERATURE : -45°F

Figure 3-30
LATERAL TEMPERATURE GRADIENTS - Crinkled aluminized Mylar.

3.5.3 Fabrication Parameters

The basic fabrication parameters for the insulation are quality of materials, handling procedure, and fabrication techniques required. Table 3-6 presents a summary of the fabrication parameters.

3.5.3.1 Materials

The aluminized Mylar is obtained per TRW Specification MT 3-14A. Strict quality control is specified at the start of sheet fabrication and aluminum deposition. Deep scratching of the aluminized Mylar films that form a blanket generally results in an increase in overall aluminum emissivity and consequent increase in thermal conductance. However, it has been found that minute scratches in the metal coating tend to increase lateral resistance to heat transfer by conduction. This decreases thermal conduction through the aluminum deposit between layer contact points. Furthermore, resistance measurement of an aluminized Mylar sheet with such minute scratches indicates that the resistance increases significantly as compared with an identical sheet without the minute scratches. Further evaluation of this phenomenon is warranted.

The effect of aluminum deposit thickness on layer lateral thermal conductance is presented in Figure 3-31, and its effect on aluminum emissivity is indicated in Figure 3-32. Applying a thick deposit to the Mylar film offers low emissivity and decreases thermal conductance. However, the thick aluminum deposit provides greater lateral thermal conductance and consequently increases overall thermal conductance. A thin aluminum coat on the Mylar film gives high aluminum emissivity, which tends to increase overall thermal conductance; but the thicker aluminum coat decreases lateral thermal conductance which results in reduction of the insulation thermal conductance. It is concluded that the optimum aluminum deposit thickness is 500 angstroms.

For a 500-angstrom aluminum deposit on a 1/4 mil Mylar film, the dominant control of lateral thermal conductance resides in the aluminum deposit by a factor of 3 to 1. This is explained by the fact that, although there is considerable cross-sectional area of Mylar,

Table 3-6. Summary, Fabrication Parameters

Parameter	Effect on Ideal* Thermal Conductance	Cost	Availability of Equipment, Tools, and Materials	Insulation Weight
A. Layer Fabrication	Conductance can increase significantly because of lack of control	Less cost than for insulation manufactured at TRW	Vendor has required equipment	No close tolerances on weight as compared to TRW manufactured insulation
1. Roll handling in shipping process	Increases conductance			
2. Scratches on sheets as received	Deep scratches on aluminum side increases conductances			
3. Fingerprints on sheets as received	If cleaned, then effect is minimum			
4. Oxidation of aluminum deposit	Tests indicate negligible increase in conductance			
5. Aluminum deposit thickness	If not controlled at 500A, can increase conductance			
6. Impurities on sheets	If not removed, can increase conductance			
7. Mylar film thickness	Should be 1/4 mil; if greater will increase conductance; if smaller, will fail in dynamic environment			If greater than 1/4 mil, adds to insulation weight
8. Sheets aluminized on one side	Will provide Voyager insulation design requirements			
9. Sheets aluminized on both sides	Not necessary for design requirements, may increase conductance because of greater aluminum thickness			Adds to insulation weight
10. Mechanical abrasion	Aluminum film may detach			
11. Quality of aluminum deposit	It should be pure and specular; otherwise conductance will be increased			

*Ideal thermal conductance does not incorporate insulation design and mission parameters

Table 3-6. Summary, Fabrication Parameters (Continued)

Parameter	Effect on Ideal* Thermal Conductance	Cost	Availability of Equipment, Tools, and Materials	Insulation Weight
12. Uncoated Mylar	Will increase conductance 1500 percent as compared to aluminized Mylar			
13. Adhesion of aluminum deposit to Mylar film	This is critical. Good adhesion gives the desired thermal conductance. Poor adhesion will result in as much as 1500 percent conductance degradation as for uncoated Mylar			
B. Insulation Blanket Construction		Minimum cost if performed at TRW	Tools and equipment are available	No effect on insulation weight
1. Lamination process	Exact cutting process; no effect on conductance		Tools and equipment are available	
2. Use of plastic gloves	Will minimize adhesion of impurities to the blanket and guard against abrasions; will maintain design thermal conductance	Not costly	Readily available	
3. Use of nylon gloves	Not effective as plastic gloves; increases conductance	Not costly	Readily available	
4. Hand wrinkling of the sheets	No assurance of repeatable pattern; cannot assess thermal conductance	Less costly than mechanical	No equipment required	
5. Mechanical wrinkling of the sheets	Repeatable pattern control, repeatable performance; good control of thermal conductance	Costlier than hand wrinkling	Must acquire the machine	
6. One large blanket for attachment on a surface	Not practical and will result in compressive loads at bends and curves; increases thermal conductance significantly	Less costly than separate blanket		Saves some weight since does not need overlaps at joints, nor closeout strips

*Ideal thermal conductance does not incorporate insulation design and mission parameters

Table 3-6. Summary, Fabrication Parameters (Continued)

Parameter	Effect on Ideal* Thermal Conductance	Cost	Availability of Equipment, Tools, and Materials	Insulation Weight
7. Size of face sheets	3 mil face sheets give rigidity with minimum degradation of thermal conductance. Greater size face sheets will degrade thermal conductance			Face sheets greater than 3 mil thick contribute significantly to insulation weight because of requirement of large size blankets
8. Wrinkled sheet aluminum side facing inward	Normal practice, in combination with face sheet aluminum facing inwards, provides low emissivity surface exposure to generally warm spacecraft components			
9. Skin acids	Will increase thermal conductance; avoid by using plastic gloves			
10. Face sheets aluminized both sides	Normally not done in practice; will not improve design conductance significantly	Costlier than for single surface aluminum		Adds to insulation weight
11. Face sheet aluminized one side	Normal design practice; will give design thermal conductance	Less costly than two-side aluminum deposit		
12. Ultrasonic welding – weld spacing	Commonly used to form blankets from layers; will not increase conductance significantly if point welding 12-inch spacing used		Weld tools available	Does not add to insulation weight
13. Ultrasonic welding and end tape caps – weld and tape spacing	End tape caps required to prevent blanket layers from slipping out partially; 3M 850 tape used for this; it will not significantly increase conductance	Not costly	3M 850 tape readily available	Does not increase insulation weight significantly
14. End tape caps only – tape spacing	Not enough to maintain all blanket layers together; will increase thermal conductance because of excessive number of caps	Less costly than ultrasonic weld	Readily available	Will increase weight as compared to ultrasonic weld

*Ideal thermal conductance does not incorporate insulation design and mission parameters

Table 3-6. Summary, Fabrication Parameters (Continued)

Parameter	Effect on Ideal* Thermal Conductance	Cost	Availability of Equipment, Tools, and Materials	Insulation Weight
15. Packing the wrinkled sheets to form required thickness	Will unavoidably increase conductance but when slight force is removed will regain most of insulation effectiveness			
16. Compression loading on the blanket edges in welding and end cap installation process	Should be minimized; will significantly increase conductance			
17. Construction of the blanket directly on the spacecraft - custom construction	Will minimize edge loss; minimum degradation of design conductance due to seam loss	Extremely costly and time consuming	Available	Save some insulation weight
18. Allowance for blanket venting				
a) Edge venting only	Increase conductance because of trapped interstitial gas; also blanket may billow and balloon and consequently tear			
b) Edge venting plus perforations – size of perforations	Will preserve design conductance because of absence of trapped gas; will degrade conductance 5 percent maximum	Costlier than if no perforations	Must acquire machine to do perforations	Save some insulation weight because of holes
19. Blanket movement	This usually means blanket handling and therefore increase in conductance			
20. Blanket storage				
a) Clean room atmosphere	Maintains design conductance especially if have Class 100, 000	Costlier than nonclean room	Clean room facilities available	
b) Nonclean room atmosphere	Degrades conductance because of impurities			
c) Special storage bags	Will maintain design conductance	Must buy bags	Available	
21. Blanket impurities	Will degrade design conductance			
22. Blanket handling	Will significantly degrade design conductance			

*Ideal thermal conductance does not incorporate insulation design and mission parameters

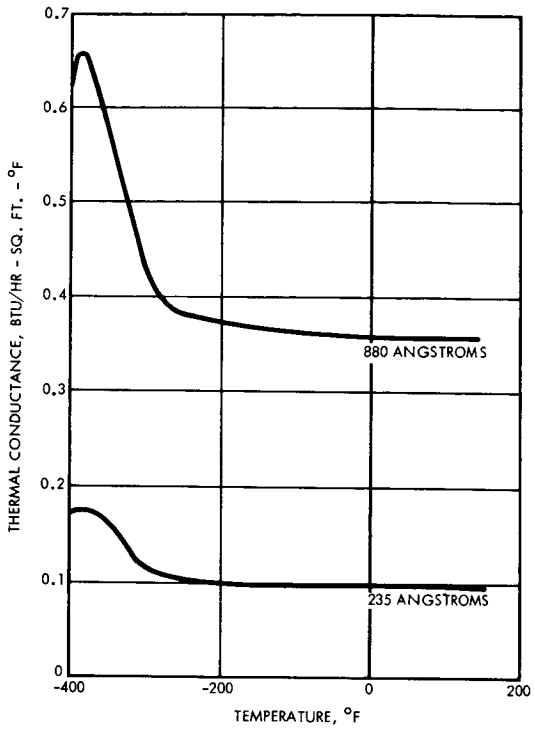

CONDITIONS:
1) IDEAL THERMAL CONDUCTANCE: EFFECTS OF FABRICATION, ATTACHMENT AND MISSION PARAMETERS NOT INCLUDED
2) 1/4 MIL MYLAR, ALUMINIZED ONE SIDE
3) STEADY STATE VACUUM
4) 70 LAYERS/INCH
5) 1 INCH BLANKET

Figure 3-31
LATERAL THERMAL CONDUCTANCE - Aluminized Mylar Vs. aluminum coating thickness and average insulation temperature.

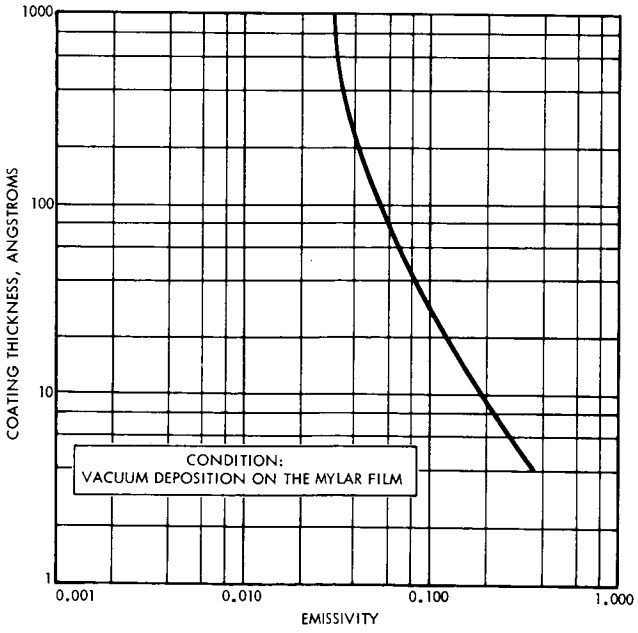

Figure 3-32
EMISSIVITY OF ALUMINUM COAT VS. COATING THICKNESS

the thermal conductivity of the aluminum exceeds that of the Mylar by a greater factor. Aluminum thickness deviations have a significant effect on insulation thermal conductance. This thickness can be checked directly during aluminum deposition since a 500 angstrom thickness provides a direct current electrical resistance of 2 ohms per square through the aluminum. The measurement cannot be made after the material is crinkled because crinkling causes mechanical interruption of the coating with corresponding indeterminate changes in electrical resistance.

The quality of the aluminum deposit on Mylar film must be carefully controlled from the time deposition takes place. First, it is required that aluminum deposit on the base film be 99.99 percent pure. The insulation should be observed at frequent intervals to ensure that the deposit appears visually uniform, has a bright silver color, and is free of yellow discoloration when viewed in white reflected light in such a manner as to preclude environmental influences. Just before crinkling, a film check by special lights should be made to ensure that the aluminum side is a bright, specular surface. After crinkling is completed, the surface condition of the coating is difficult to appraise and impossible to measure with present techniques. Development of new methods is required to assess the insulation in its final form.

Adhesion of the aluminum deposit to its Mylar substrate is an important parameter. Poor adhesion can result in significant loss of aluminum with a consequent increase in thermal radiation energy transfer between insulation interior and exterior. A 250 3M tape test is performed to check adhesion and consists of applying the tape to a 4-inch square of coated surface and removing the tape in one quick motion. Visual inspection of the tape and tested area is made to note any evidence of coating removal. Adhesion failure on 5 percent of the entire surface or small points of poor adhesion distributed widely over the sample should be cause for rejection.

3.5.3.2 Fabrication Techniques

Once the sheets are available the blankets are constructed by a lamination process. This procedure requires exact cutting and the use of specialized hand tools and templates. This layup technique prevents compacting of layers and inclusion of contaminants. Blankets will be cleaned in vacuum prior to installation and plastic gloves are to be worn at all times to reduce contamination by skin acids and other contaminants. Blankets will be stored in clear plastic bags to minimize effects of environment and handling.

Packing of the insulation or otherwise applying a compressive load to the blanket results in a significant degradation of thermal conductance because of increased solid conduction through interlayer contacts. The quantitative effect is indicated in Figure 3-33 (Reference 3-17) in terms of thermal conductance and heat flux ratio. The greatest increase in thermal conductance occurs during the initial load application. Further increases in load result in smaller changes in insulation effectiveness. Figure 3-33 indicates that thermal conductance varies directly with the load taken to the two-thirds power. The closeouts between blankets greatly affect thermal performance. Increased heat flux, as a result of overlapping blanket layers at a joint, is shown in Figure 3-34 (Reference 3-18). The results are specifically for 30 layers of Dimplar interleaved at a joint on a cryogenic tank. The curves indicate that, for a 2-inch overlap, the increased heat flux or increase in thermal conductance is 25 percent. This increase is due to edge effects. Edges of inner layers are exposed to the environment or to cold layers in adjacent blankets. With the proposed attachment scheme of two blankets, separated by a minute gap and covered by a multilayer blanket strip, it is felt that degradation will be considerably less than 25 percent. The closeout in combination with the blankets provides a total of 140 blanket layers, two inches thick at the closeout. The effect of blanket compaction is minimized in this method. It is not dependent on the fabrication procedure. Care should be taken in attaching the blanket to the spacecraft and the closeout to the blankets to minimize the compaction.

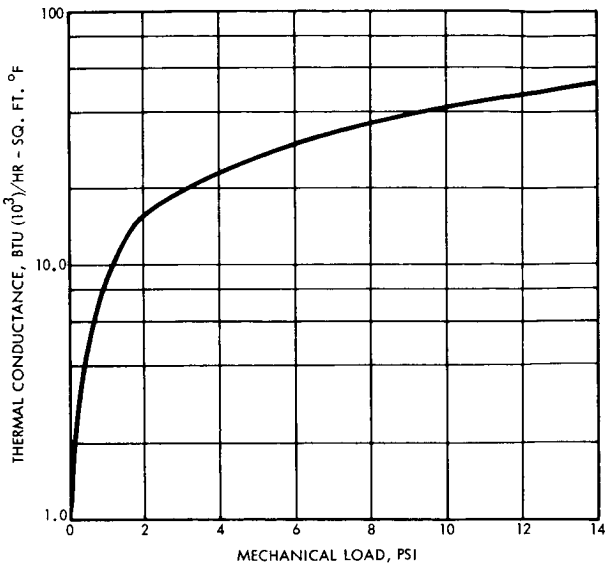

CONDITIONS:
1) 70 1/4 MIL MYLAR LAYERS BOUNDED BY 3 MIL FACE SHEETS
2) HOT BOUNDARY TEMPERATURE: 85°F
3) COLD BOUNDARY TEMPERATURE: -315°F
4) STEADY STATE VACUUM
5) 1 INCH THICK INSULATION BLANKET

Figure 3-33
EFFECT OF MECHANICAL LOAD ON THERMAL CONDUCTANCE - Aluminized Mylar.

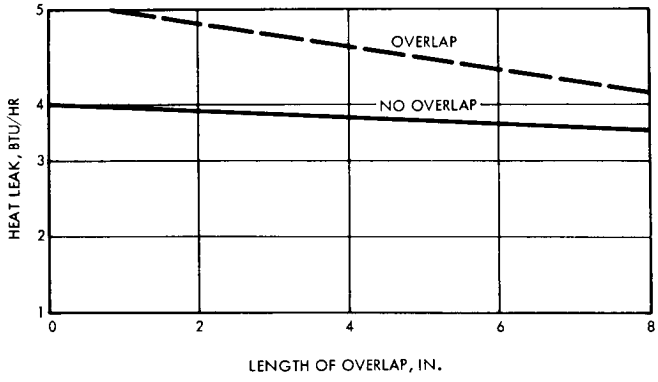

CONDITIONS
1) DIMPLAR
2) LAYERS ARE INTERLEAVED AT JOINT

Figure 3-34
EFFECT OF OVERLAP LENGTH ON HEAT LEAK - Multilayer insulation.

The effects of gaps between insulation blankets and/or the closeouts on thermal conductance is presented in Figure 3-35. For a gap width as low as 1/16 inch, conductance increases 190 percent, and for a gap width of 1/4 inch, conductance increases 460 percent. Heat transfer through the gap consists of radiation directly through the gap and radiation from each layer through the gap. All gaps are covered with a closeout, and the fabrication technique must assure no gap between blankets or between blankets and closeouts exposed to space.

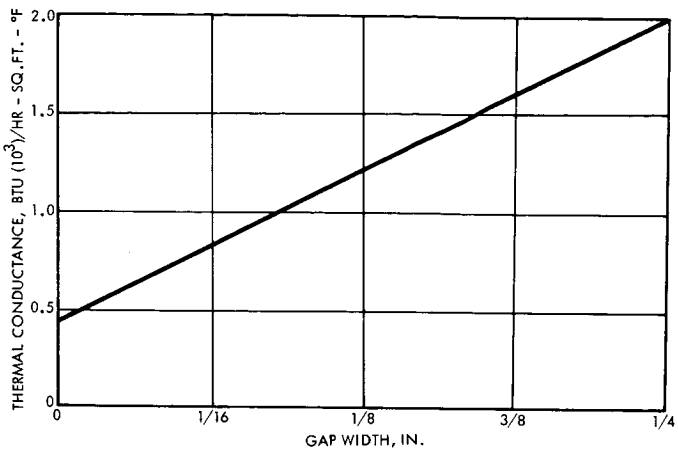

CONDITIONS:
1) IDEAL THERMAL CONDUCTANCE: EFFECTS OF FABRICATION, ATTACHMENT AND MISSION PARAMETERS NOT INCLUDED
2) 70 LAYERS 1/4 MIL MYLAR BOUNDED BY THREE MIL FLAT MYLAR SHEETS
3) ALL LAYERS AND SHEETS ALUMINIZED ON ONE SIDE
4) HOT BOUNDARY TEMPERATURE: 85°F
5) COLD BOUNDARY TEMPERATURE: -315°F
6) STEADY STATE VACUUM
7) 1 INCH THICK INSULATION BLANKET

Figure 3-35
EFFECT OF DISCONTINUITY ON THERMAL CONDUCTANCE - Aluminized Mylar.

REFERENCES

3-1 Volume 1, Voyager Spacecraft System Technical Proposal

3-2 Volume 5, Phase IA Study Report, Voyager Spacecraft, Alternate Designs, System Considerations

3-3 Volume 4, Phase IA Study Report, Voyager Spacecraft, Alternate Design, System Considerations Appendices, dated 30 July 1965

3-4 Volume 2, Phase IA Task B, Voyager Spacecraft, Preferred Design: Subsystem, dated 17 January 1966

3-5 TRW IOC 66-3331.9-8, "The Development of a Mechanical Design for a Bellows Actuated Thermal Switch," dated 31 March 1966, by J. S. Townsend

3-6 TRW IOC 66-3331.9n-1, "Conductance Tests of the TRW Thermal Switch in Vacuum", by L. R. Kelley, dated 10 March 1966

3-7 Test Report 2321-6012-TU-000, "Orbiting Geophysical Observatory Temperature Control Louvers Life Test", (OGO-V21-25), dated 23 April 1963

3-8 AICh. E. Preprint, "Heat Transfer as applied to the Thermal Design of the Nimbus Control System", dated August 1965 by Alexander London

REFERENCES (Continued)

3-9 GE Report, VC-235-101, "Phase IA Task B, Voyager Spacecraft Preferred Design"

3-10 "Reliability Engineering Data Series, Failure Rates", dated April 1962, AVCO Corporation, Research and Advanced Development Division

3-11 TRW Proposal No. 7192.000, "A Proposal for Planetary Vehicle Thermal Insulation Systems, Development Program, Volume 1," dated 22 April 1966

3-12 Douglas Missile and Space Systems Division, "Thermodynamic Design Fundamentals of High Performance Insulation," dated March 1967, N. R. Foliman and T. G. Lee

3-13 General Electric Missile and Space Division, "Planetary Vehicle Thermal Insulation Systems, Phase I Summary Report," Document No. 675D4289, dated 3 March 1967

3-14 Douglas Missile and Space Systems Division, "High Performance Insulation System Development," Douglas Report SM-48806, dated October 1965

3-15 TRW IOC 67-3346.81a-12, "The Effect of Relative Humidity on Aluminized Mylar Films," dated 15 August 1967, J. W. Verbeck

3-16 Lockheed Missile and Space Company, "Lockheed Multilayer Insulation Independent Development Program," LMSC-A 777990, 1963-1964

3-17 A. D. Little Co., "Multilayer Insulation Development Program," 1965.

3-18 TRW Report No. 9990-7306-T0000, "Cryogenic Insulation Development Program - Phase II Report," O. O. Haroldsen, W. M. Pence and J. C. Elizalde, dated July 1966

4. PLUME HEATING

4.1 GENERAL DESCRIPTION

4.1.1 Scope of Work

This engineering task investigated: 1) engine plume heating and areas of impingement of the Voyager spacecraft from the LM Descent Engine; 2) nozzle radiation heating to spacecraft from the LM Descent Engine nozzle extension; and 3) effect of engine plume heating and nozzle radiation heating on critical spacecraft components.

4.1.2 Summary

The temperature and pressure gas dynamics was determined for the LM Descent Engine. A one-phase, inviscid flow field was developed to depict the liquid propellant engine plume. Determination of the discernible plume (Section 4.2.1) indicated that there are no areas of impingement either on the spacecraft or the external equipment from the firing of the LM Descent Engine. The chemical composition of the plume (Section 4.2.2) was determined accounting for N_2, CO, CO_2, and H_2O (vapor). The total incident radiation heat flux from the engine plume was calculated to each of the critical spacecraft components by the line-of-sight method.

Based on the nozzle extension temperatures generated by the engine firing program and shape factors calculated by the method in Reference 4-1, the heat fluxes from the nozzle to the critical spacecraft components were calculated. During the analysis of Task C it was found necessary to use an ablative nozzle extension to keep the solar arrays on the base below 300°F. During Task D it was found that an insulated nozzle extension using Fiberfrax with low emittance metallic coating would keep the solar arrays below 300°F. The insulated nozzle extension weighs much less than the ablative nozzle.

The effect of engine plume heating and nozzle radiation heating when coupled with the normal spacecraft environments during engine firing is presented in Section 4.5. There is no deleterious effect on the spacecraft or any of its components as a result of engine firing.

4.2 DEFINITION OF PLUME CHARACTERISTICS

4.2.1 Temperature and Pressure Gas Dynamics

Thermal radiation from the LM Descent Engine plume to the spacecraft surfaces could affect the performance of those surfaces. Figure 4-1 shows the relationship between the critical spacecraft components and the engine. As a result of the possible deleterious effects of the plume, it is important that an accurate prediction of the thermal environment during the engine firing be made. For a liquid propellant motor (i.e., LM Descent Engine), the gaseous plume is the sole radiator. In this case, the radiation is a function of temperature, pressure, and chemical composition of the plume.

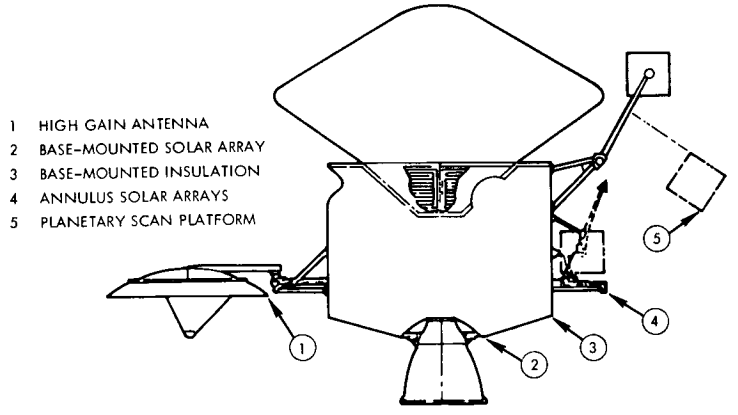

Figure 4-1
VOYAGER SPACECRAFT - Critical components subjected to engine plume heating.

To initiate the study, the plume flow field was generated using the TRW computer program, "Jet Wake Study Program." The flow field for the gaseous plume was determined using the pertinent propulsion data in Table 4-1. This program calculates the lines of constant Mach and defines the discernible plume for a one-phase (ideal gas) inviscid flow field (Figure 4-2). The flow field is used with the composition (Section 4.2.2) to determine the plume heating (Section 4.3).

An ideal gas analysis was used in this study. For the high-temperature high-pressure region (chamber), very large kinetic energies exist and the gases are in an equilibrium state. When temperature and

Table 4-1. Pertinent Propulsion Data

Item	Units	First Interplanetary Trajectory Correction	Mars Insertion
Chamber pressure	(psia)	18	100
Chamber temperature	(^{o}R)	5501	5501
Gas constant	(ft/^{o}F)	75.1	75.1
Specific heat ratio	(γ)	1.24	1.24
Ambient pressure	(psia)	0.695×10^{-5}	0.695×10^{-5}
Nozzle exit radius	(ft)	2.38	2.38
Nozzle exit Mach number	(M)	4.18	4.18
Nozzle lip angle	(θ)	11	11

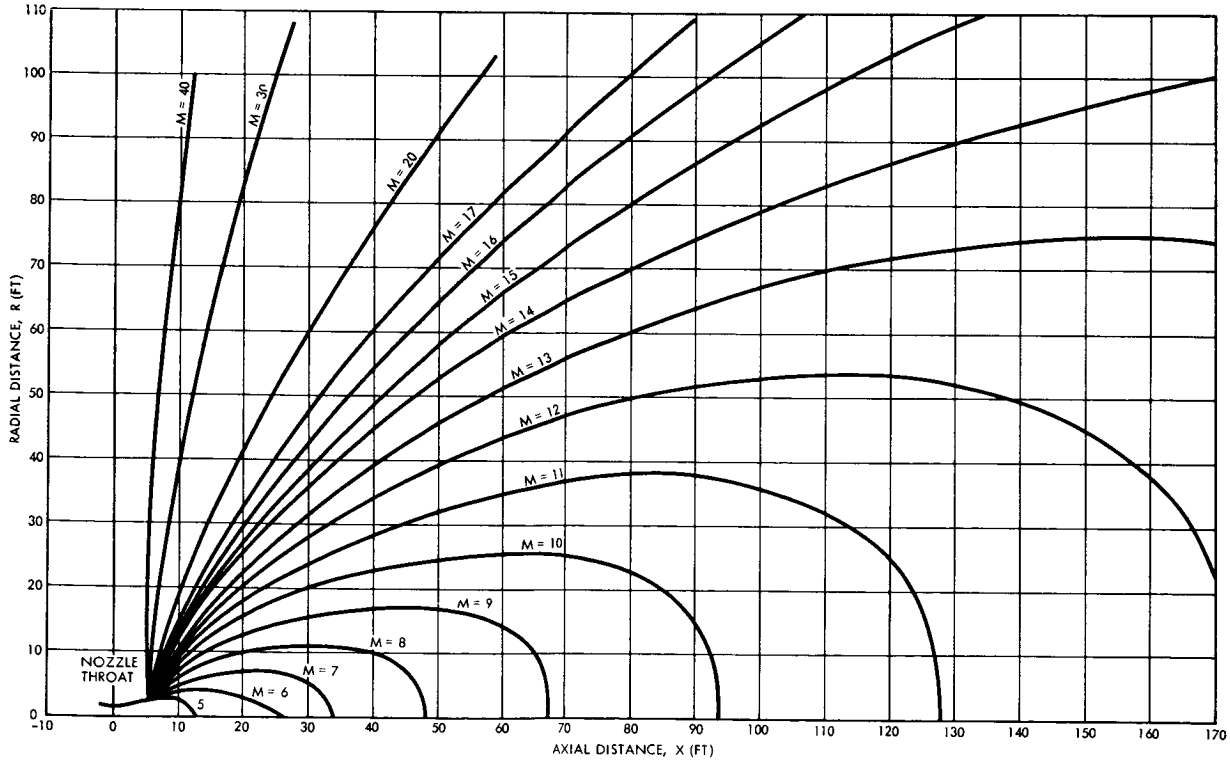

Figure 4-2
PLUME FLOW FIELD - Constant mach number lines.

pressure drop (somewhere in the nozzle), the gas shifts to a nonequilibrium state and the real gas effects become significant. When temperature and pressure drop to very low values (somewhere in the divergent section of the nozzle or outside of the nozzle), the kinetic energy is almost zero and no critical reactions can take place. Consequently, ideal gas assumptions are valid in this region. For this particular analysis the only area we are concerned with is the plume as it forms outside the nozzle.

4.2.2 Plume Composition

The plume chemical composition was determined using the TRW computer program, "Rocket Chemistry Program." This program accounts for N_2, CO, CO_2, and H_2O (vapor). It ignores all free carbon. From the LM Descent engine test presently in progress, TRW has motion pictures taken through the engine plume which show that it is very clear and that very little free carbon exists in the plume. In the analysis only CO, CO_2, and H_2O (vapor) were considered as radiation sources. The N_2 was neglected because of its very low emittance. Table 4-2 gives the chemical composition of the plume at nozzle exit.

Table 4-2. Plume Composition

Constituent	Mole Fraction	Radiation Source
N_2	0.497	No
CO	0.078	Yes
CO_2	0.053	Yes
H_2O (Vapor)	0.372	Yes
	1.000	

4.3 PLUME RADIATION HEATING

To determine the radiant heat flux incident to a given surface point, the plume is first divided into a number of small segments with view planes emanating from the surface point to which the heat flux is to be calculated. The heat flux from each of these segments is then computed, and by summing up the contributions from all the segments, the total heat flux incident

to the surface point is obtained. In computing the incident heat fluxes from the individual segments, a mean grey body emissive power was computed. Figure 4-3 shows an example of the method of calculation.

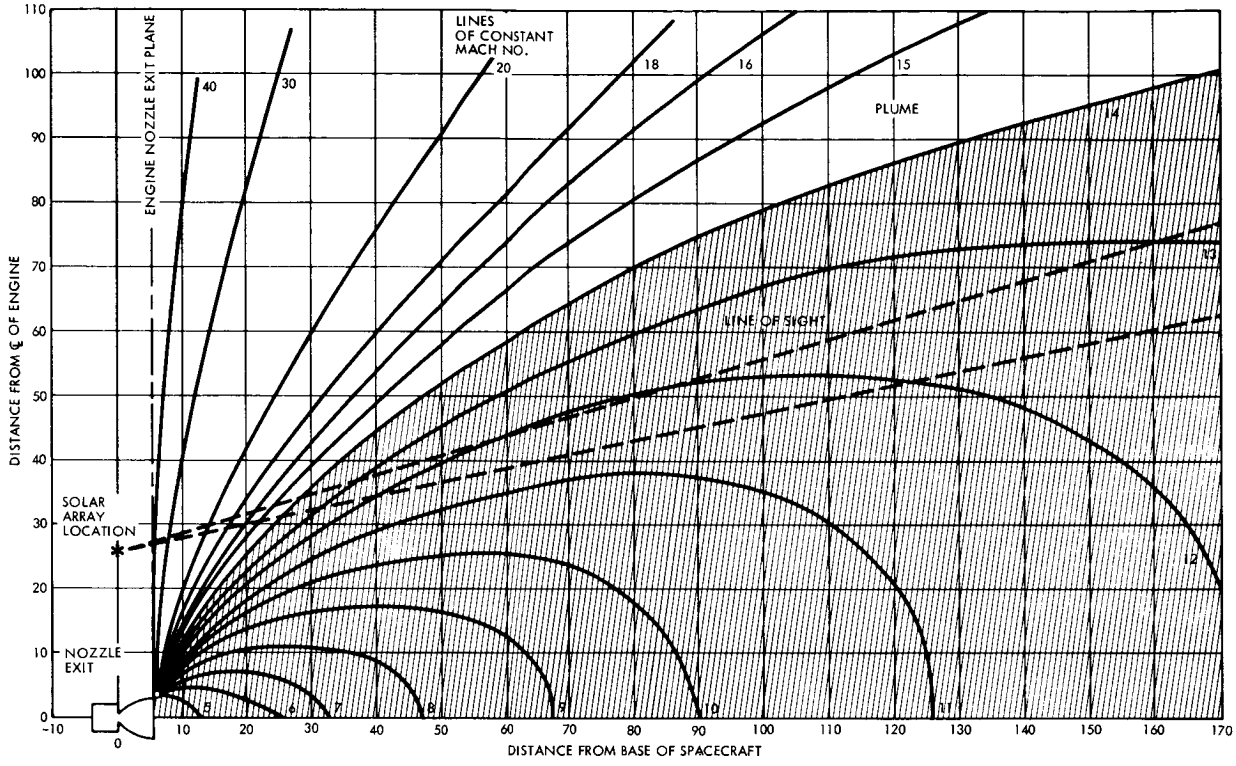

FIGURE 4-3
PLUME HEATING EFFECT - Typical calculation.

For the prediction of gaseous plume radiation, the following computing technique is used. Since total heat flux is being calculated, then the emissivity values for individual species are determined from Hottel's emissivity data as functions of temperature and the product of partial pressure and beam length. These emissivity values are combined with the black body emissive power and the shape factor for each individual segment to determine the heat flux from that segment.

4.4 NOZZLE RADIATION HEATING

The nozzle radiation heating in conjunction with the engine plume heating and normal solar heating posed the potential problem of overheating critical spacecraft components during the engine firing. The

maxiumum heat flux occurs during first interplanetary trajectory correction. The next highest heat flux occurs during the Mars orbit insertion. Previous studies have shown that a radiation-cooled nozzle exhibits thermally destructive effects upon base-mounted solar arrays. The current design of the LM Descent engine employs a radiation-cooled extension For the Voyager application the heat radiation from the nozzle extension must be limited due to the proximity of the solar arrays. During Task C, an ablative nozzle extension was proposed. This would limit radiation heating to the base-mounted solar arrays, but its weight is prohibitive. During Task D an insulated nozzle extension concept was studied and found to be effective in limiting the heat radiation. The weight of the insulated nozzle extension is considerably less than that of the ablative nozzle extension. The present nozzle extension uses Fiberfrax insulation with the low-emittance ($\epsilon = 0.2$) metallic coating.

Near-earth and near-Mars steady state temperatures were used as the initial temperature for the first interplanetary trajectory correction and the Mars orbit insertion, respectively. The extremely high values obtained near-earth steady state are especially important from the solar array standpoint since this, coupled with the high heat flux due to engine firing, tend to cause the solar arrays to experience high temperature ($300^{\circ}F$). The near-Mars steady state temperatures, coupled with the engine firing for the Mars orbit insertion, cause the solar arrays to reach high temperature ($195^{\circ}F$), but are not as critical since these are within the temperature limits of the solar arrays.

The nozzle extension radiation was considered to the following areas: 1) high-gain antenna, 2) base-mounted solar arrays, 3) base insulation, 4) solar arrays on the annulus, and 5) planetary scan platform. The solar panels and nozzle extension have emissivities of 0.82 and 0.2., respectively. For the thermal radiation from the nozzle to the critical spacecraft components, shape factors were determined analytically. Curves of component temperatures versus engine firing time during the first interplanetary trajectory correction and the Mars orbit insertion are presented in Figure 4-4. These temperatures, combined with the shape factors between the nozzle and the spacecraft components, yield the heat

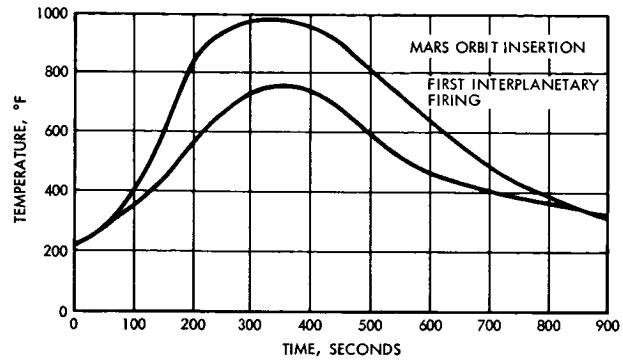

Figure 4-4
NOZZLE TEMPERATURES

flux for the critical spacecraft components. Table 4-3 indicates the maximum radiation heat flux each of the critical spacecraft components receives from the nozzle extension.

Table 4-3. The Base-Mounted Solar Array, Base Insulation, and High-Gain Antenna Radiant Heat Flux.*

Description	Near-Earth Heat Flux $Btu/sec\text{-}ft^2$	Near-Mars Heat Flux $Btu/sec\text{-}ft^2$
Base-mounted solar array	0.001	0.026
Base insulation	0.003	0.006
High-gain antenna	0.001	0.003

* The base-mounted solar array, base insulation, and high-gain antenna receive a radiant heat flux from the nozzle extension during engine firing.

4.5 THERMAL EFFECT OF PLUME HEATING ON SPACECRAFT AND EXTERNAL EQUIPMENT

A thermal analysis has been performed to determine the effect of engine plume heating on critical spacecraft components. Short-term temperature excursions associated with engine firing are an important

area of concern. The two firings which produce maximum temperature excursions are the first interplanetary correction and the Mars orbit insertion.

Results from the steady state, near-earth and steady state, near-Mars analyses are taken as the initial temperatures for the present analysis. The radiant plume energy incident upon the spacecraft during engine firing was determined by the total radiant energy method. A detailed description of the study performed to determine the radiant heat fluxes incident to critical components of the spacecraft from the engine plume is presented in Section 4.3. The critical spacecraft components receiving radiant energy from the engine plume are as follows: annular solar array, base-mounted solar array, base insulation, planetary scan platform and high-gain antenna.

The first interplanetary trajectory correction is an upper bound hot condition near-earth. All of the critical areas receive a solar heat flux of 442 $\frac{\text{Btu}}{\text{hr-ft}^2}$ in addition to radiant energy from the engine plume and nozzle (nozzle radiation heating is duscussed in Section 4.4). The results as shown in Figure 4-5 provide data for the 380 second engine firing as well as soakback after firing. The results of the analysis indicate that all of the critical components, with the exception of the base mounted solar array, are well within their respective temperature limits. The near-earth, steady-state temperature of the base mounted solar array is only a few degrees under its 248°F temperature limit. Therefore, during engine firing the heat flux received from the engine plume causes a short duration temperature excursion to 300°F. Although the upper temperature limit is 248°F, temperatures to 300°F have been tested in the course of the Vela satellite program, demonstrating that the structural integrity of the array can be maintained if proper aluminum venting and mounting structure expansion requirements are implemented. The near-earth, steady-state temperatures of the other critical components are well below their upper limits; therefore, the temperature excursions experienced during firing do not constitute a problem.

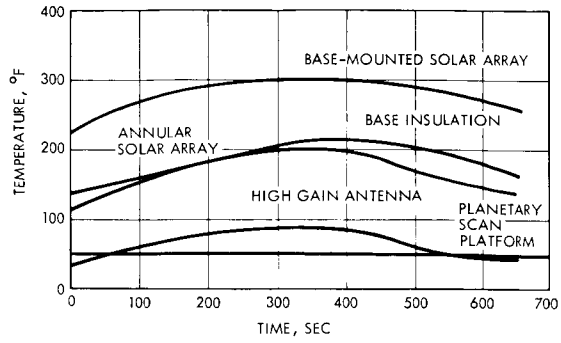

Figure 4-5

FIRST TRAJECTORY CORRECTION provides maximum temperatures for the spacecraft and its components.

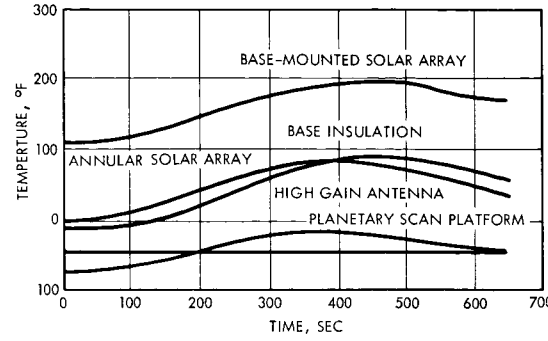

Figure 4-6

MARS ORBIT INSERTION TEMPERATURES do not exceed those of first trajectory correction burn in spite of longer burn time during orbit insertion. This is due to lower solar flux near Mars.

During Mars orbit insertion the critical areas discussed above receive a solar flux of 159 $\frac{\text{Btu}}{\text{hr-ft}^2}$ and, as in the case of the first interplanetary firing, they also receive incident energy from the engine plume and nozzle. As is shown in Figure 4-6, these areas experience a temporary temperature excursion during the 380 second engine firing. Because of the lower near-Mars, steady-state temperatures, the temperature rises during Mars orbit insertion engine firing are well within the allowable temperature range.

4.6 CONCLUSION

The effect of the engine plume and the nozzle radiation combined with the spacecraft environment during the engine firings does not cause any deleterious effects on the spacecraft or its components. There are no areas on the spacecraft or its external equipment where the engine plume impinges. All the spacecraft critical components are within their allowable temperature limits. The solar arrays on the base of the spacecraft reach 300°F for a short period of time during the first interplanetary trajectory correction, but this is not injurious to the array.

REFERENCES

4-1 S. J. Morizumi, "Analytical Determination of Shape Factors from a Surface Element to an Axisymmetric Surface," AIAA J., 2 (Nov. 1964).

APPENDIX A

SHROUD VENTING ANALYSIS

1. INTRODUCTION AND GUIDELINES

An ascent venting analysis has been performed on the Voyager Spacecraft shroud configuration. The size and location of all the vents required to ensure the adequate venting of each of the two Voyager capsules, the two planetary vehicle compartments, and all the shroud interior compartments during the ascent portion of the trajectory have been determined.

The Voyager launch vehicle configuration upon which this analysis is based appears in Figure A-1. The detailed shroud configuration used in this analysis is shown in Figure A-2.

Prior to launch there will be an ETO purge of the planetary vehicle compartments followed by a drying N_2 purge until the ETO mixture has been completely dispelled. At the completion of this purge, a 0.5 psi N_2 overpressure in each planetary vehicle compartment and a 3.5 psi N_2 overpressure in each of the capsules will be maintained. The vent concept for this study is controlled venting of each capsule, controlled venting of each planetary vehicle compartment, and uncontrolled venting from each shroud compartment to the atmosphere.

The ascent trajectory parameters used in the present analysis are in Figures A-3 and A-4. The maximum value of the angle of attack envelope during ascent, induced by winds, is α = 7-1/2 degrees.

A literature survey was made to find test data on a biconic cylindrical configuration geometrically similar to the shroud. Reference A-1 contains pressure data for the Mach number range 0-1.18 for such a geometric shape. Pressure coefficient data for the Voyager shroud configuration is presented in Figures A-5 through A-13 for the entire Mach number range of interest. Pressure coefficient distributions at angles of attack (α) of 0 and 7-1/2 degrees are presented for the proposed vent and critical loading locations in Figures A-14 and A-15.

There are two ways to vent each planetary vehicle compartment: locate the vent on the forward bulkheads (concept A), or locate the vents on the aft bulkheads (concept B). Both vent arrangements are studied.

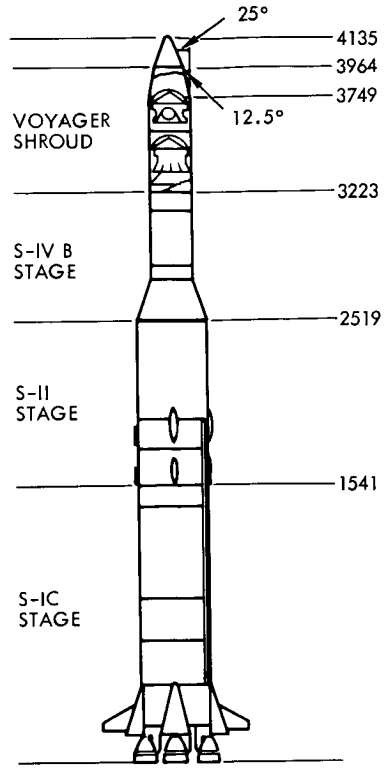

Figure A-1. A Preliminary Ascent Venting Analysis

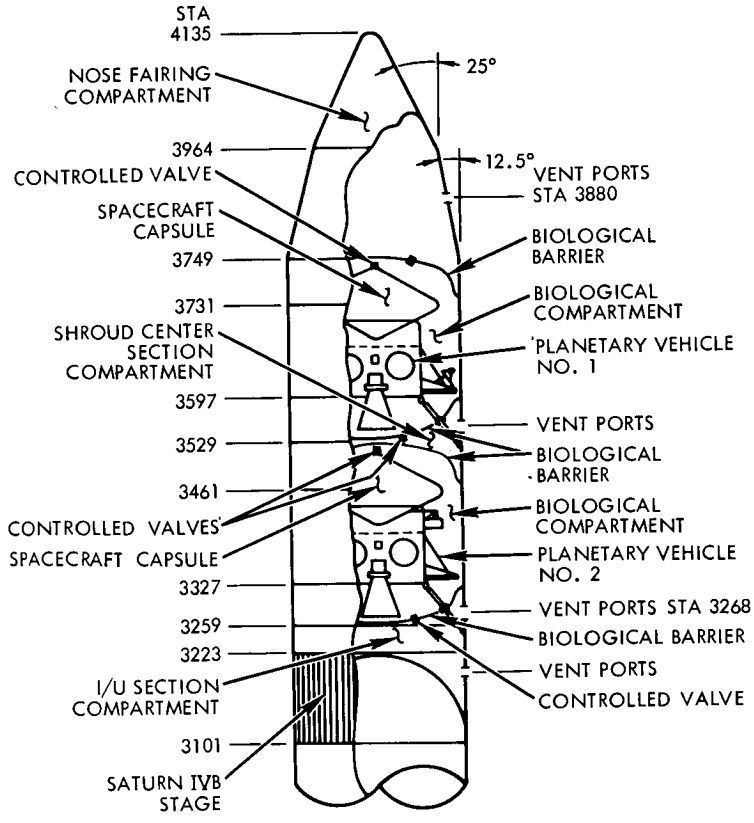

Figure A-2. Planetary Vehicle/Shroud Configuration

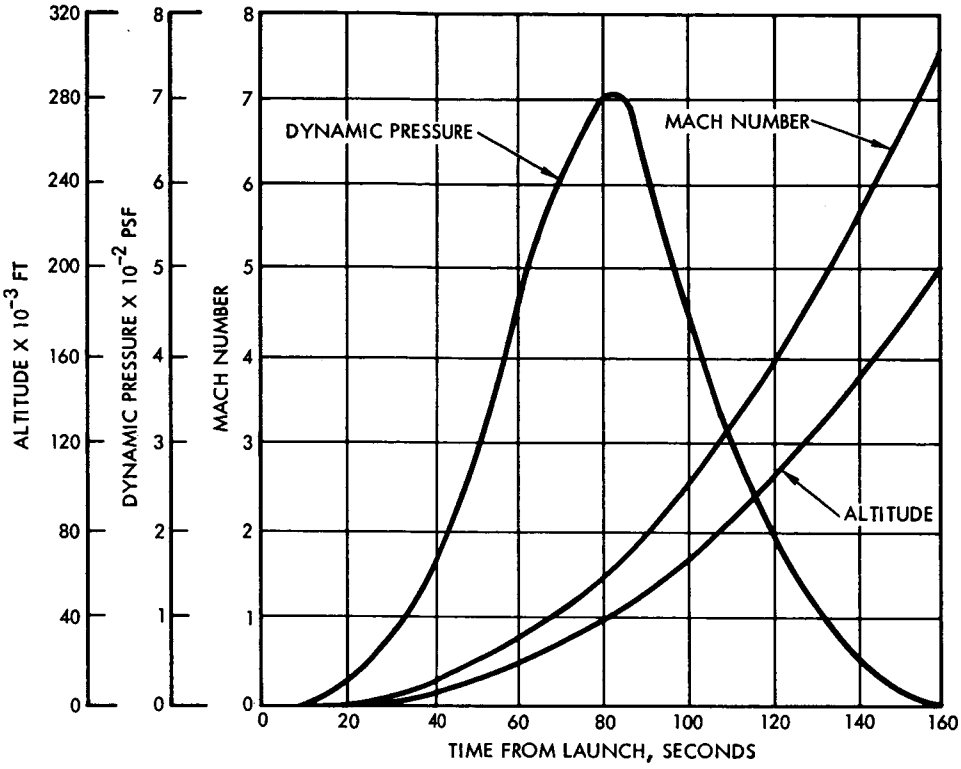

Figure A-3. Ascent Trajectory

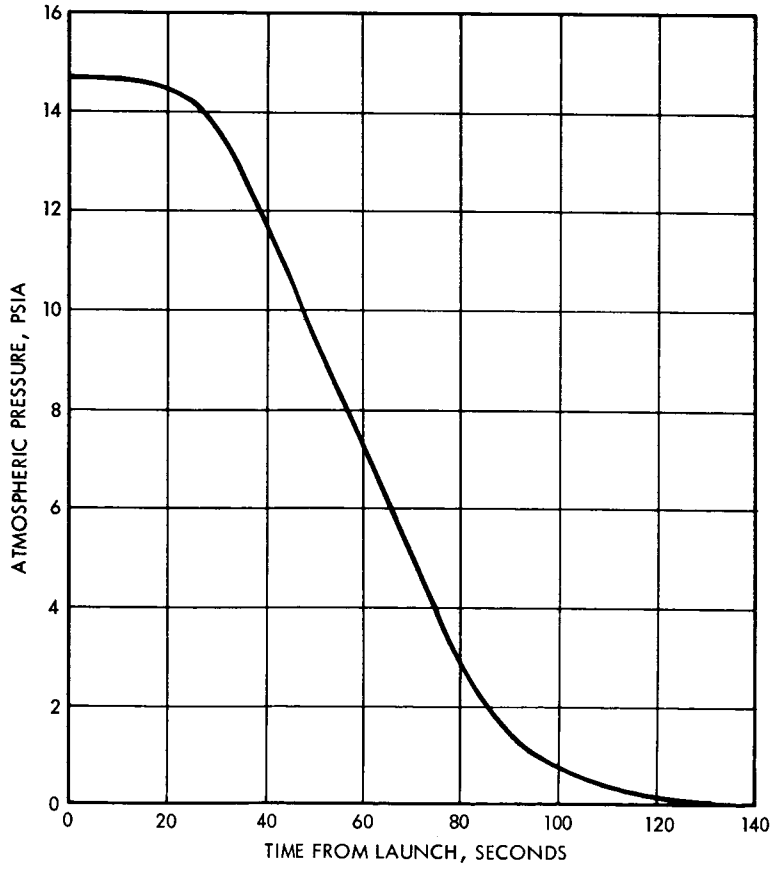

Figure A-4. Ascent Trajectory Atmospheric Pressure Versus Time From Launch

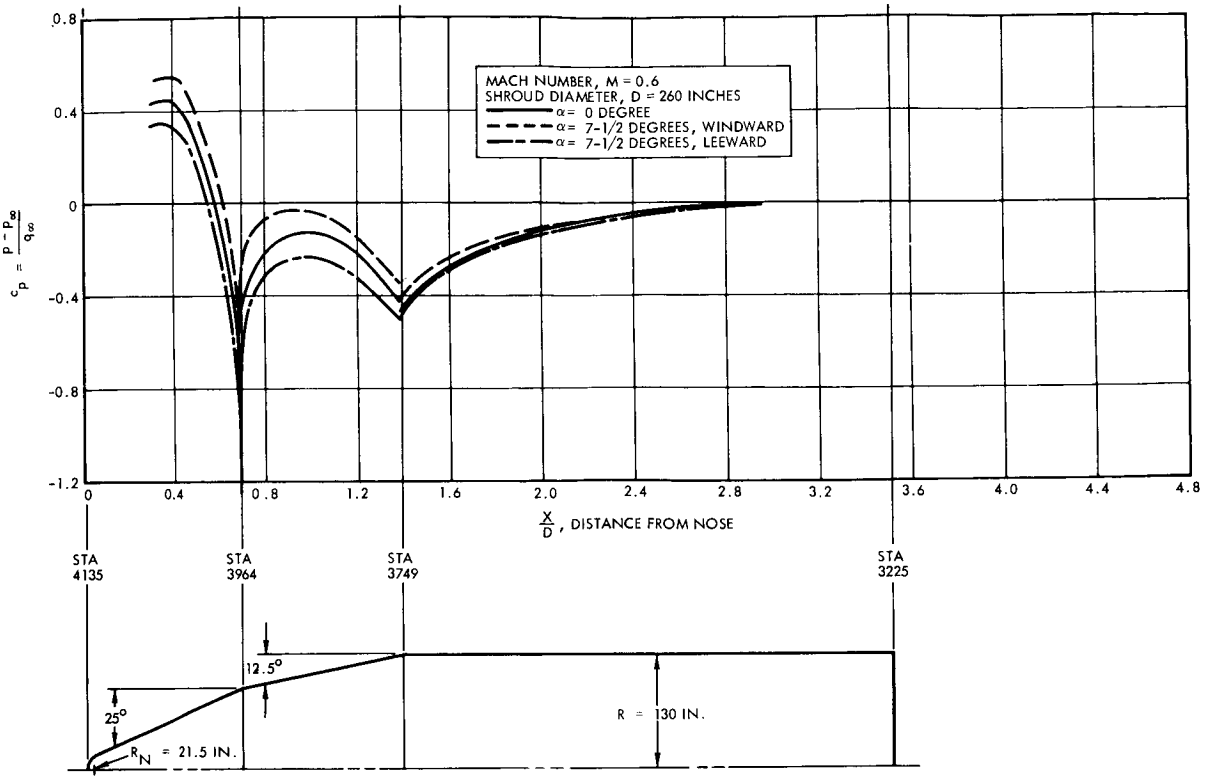

Figure A-5. Shroud Pressure Distribution - Mach 0.6

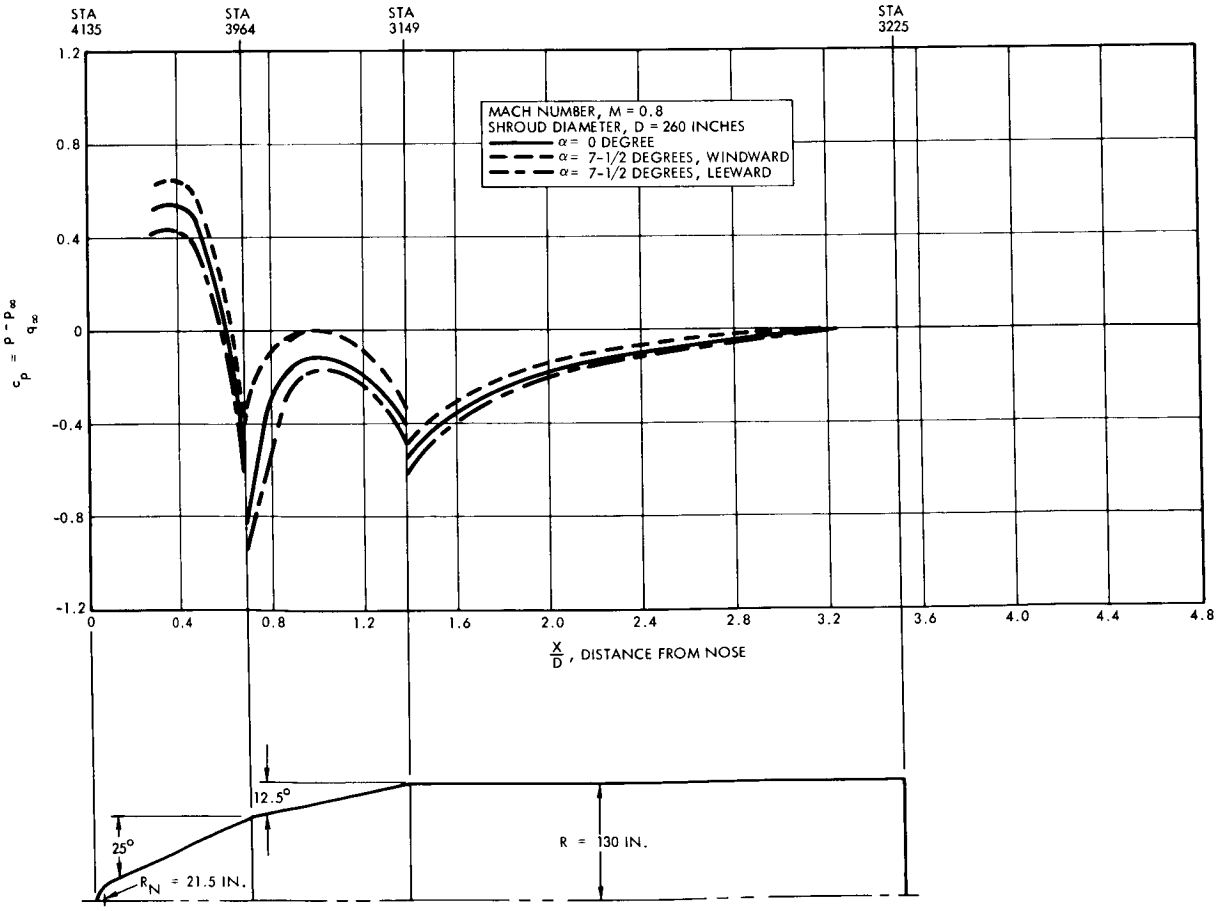

Figure A-6. Shroud Pressure Distribution - Mach 0.8

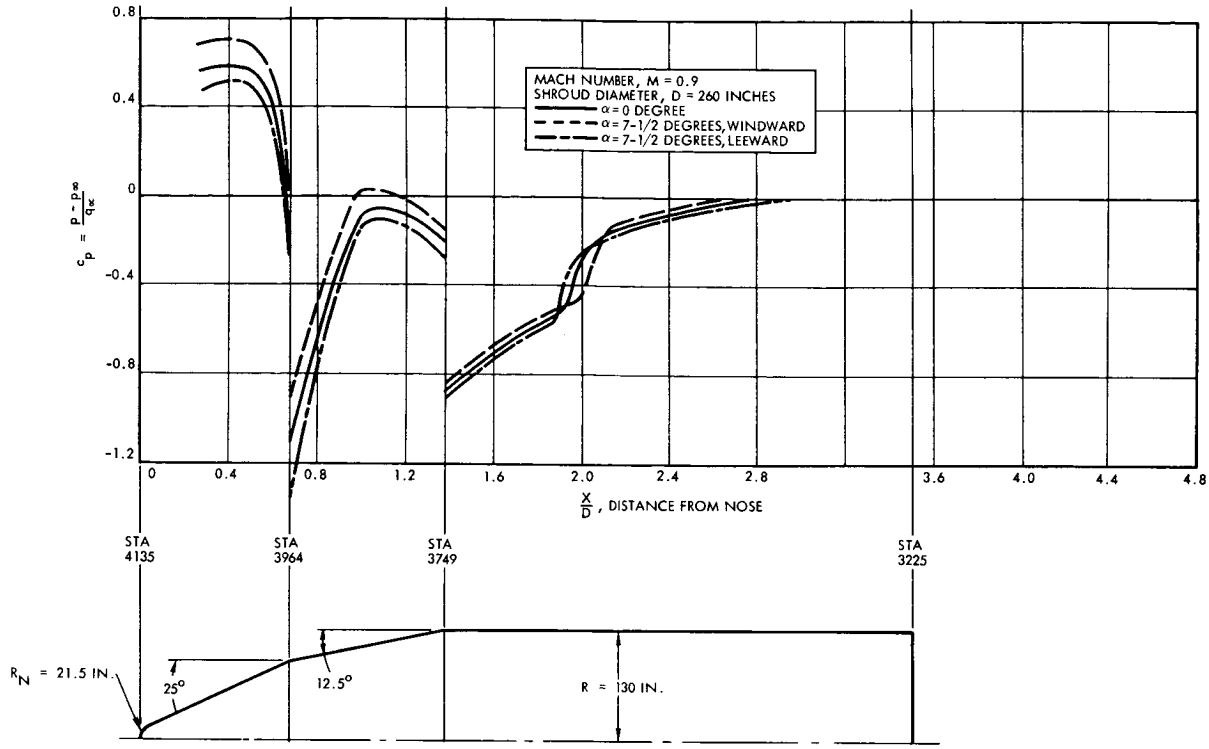

Figure A-7. Shroud Pressure Distribution - Mach 0.9

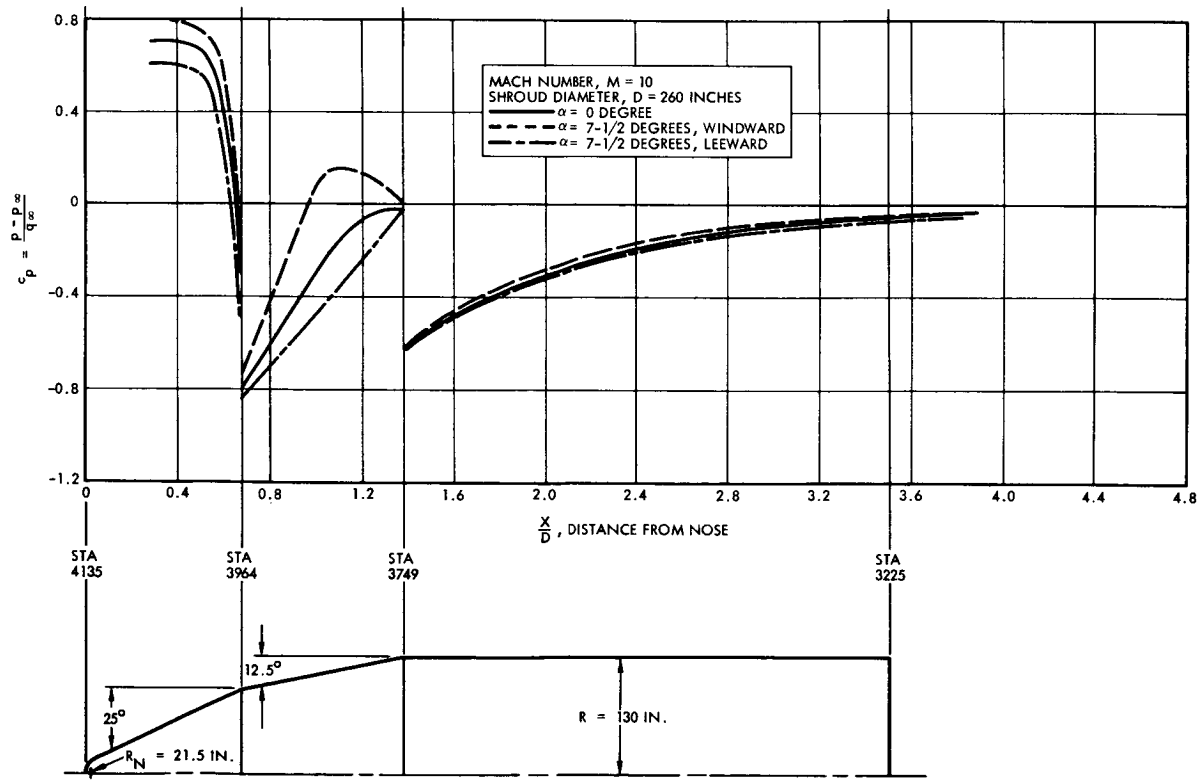

Figure A-8. Shroud Pressure Distribution - Mach 1.0

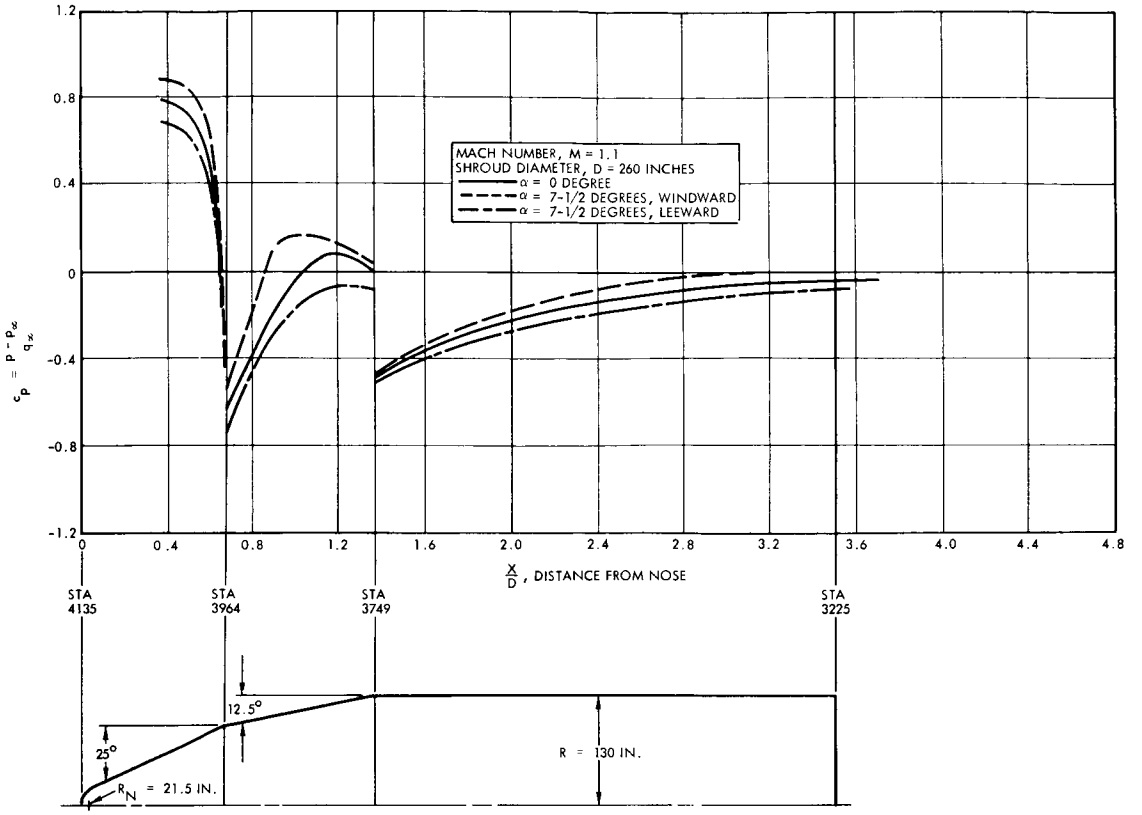

Figure A-9. Shroud Pressure Distribution - Mach 1.1

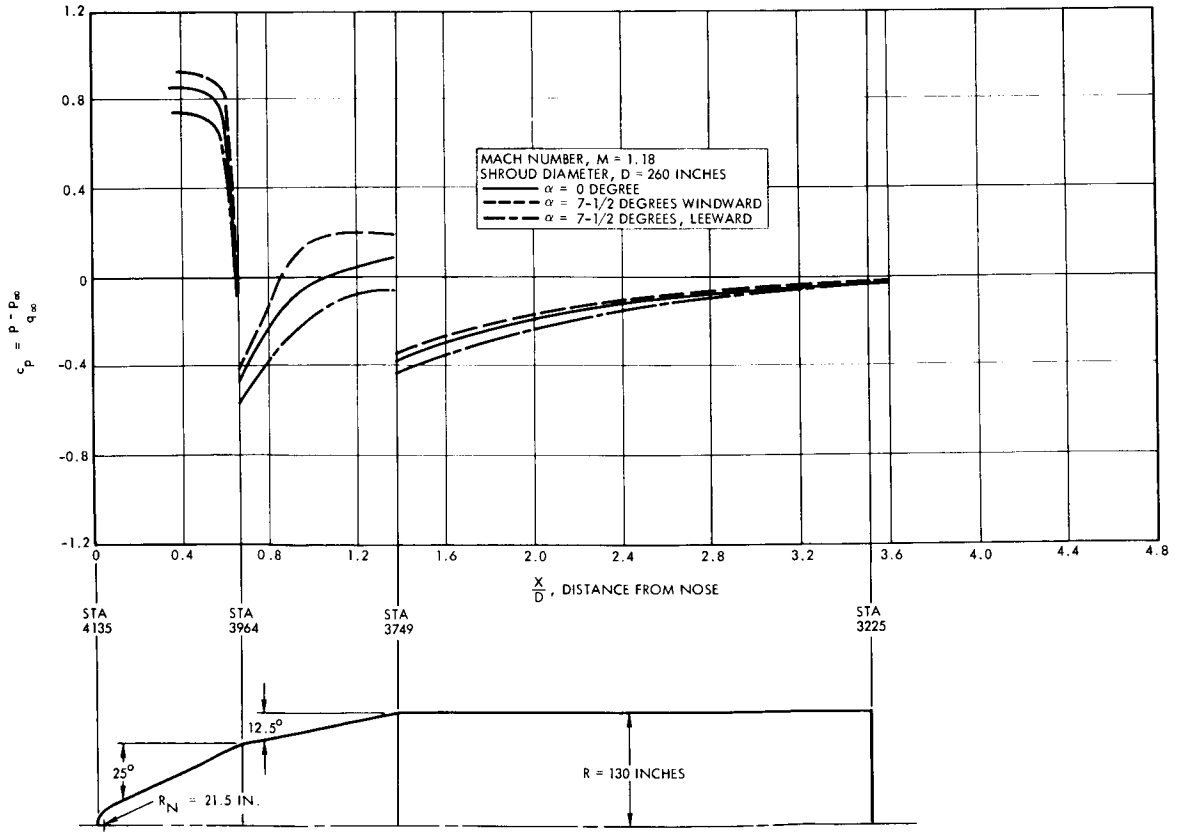

Figure A-10. Shroud Pressure Distribution - Mach 1.18

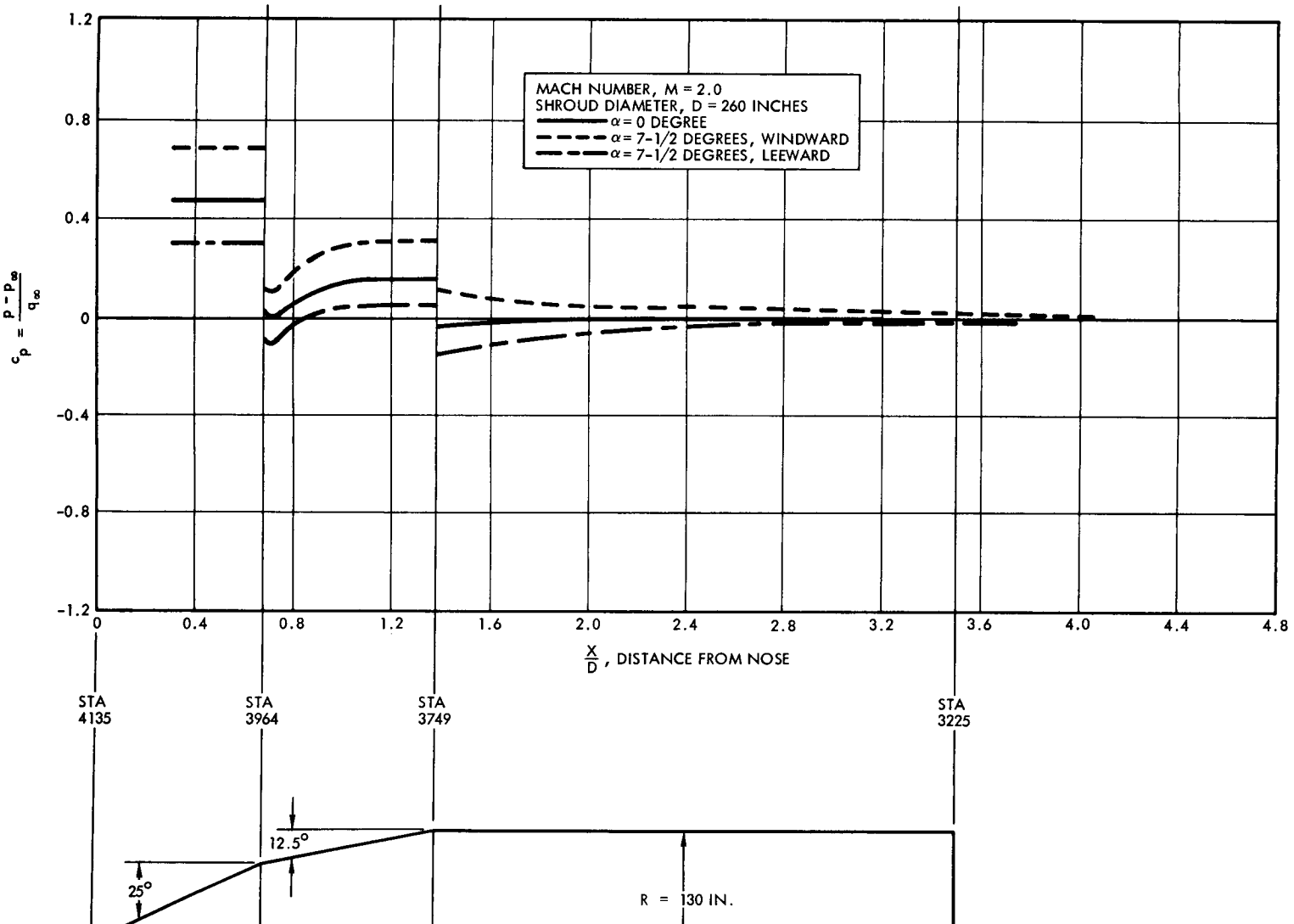

Figure A-11. Shroud Pressure Distribution - Mach 2.0

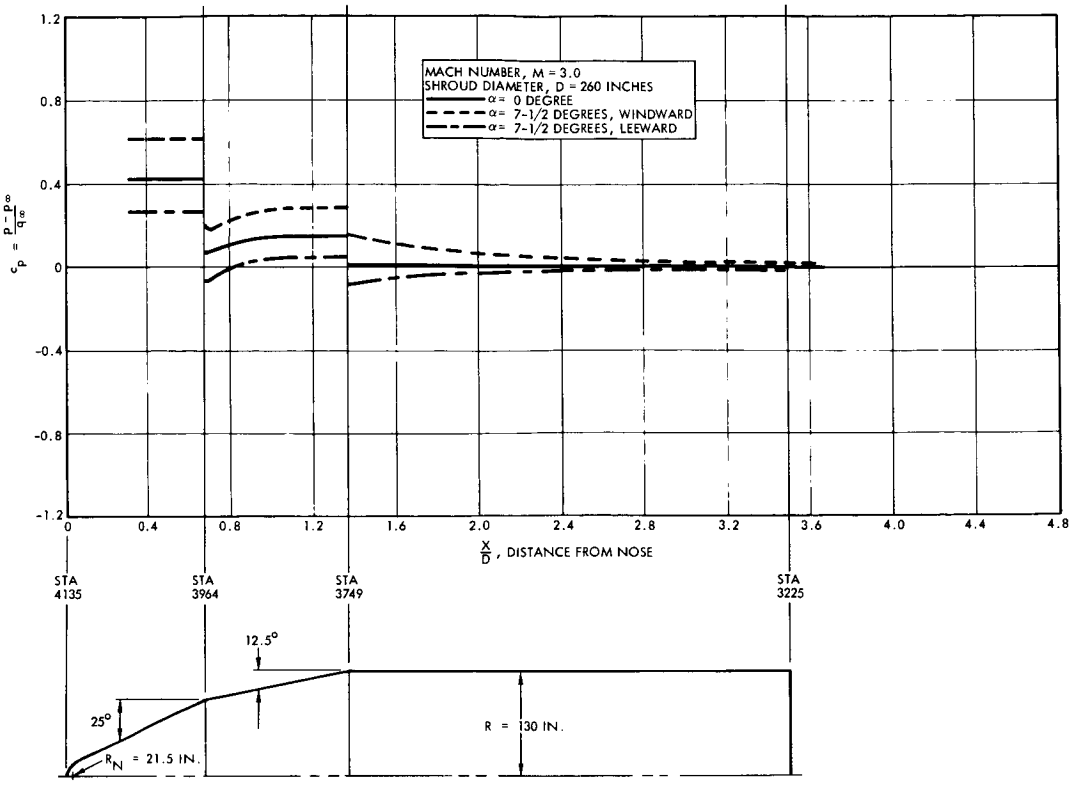

Figure A-12. Shroud Pressure Distribution - Mach 3.0

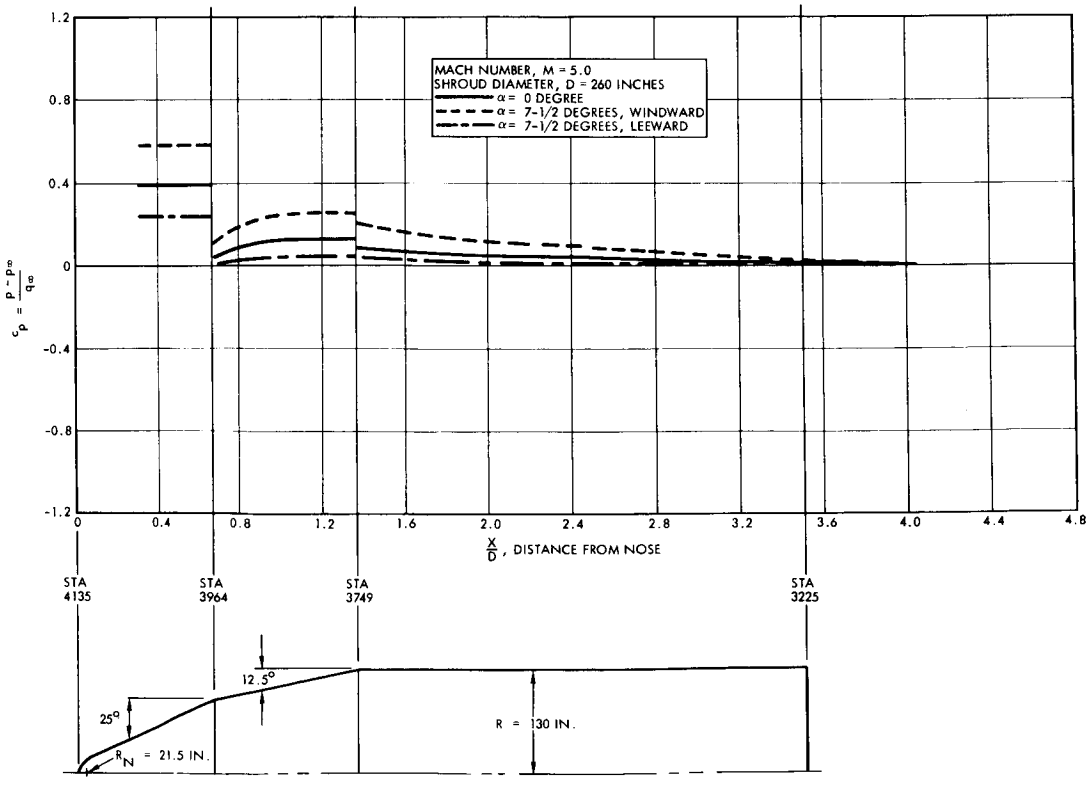

Figure A-13. Shroud Pressure Distribution - Mach 5.0

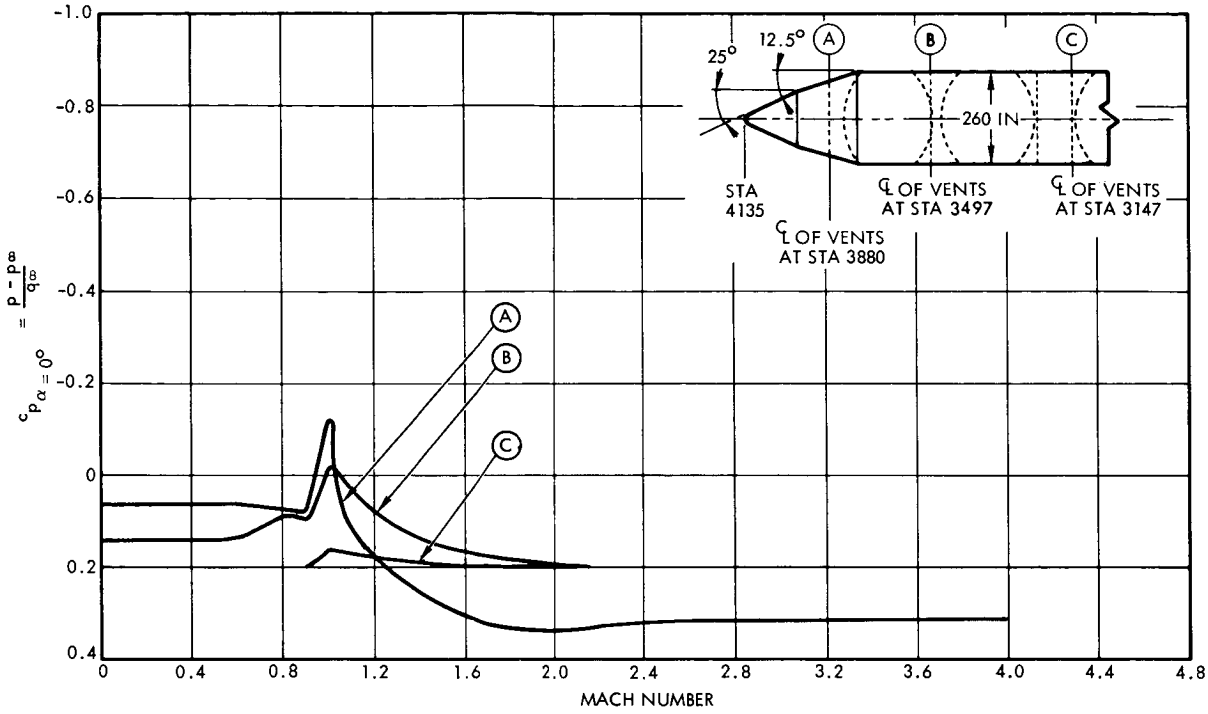

Figure A-14. Pressure Coefficient Distributions Versus Mach Number (α = 0 degrees)

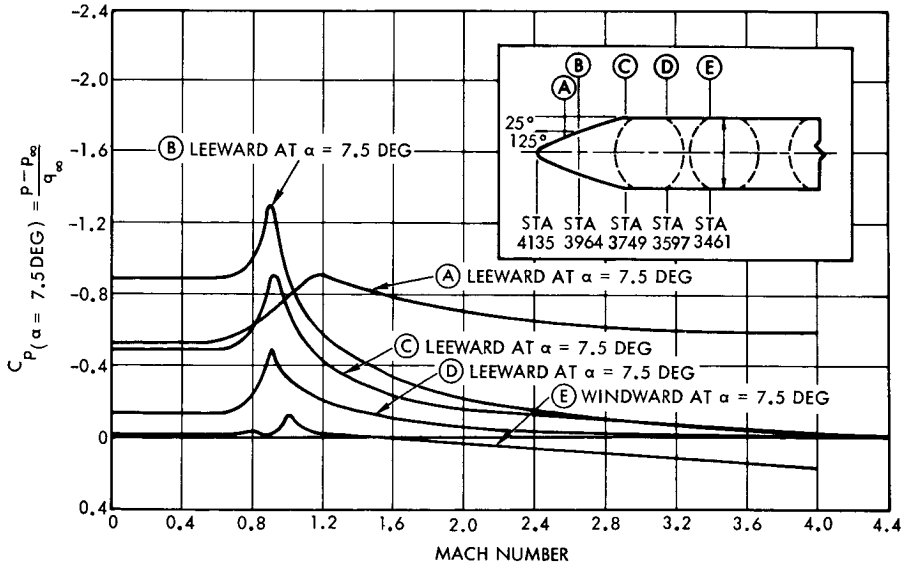

Figure A-15. Pressure Coefficient Distribution vs Mach Number (α = 7.5 degrees)

Because of the presence of external boundary layer flow adjacent to each vent orifice on the shroud, the discharge coefficient of the sharp edge orifice is a function of the pressure ratio across the vent, and the Mach number of the external flow. The experimental data of References A-2 and A-3 have been incorporated in the present analysis to include the functional dependence of the discharge coefficient upon the pressure ratio and Mach number of the flow.

The free volumes of the compartments which must be vented are:

a) Voyager capsule: 1050 ft^3

b) Each planetary vehicle compartment: 6400 ft^3

c) Nose fairing: 3800 ft^3

d) Shroud center section: 970 ft^3

e) Instrument unit and forward S-IVB skirt volume: 3700 ft^3.

The nominal internal pressures within the above compartments at launch are listed below:

a) Voyager capsule: 3.5 psig

b) Each planetary vehicle compartment: 0.5 psig

c) Nose fairing compartment: ambient pressure

d) Shroud center section compartment: ambient pressure

e) IU/forward S-IVB skirt volume: ambient pressure.

Additional ground rules are:

a) There shall be a maximum of 5 psi burst across the shroud structure.

b) There shall be a positive pressure differential between the planetary vehicle compartment and adjacent volume of not less than 0.5 psi, as long as the stage is within the sensible atmosphere.

2. METHOD OF ANALYSIS

The size of the vent areas required to adequately vent the compartments is determined by considering the mass flow of the nitrogen leaving

the compartments during the ascent portion of the trajectory. As the missile ascends there will be a net mass flow out of the compartment as the volume of nitrogen contained within the compartment escapes through the vent to the lowering external pressure at the vent location. If the compartment is completely sealed everywhere except at a single vent, then the mass flow through the vent is given by the following:

For subsonic flow through the vent, $\left(\frac{2}{\gamma+1}\right)^{\frac{\gamma}{\gamma-1}} < \frac{P_e}{p} < 1$, and

$$\dot{m} = -C_d A \sqrt{\frac{2\gamma}{\gamma-1} p\rho \left(\frac{p_e}{p}\right)^{\frac{2}{\gamma}} \left[1 - \left(\frac{p_e}{p}\right)^{\frac{\gamma-1}{\gamma}}\right]} \quad \text{(subsonic)}$$

For sonic (choked) flow through the vent, $\frac{p_e}{p} \leq \frac{2}{\gamma+1}^{\frac{\gamma}{\gamma-1}}$, and the mass flow is independent of p_e:

$$\dot{m} = -C_d A \sqrt{\gamma p\rho \left(\frac{2}{\gamma+1}\right)^{\frac{\gamma+1}{\gamma-1}}} \quad \text{(supersonic)}$$

where p and ρ are the compartment pressure and density, respectively, at any time, and the minus sign indicates that the mass of nitrogen within the compartment decreases with time. Basically, these are simple nozzle flow equations corrected for the effects of the actual non-nozzle geometry of the vent by means of the discharge coefficient.

The discharge coefficient is defined as the ratio of the actual mass flow to the mass flow calculated for isentropic flow through an equivalent rounded-entrance converging nozzle having the same exit area as the vent.

$$C_d = \frac{\text{actual mass flow}}{\text{isentropic mass flow}}$$

The discharge coefficient for a sharp-edged orifice is due primarily to the contraction (vena contracta) in the stream following the orifice, hence the product $C_d A$ can be thought of as an equivalent exit area of a smaller converging nozzle, and thus all the aerodynamic flow parameters through the vent can be described by isentropic flow relations. The discharge coefficient is a function of the vena contracta, and either the pressure ratio across the vent (for flow into stagnant air), or both the pressure

ratio across the vent and the Mach number of the flow past the vent opening (for flow discharging into a moving stream).

The mass flow equations describe the characteristics of the nitrogen in the vicinity of, and through the vent. It is then necessary to describe the characteristics of the general gas mass in the compartment; in particular, it must be specified as to how the compartment gas density, ρ, changes as the pressure in the compartment drops. The assumption is made that the nitrogen remaining in the compartment expands adiabatically. This means that all heat inputs to the nitrogen are neglected, such as that due to external aerodynamic heating, or that due to operation of electrical equipment inside the compartment.

For an adiabatic process, the pressure and density are related by

$$\frac{p}{\rho^{\gamma}} = \text{constant}$$

The constant can be evaluated by considering the initial conditions of the nitrogen in the compartment at t = 0 (launch). Thus,

$$\frac{p}{\rho^{\gamma}} = \frac{p_o}{\rho_o{}^{\gamma}}$$

and by substituting

$$\rho = \frac{m}{VOL}$$

where VOL = free volume of the compartment, then the pressure in the compartment as a function of the mass of gas remaining in the compartment is

$$p = \frac{p_o\, m^{\gamma}}{(\rho_o\, VOL)^{\gamma}}$$

By combining either the subsonic or supersonic mass flow equation with the foregoing equation, a relation for the compartment pressure as a function of the external pressure is obtained. A number of computer programs have been set up which will give the exact relation for the compartment pressure as a function of time. For the Voyager analysis, these consisted of TRW's CDRC Program AFG4A and the G. E. Time Sharing Programs designated "VOYAGE" and "BLAHS."

NOMENCLATURE

A	area of vent, ft^2
C_d	discharge coefficient, dimensionless
m	mass of gas in compartment, slugs
$\dot{m}$	$= \frac{dm}{dt}$, mass flow of compartment gas, slugs/sec
p	compartment pressure, lb/ft^2 absolute
p_e	local external pressure at vent location, lb/ft^2
VOL	compartment free volume, ft^3
γ	ratio of specific heats
ρ	compartment gas density, $slug/ft^3$
ρ_o	compartment gas density at $t = 0$, $slug/ft^3$

3. NOSE FAIRING COMPARTMENT

The 12-1/2 degree frustum section of the nose fairing structure and the cylindrical section of the nose fairing can not resist large crushing pressures as efficiently as the 25 degree frustum nosecone. With this in mind, and the fact that burst pressures must be limited to 5 psi maximum, the location for the nose fairing vent was chosen at station 3880, at approximately the mid-section of the 12-1/2 degree frustum. This location was selected because the pressure coefficient distributions shown in Figures A-5 through A-13 indicate that the external pressure in this region will be near ambient. Therefore, with properly sized vents, only small crushing pressures will be induced on the 12-1/2 degree frustum and no crushing pressures will be induced on the cylindrical section. The somewhat significant crushing load on the 25 degree forward portion should not impair its structural integrity.

The recommended nose fairing compartment vent area is 3.0 ft^2 if the planetary vehicle compartments are vented aft, and is 8.9 ft^2 if they are vented forward. There are two reasons for this large difference:

a) If the planetary vehicle compartments are vented forward, their free volume must be considered in sizing the vent holes of the compartment they are venting into.

b) A plot of the maximum pressure lag between the internal and external pressure at the vent location station 3880 (Figure A-16) shows that very large pressure lags may exist if the vent area selected is small and if the vent and/or aerodynamic characteristics deviate only slightly from that anticipated.

In order to provide a compartment pressure which is approximately independent of angle of attack, the vent area should be equally distributed around the circumference of the shroud. The internal nose fairing compartment pressure history, together with the external pressure histories at the vent and other critical loading stations, are represented in Figure A-17. This figure indicates that for either fore or aft planetary compartment venting: The maximum collapsing pressure on the 25 degree nosecone leeward meridian forward of station 3968 is 4.1 psia and occurs at approximately 75 seconds after liftoff, at Mach 1.3. The maximum collapsing pressure on the 12.5 degree frustum is 0.45 psia and occurs at station 3849 at approximately 68 seconds after launch, at a Mach number of 1.05. Maximum bursting pressure at the 12.5 degree frustum/shroud cylinder interface (station 3749) is 3.4 psia and occurs at approximately 64 seconds after launch, at a Mach number of 0.90.

The internal pressure history of the nose fairing and the internal pressure of the forward planetary vehicle compartment is shown in Figure A-18. The maximum pressure differential is 0.8 psi at t = 62 seconds.

The vent areas were sized so that the pressure differential across the vents would never exceed 0.6 psi. Therefore, the upper limit for the internal pressure is the vent external pressure plus 0.6 psi. In order for the internal shroud pressure to remain within these limits, a study was conducted to investigate what effect leakage to either a low or high pressure region would have on the internal compartment pressures. A leakage area was assumed to exist at station 3964 on the nose fairing compartment. This location was chosen because it is the least desirable location, the region of lowest external pressure. The leakage analysis shows that if the total leakage area is less than 10 square inches the internal pressure would not fall more than 0.1 psi below the previously determined compartment internal pressures. Another critical area investigated for possible leakage was on the 25 degree nosecone forward of station 3964 where there is high

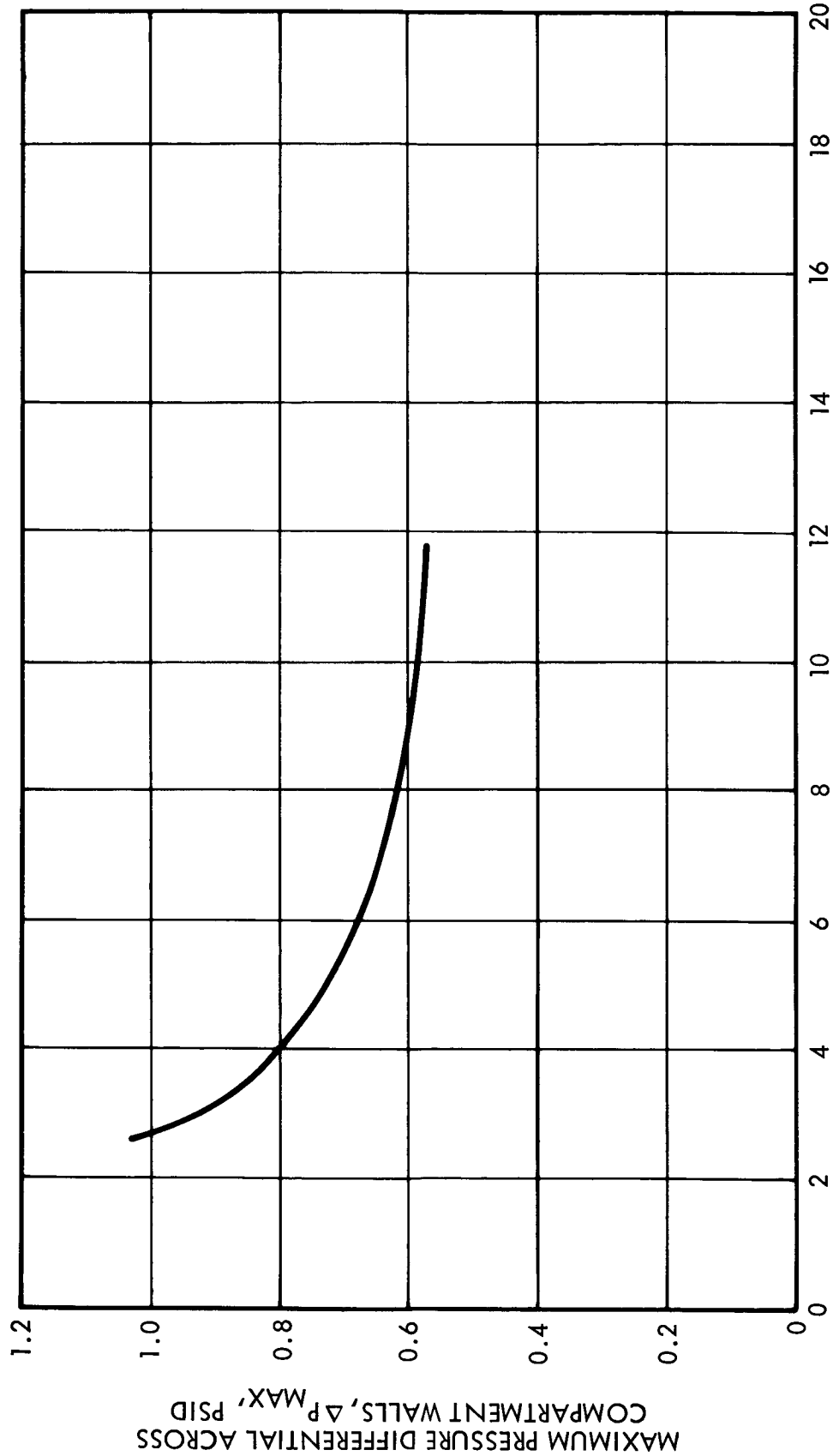

Figure A-16. Nose Fairing Compartment Pressure Lag Versus Vent Area

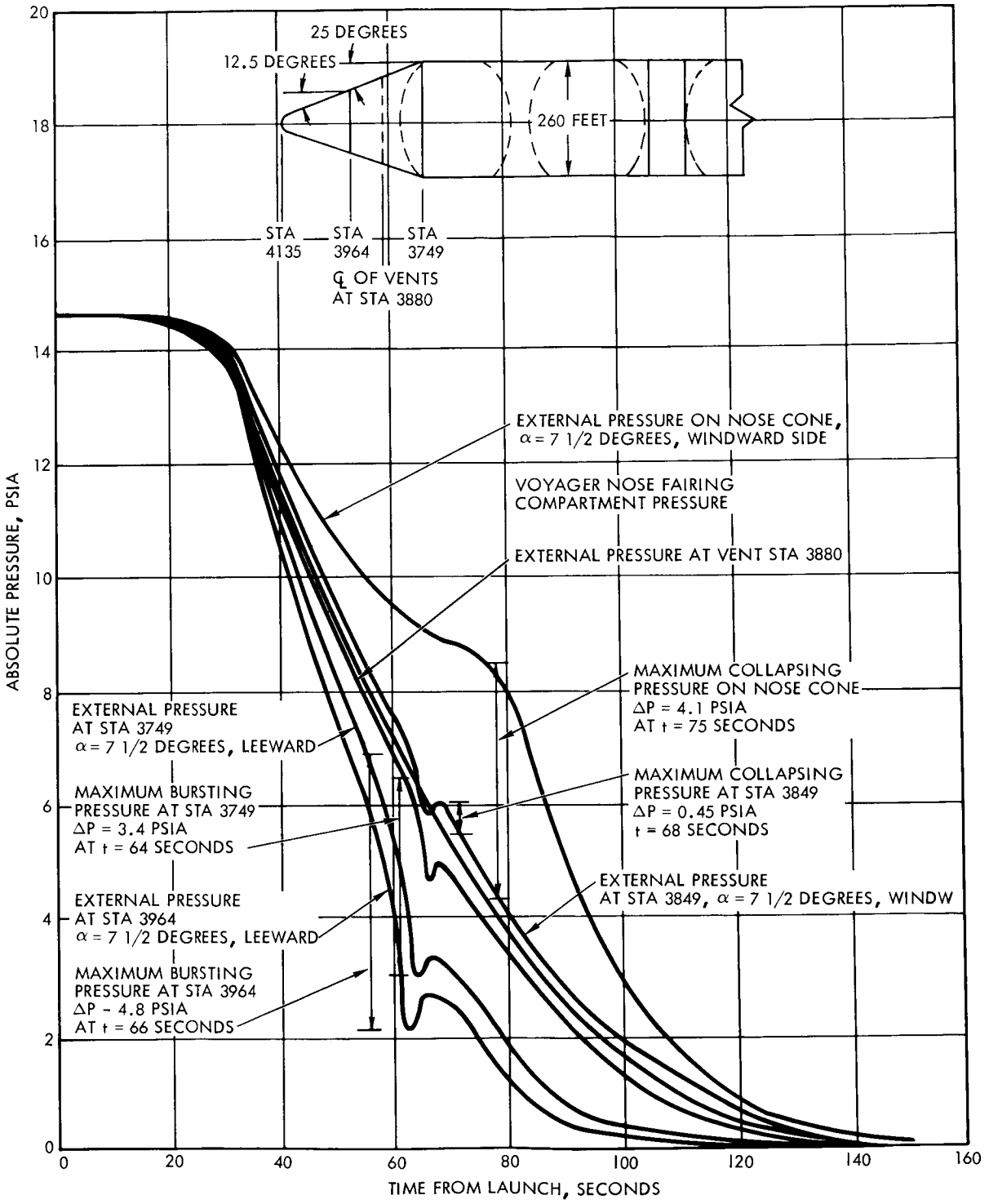

Figure A-17. Nose Fairing Compartment Internal and External Pressure Versus Time From Launch

external pressure. The study showed that if the total leakage area is less than 5 square inches the compartment pressure will not exceed the previously determined internal pressure by more than 0.1 psi.

Venting on the 12-1/2 degree frustum could result in excessive cross flow through the nose fairing compartment at angles of attack. Therefore, the effects of any inflow into the nose fairing compartment was investigated. In order to simplify this study, one-half of the maximum concept A vent area (4.44 square feet) was considered lumped on the windward surface of the nose fairing at station 3880, and one-half lumped on the leeward surface at station 3880, and the vehicle was considered at an angle of attack of α = 7-1/2 degrees. Figure A-19 shows that the internal pressure "follows" the external pressure on the windward surface more closely than it follows the external pressure on the leeward surface, deviating a maximum of $\sim$0.2 psia. This is a desirable result as it indicates that crushing loads will be lower on the compressive side of the nose fairing structure than on the tension side. At an angle of attack α = 7-1/2 degrees, the inflow reaches a velocity of 27 ft/sec and a dynamic pressure of 14.5 psia. It does not appear likely that any harmful loads could be imposed upon any nose fairing equipment or the biological compartment by the inflow conditions; however, it is conceivable that a local "hot spot" could be present on equipment in a direct line with the vent due to the rapidly rising stagnation temperature of the inflow after liftoff. Small deflectors to diffuse the inflow and direct it away from the equipment would be sufficient to relieve this condition since the overall compartment temperature would be low. This is due to the rapid venting of the compartment (in spite of the local inflow) causing the gas temperature in the compartment to drop.

4. SHROUD CENTER SECTION COMPARTMENT

The vent area required to adequately vent the shroud center section compartment is 0.87 ft^2 (vent concept A) and 1.5 square feet (vent concept B). In order to provide a compartment pressure which is approximately independent of angle of attack, the venting area should be equally distributed around the circumference of the section at station 3529. As explained before, the discharge coefficient is dependent both on the Mach number of the flow and the pressure ratio across the vent opening. A plot

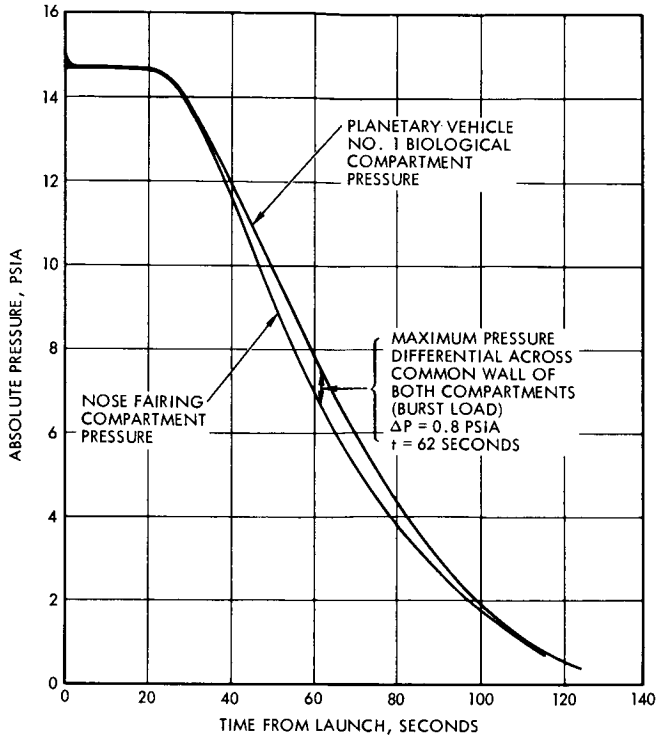

Figure A-18. Nose Fairing Compartment and FWD Planetary Vehicle Compartment Internal Pressure Versus Time From Launch

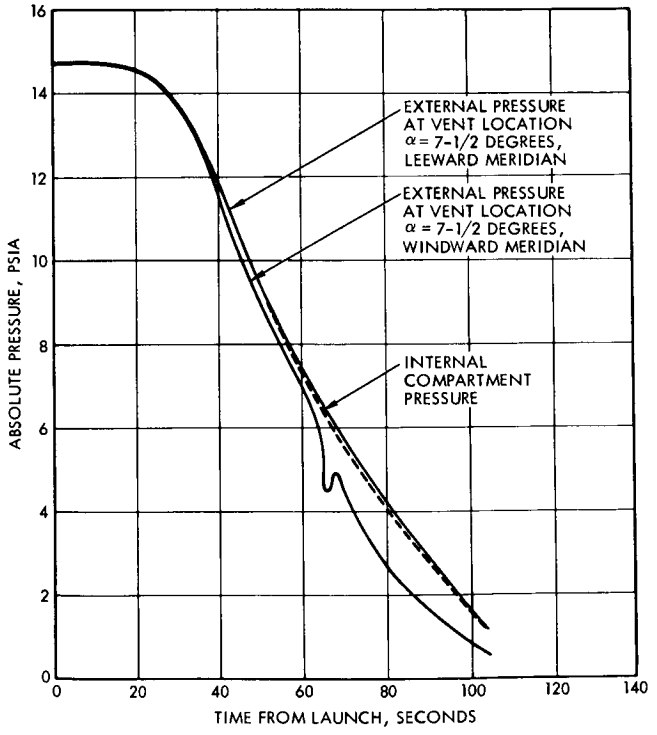

Figure A-19. Nose Fairing Compartment - Internal and External Pressure Versus Time From Launch

of the maximum pressure lag between the internal compartment pressure and the external pressure at the vent location is presented in Figure A-20. The required vent area will result in a maximum pressure lag of 1.7 psi. Assuming no leakage area, the internal compartment pressure history and the external pressure at the vent opening are presented in Figures A-21 and A-22 for vent concepts A and B, respectively. These figures show that for:

a) Concept A – The maximum bursting pressure on this section of structure, which occurs on the leeward meridian, is 2.4 psi and occurs at station 3597 at t = 62 seconds, when the Mach number = 0.85. The maximum bursting pressure on the leeward meridian at station 3461 is 1.7 psi and occurs at t = 67 seconds, when the Mach number = 1.0. No collapsing pressures occur on this section.

b) Concept B – The maximum bursting pressure at station 3597 is 2.2 psi and occurs 62 seconds after liftoff, at a Mach number of 0.85. The maximum bursting pressure at station 3461 is 1.3 psid and occurs 82 seconds after liftoff, at a Mach number of 1.6.

5. INSTRUMENT UNIT/FORWARD S-IVB SKIRT

The vent area required to adequately vent the instrument unit (I/U) compartment is 1.0 ft^2 for concept A and 2.4 ft^2 for concept B. A plot of the maximum pressure lag between the internal compartment pressure and the external pressure at the vent locations is shown in Figure A-23. The required vent area will result in a maximum pressure lag of 1.25 psi. Assuming no leakage in the I/U, the internal and external pressure histories at the vent are presented in Figure A-24. The maximum bursting pressure on the I/U compartment structure is 1.3 psia and occurs on the leeward meridian along the entire section length at t = 70 seconds and at a Mach number = 1.1. No collapsing pressure occurs on the structure. These conclusions apply to both vent concepts.

6. CAPSULE

The vents for the capsule were sized so that the pressure differental across the capsule would not exceed 3.0 psi. Because of the planetary vehicle compartment interchangeability requirement, the largest vent area

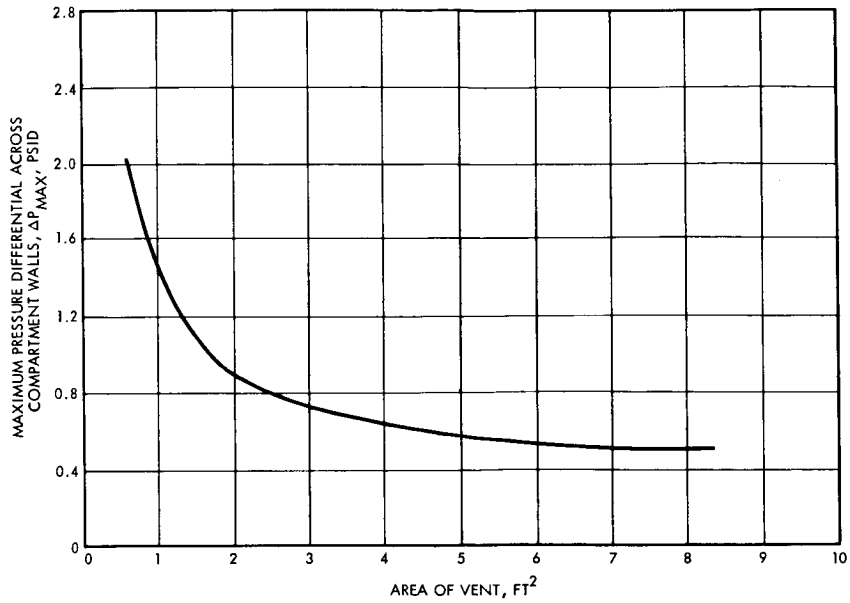

Figure A-20. Shroud Center Section Pressure Lag Versus Vent Area (Vent 3538)

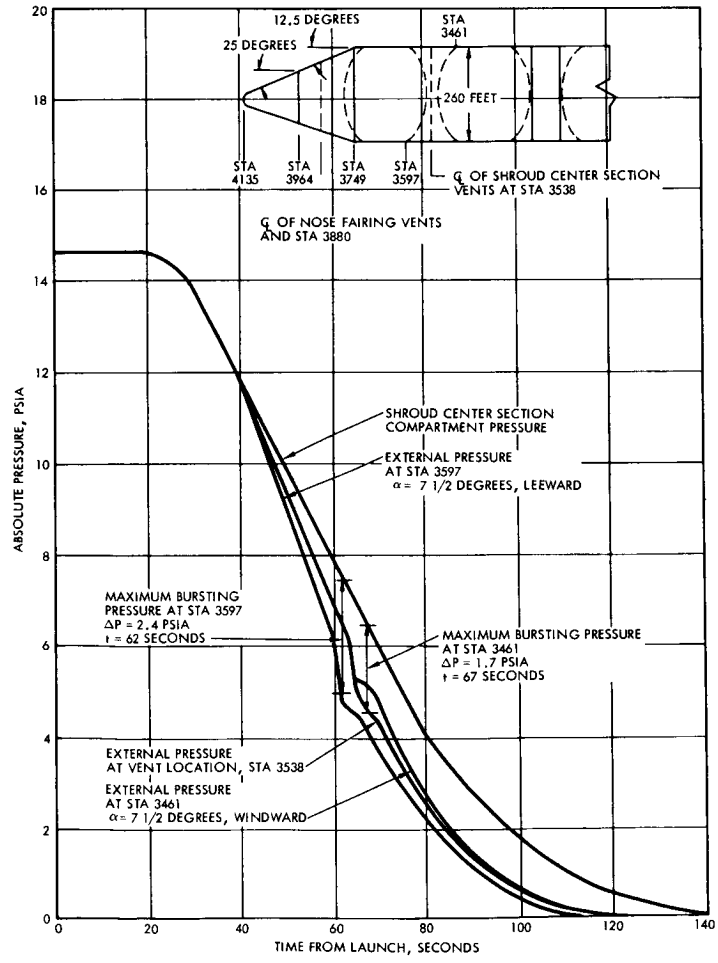

Figure A-21. Shroud Center Section Internal and External Pressure Versus Time From Launch (Concept A)

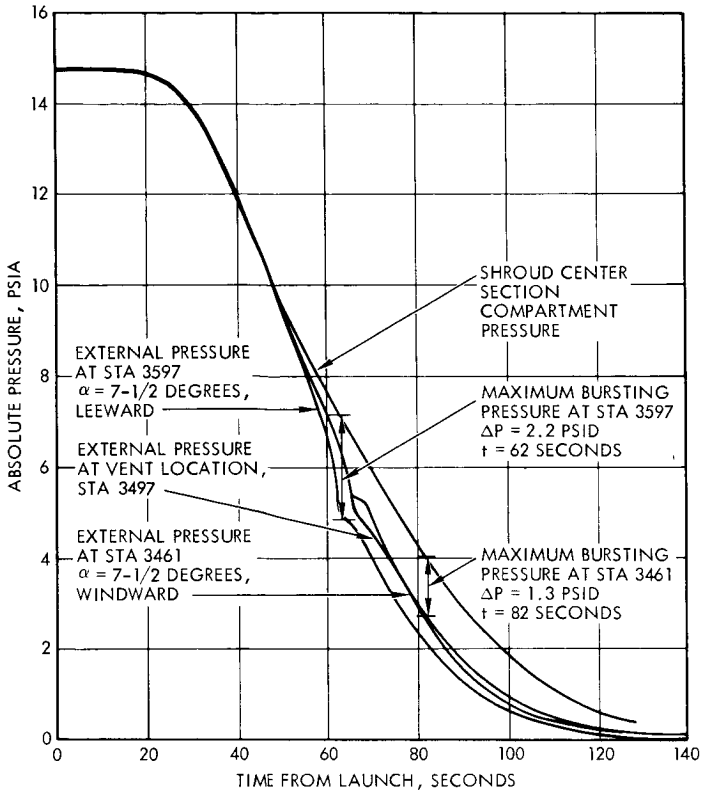

Figure A-22. Shroud Center Section Internal and External Pressure Versus Time From Launch (Concept B)

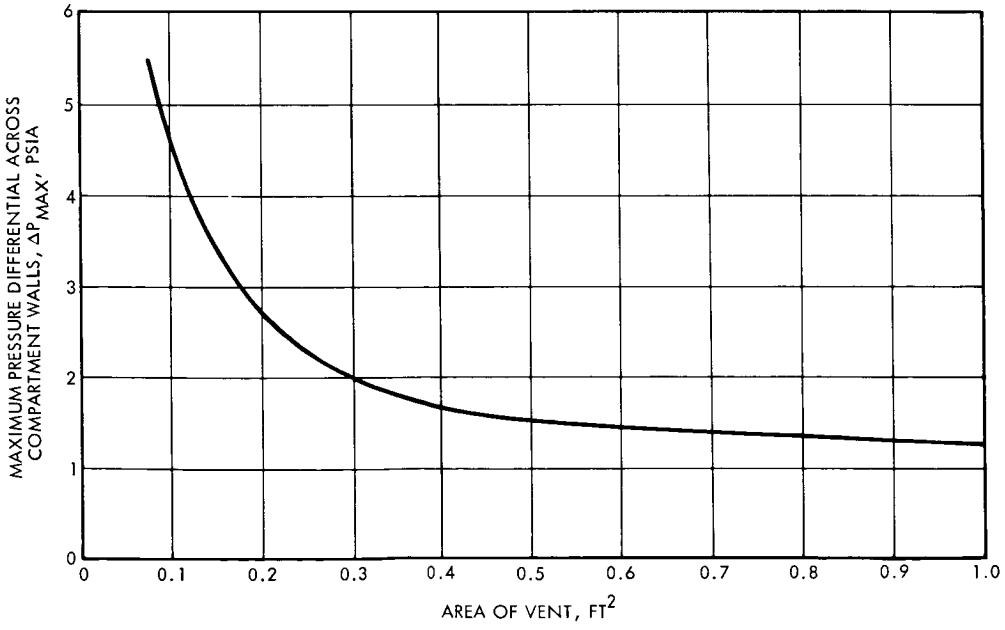

Figure A-23. Instrument Unit/FWD SIVB Skirt Pressure Lag Versus Vent Area

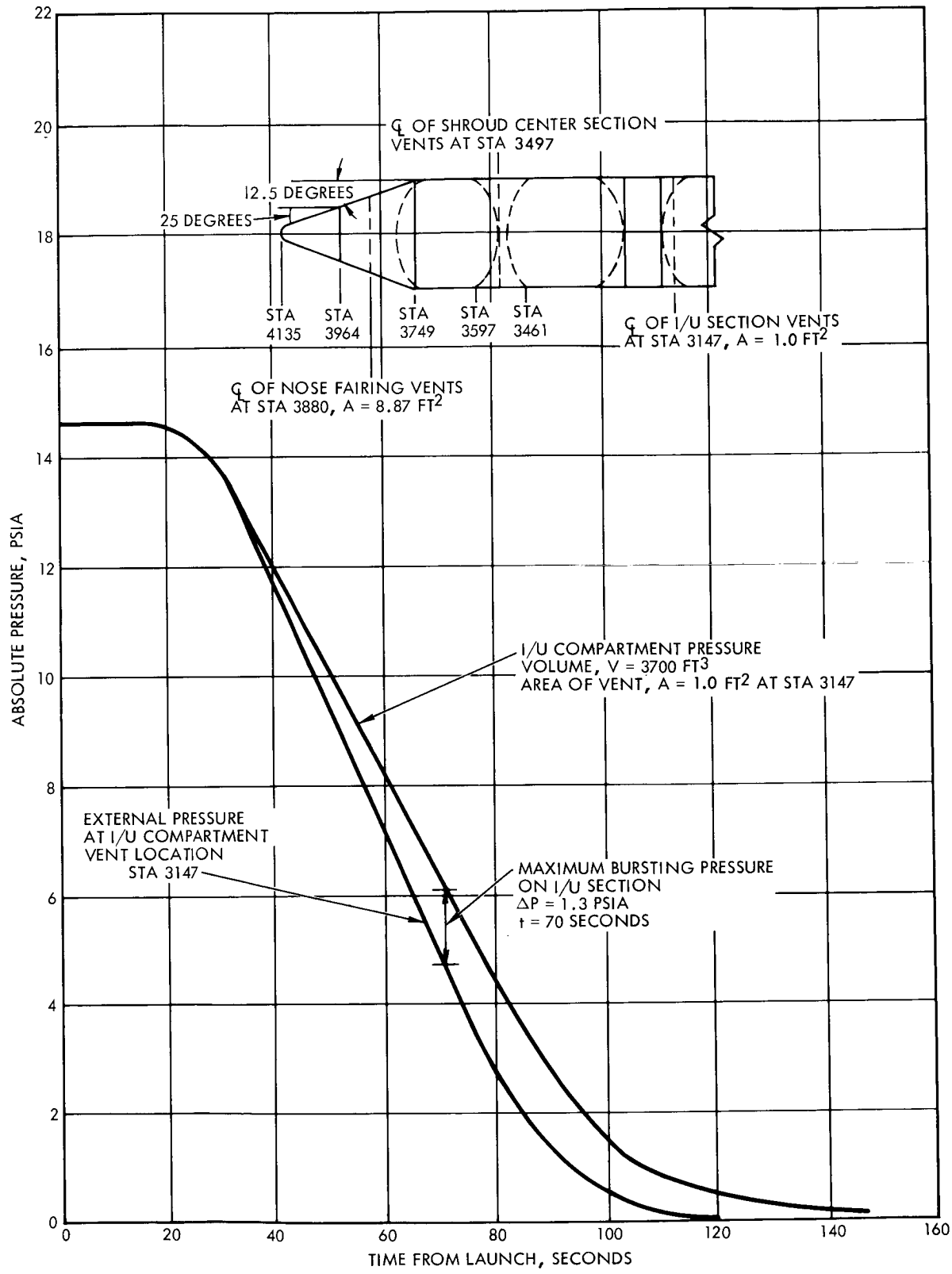

Figure A-24. Instrument Unit/FWD SIVB Internal and External Pressure Versus Time From Launch

required for either must be used for both capsules. The capsules vent into the interior of the planetary vehicle compartments which, for the analysis, are assumed to be at the external ambient pressure at the vent location. This assumption will result in larger pressure differentials across the capsule walls for a given capsule vent area than would actually be anticipated, since the exhaust pressure is typically higher than atmospheric. A plot of the variation of maximum pressure lag with vent area is presented in Figure A-24. Since there is no flow past the vent opening, the discharge coefficient is a function only of the pressure ratio across the vent opening. The capsule pressure lag is essentially independent of the vent concept.

In order to satisfy the contamination criteria, control valves (check valves) are required for the capsule vents. In this way there is assurance that there will be no flow into the capsule of possibly contaminate gas. As shown in Figure A-25, as the area of the valve opening decreases the pressure differential across the capsule wall increases very rapidly. It therefore is prudent to avoid a valve area which corresponds to this portion of the curve, for if the flow out is in any way restricted or if the valve area is slightly undersized, the differential will get very large. A 0.25 square foot unit area (minimum) is required.

The controlled valve remains closed as long as the pressure differential across the capsule is 3.0 psi or less. As the external (i.e., planetary vehicle compartment) pressure decreases and the pressure differential begins to exceed 3.0 psi, the valve begins to open. For small openings, the pressure may continue to build up, which will tend to open the valve farther. In its fully opened position, corresponding to the minimum required area, the pressure differential will be 3.0 psi. As described in Section 2.2, the controlled valves must have a solenoid-type override to completely vent down the shroud section before any separation events.

7. PLANETARY VEHICLE COMPARTMENT

The vents for each planetary vehicle compartment were sized such that the burst pressure differential across the compartment walls would not exceed 0.5 psi. Because of the compartment interchangeability requirement, the largest vent area required for either of the compartments must be used for both compartments. The forward and aft compartments vent

into volumes that are assumed to be at the external pressure that exists at the vent opening. A plot showing the variations of the maximum pressure lag with vent area is presented in Figure A-25. To satisfy the contamination criteria, controlled valves are required similar to those of the capsule as described in paragraph 6, except that the differential pressure is 0.5 psi.

Internal pressure histories for the capsules, planetary vehicle compartments and shroud compartments, together with the external pressures at the vent locations, are shown in Figures A-26 and A-27. The pressure lag across each element is essentially the same for both vent configurations.

A comparison of the internal pressure history of the shroud center section and the internal pressure of the forward planetary vehicle compartment is presented in Figure A-28 for vent concept A. The maximum pressure differential across the bulkhead is 0.5 psi and occurs at t = 62 seconds.

The internal pressure history of the instrument unit and the internal pressure of the aft planetary vehicle compartment is presented in Figure A-29 for vent concept A. The maximum pressure differential across this bulkhead is 0.5 psi and occurs at t = 95 seconds.

The pressure histories of the aft planetary vehicle compartment and the shroud center section are presented in Figure A-30 for vent concept B. The maximum burst pressure across the bulkhead is 0.8 psi and occurs 70 seconds after launch. This bulkhead is designed to withstand a burst pressure of 5.0 psi (Section 2.5.5).

8. RESULTS AND RECOMMENDATIONS

The analysis results and vent system design recommendations for Concept B are summarized below:

Nose Fairing Compartment

a) Required vent area, A = 3.0 ft^2. Eight vent holes will be equally spaced around the nose fairing circumference centered near station 3880;

b) Load

- The maximum collapsing pressure on the nosecone (forward of station 3964) is 4.1 psid and occurs at t = 75 seconds and at Mach number M = 1.3.

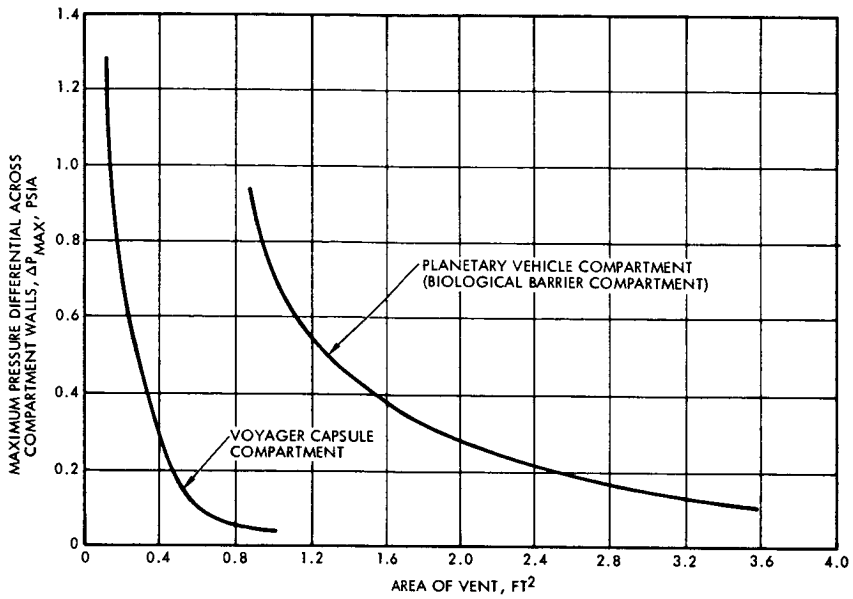

Figure A-25. Planetary Vehicle Compartment and Capsule Pressure Lag Versus Vent Area

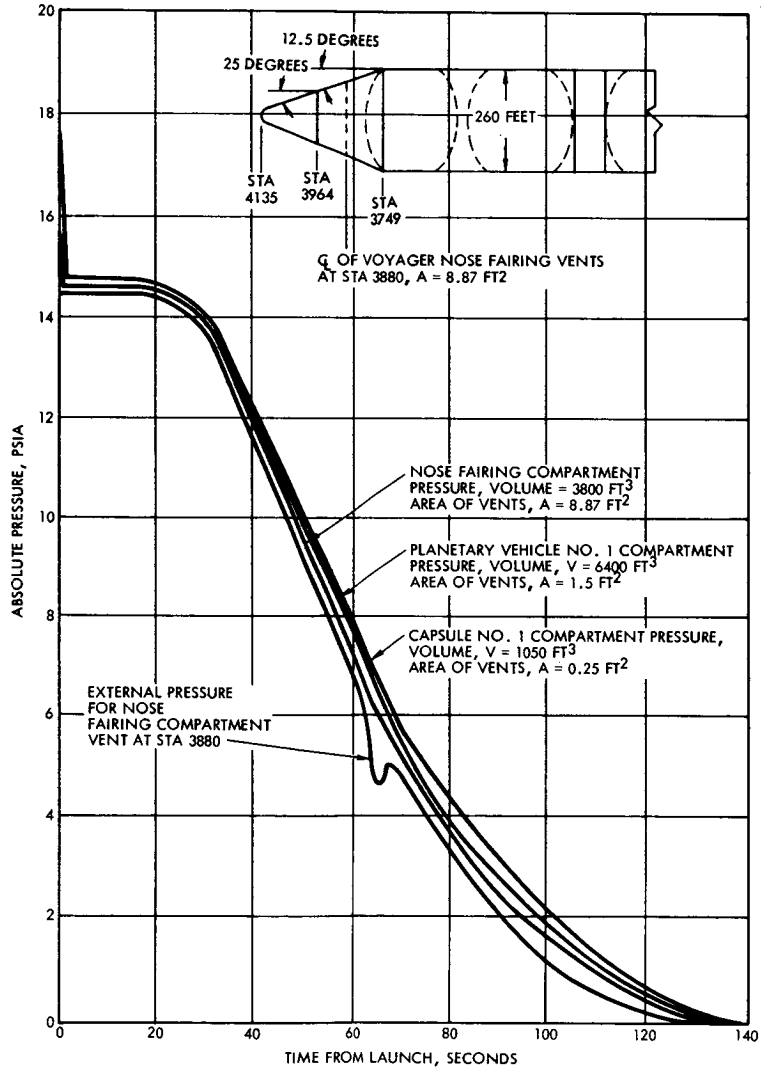

Figure A-26. Shroud Center Section, Aft Planetary Vehicle Compartment and Aft Capsule Pressures Versus Time From Launch

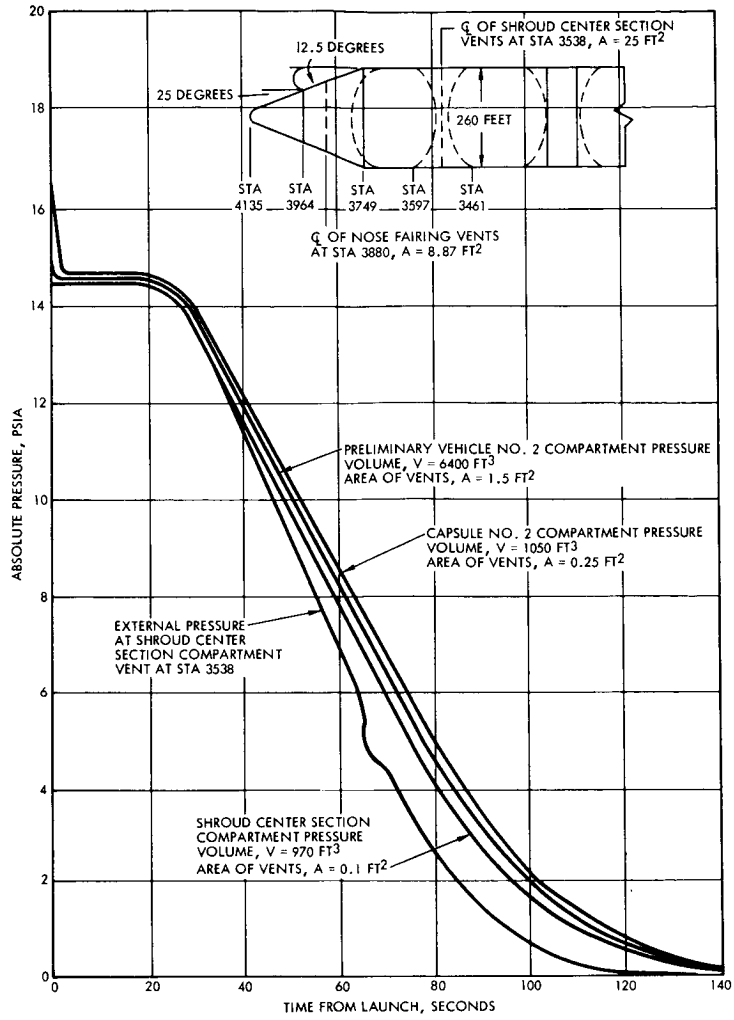

Figure A-27. Shroud Center Section, Aft Planetary Vehicle Compartment and Aft Capsule Pressures Versus Time From Launch

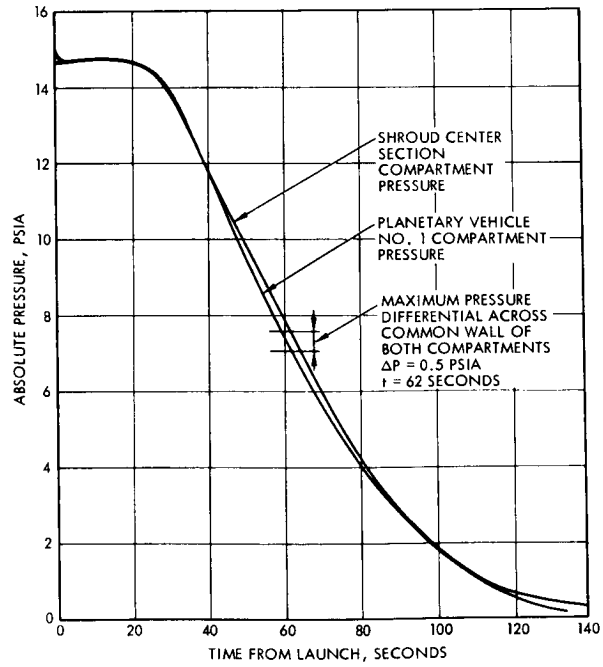

Figure A-28. Shroud Center Section and FWD Planetary Vehicle Compartment Internal Pressure Versus Time From Launch

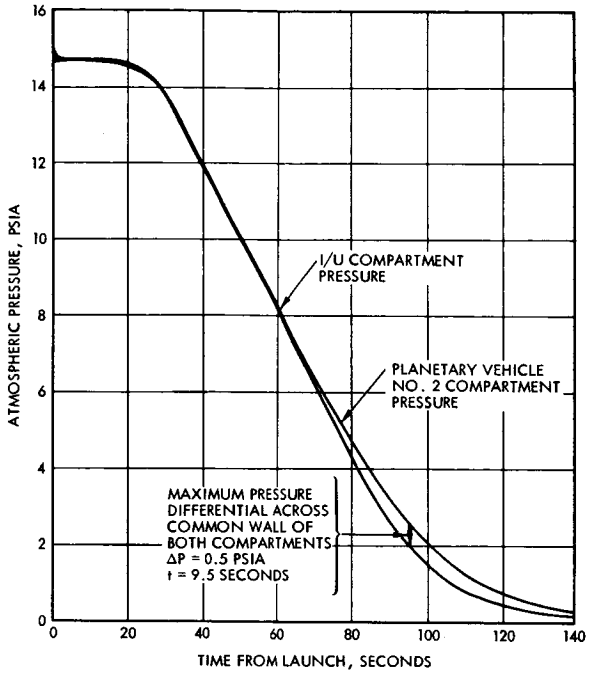

Figure A-29. Instrument Unit/FWD SIVB Skirt and Aft Planetary Vehicle Compartment Pressure Versus Time From Launch

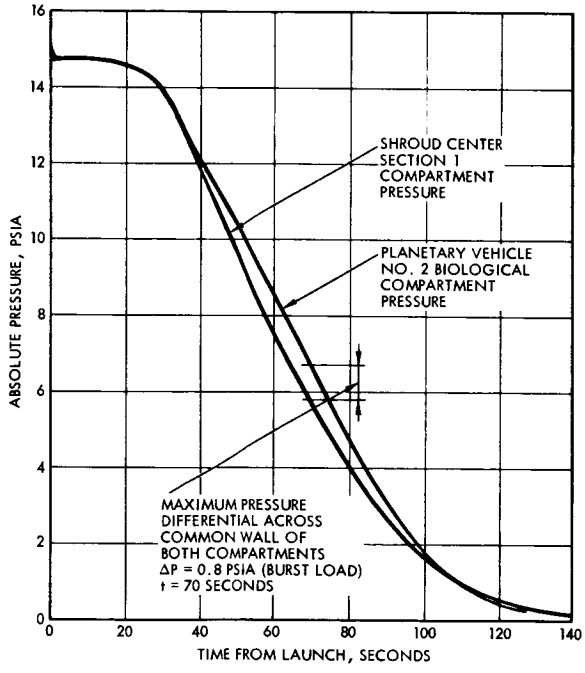

Figure A-30. Shroud Center Section and Aft Planetary Vehicle Compartment Internal Pressure Versus Time From Launch

- The maximum collapsing pressure on the 12-1/2 degree frustum section is 0.45 psid and occurs at station 3849 at t = 68 seconds and at Mach number M = 1.05.

- The maximum burst pressure in the nose fairing is 4.8 psid and occurs at the 25 degree nose cone - 12-1/2 degree frustum interface (station 3964) at t = 66 seconds and Mach number M = 0.95.

- The maximum burst pressure at the 12-1/2 degree frustum - cylinder interface (station 3749 is 3.4 psid and occurs at t = 64 seconds and Mach number M = 0.9.

c) Leakage area at station 3964 and station 3749 (low external pressure regions) may not exceed a total of 10 in^2.

d) Leakage area on the nose cone (forward of station 3964; high external pressure region) may not exceed 5 in^2.

e) No harmful loads will be imposed on any nose fairing equipment as a result of inflow under an angle of attack condition α = 7-1/2 degrees.

f) It is conceivable that a local "hot spot" could occur on equipment in a direct line with the vents due to rapidly rising stagnation temperature of the inflow approximately 50 seconds from liftoff. Small deflectors, to diffuse the inflow and direct it away from the equipment, would be sufficient to relieve this condition. The overall compartment temperature would be low.

Shroud Center Section Compartment

a) Required vent area, A = 1.5 ft^2. Eight vent holes will be equally spaced around the section circumference at station 3538.

b) Loads

- The maximum burst pressure is 2.2 psia and occurs at station 3597 at t = 62 seconds and Mach number M = 0.85.

- The maximum burst pressure at station 3461 is 1.3 psia and occurs at t = 82 seconds and Mach number, M = 1.6.

- No collapsing pressures occur on this section.

Instrument Unit Compartment

a) Required vent area, A = 2.4 ft^2. Eight vent holes will be equally spaced around the section circumferences at station 3264.

b) Loads

- The maximum burst pressure on the section is 1.3 psia and occurs at t = 70 seconds at Mach number M = 1.1.
- No collapsing pressures occur on the section.

Planetary Vehicle Compartments

a) Required vent area is A = 1.5 ft^2.

b) Controlled venting is recommended (check valves); use of four individual vents is recommended to enhance reliability.

Voyager Capsules

a) Required vent area, A = 0.25 ft^2.

b) Controlled venting is recommended (check valves).

REFERENCES

A-1 "Aerodynamic Data, WS-107A-2, "Transonic Wind Tunnel Tests, 3, 87 Percent Scale Model," G. L. Martin Company document, WDD-M-SR-57-40, March 1957.

A-2 "An Investigation to Determine the Discharge and Thrust Characteristics of Auxiliary-Air Outlets for a Stream Mach Number of 3.25," by Allen R. Vick, Langley Research Center, NASA TN D-1478, dated October 1962.

A-3 "An Investigation of the Discharge and Drag Characteristics of Auxiliary-Air Outlets Discharging into a Transonic Stream," by Paul E. Dewey and Allen R. Vick, Langley Aeronaturical Laboratory, NASA TN 3466, dated July 1955.

APPENDIX B

SPRING PERTURBATION ANALYSIS (GUIDED VERSUS UNGUIDED SEPARATION)

An analysis was performed to establish the probability of recontact of planetary vehicles and shroud elements during separation and to identify the optimum separation planes for nose fairing, shroud, and planetary vehicle separation. By varying the nose fairing separation plane and by treating the spring force perturbation as a two-part problem it is concluded that the optimum arrangement required guiding the planetary vehicle, locating the separation plane 4.6 feet below the capsule maximum diameter, and allowing the nose fairing and shroud center section to separate unguided.

The analysis initially assumes that the planetary vehicle separates unguided. The two spring perturbation forces are:

1) A lateral component of the spring force due to a misalignment of the force vector of the spring with the geometric axis of the spring.

Spring Force Misalignment

2) A lateral component of the spring force due to misalignment of the two ends of the spring.

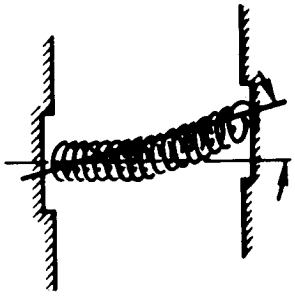

Spring Misalignment

A standard deviation (σ) for both lateral velocity and tumble rates was determined by taking the square root of the sum of the square of the expected variation in lateral velocity and tumble rates due to each spring.*

$$\sigma_{vf} = \sqrt{n\,(E_{vf})^2}$$

$$\sigma_{vs} = \sqrt{n\,(E_{vs})^2}$$

$$\sigma_{\omega s} = \sqrt{n\,(E_{\omega s})^2}$$

$$\sigma_{\omega f} = \sqrt{n\,(E_{\omega f})^2}$$

where

n = number of springs

E_{vf} = variation in lateral velocity due to spring force misalignment

E_{vs} = variation in lateral velocity due to spring misalignment

$E_{\omega s}$ = variation in rotation rate due to spring misalignment

$E_{\omega f}$ = variation in rotation rate due to spring force misalignment

The above standard deviations were computed for both spring force misalignment (assumed to be 1 percent of axial force) and spring misalignment (assumed to be 1^{o} of nominal).

The probability of failure can be determined by computing Z (the number of standard deviations needed for collision). Assuming a two-tailed distribution, the probability of failure (P) can be determined from tables relating (P) to Z. The values of Z for spring force misalignment (Z_s) are given by

$$Z_f = \frac{\delta_{collision}}{\delta_f}, \quad Z_s = \frac{\delta_{collision}}{\delta_s}$$

*TRW memo 67-3522.1-111, "Basic Language Program for Spring Separation of Spacecraft," 29 August 1967.

where

$\delta_{collision}$ = clearance between planetary vehicle and shroud

δ_f = lateral displacement due to spring force misalignment

$= t\left[\sigma_{vf} + \sigma_{\omega f}(h)\right]$

δ_s = lateral displacement due to a spring misalignment

$= t\left[\sigma_{vs} + \sigma_{\omega s}(h)\right]$

t = time necessary for planetary vehicle to fly out of shroud

h = height of planetary vehicle center of mass above the separation plane

The total probability of collision (P) is

$$P = P_f + P_s - P_f P_s$$

There are two questions of interest:

1) What is the maximum nose fairing length such that it can still be flown over the capsule maximum diameter unguided ?

2) What is the probability of collision for a guided planetary vehicle flying out of its shroud ?

Considering the first question let the design criterion be Z = 4.5 minimum which for a normal distribution gives a probability of collision of (P) = 3.4×10^{-6}.

The time allowed for the fairing to clear the maximum capsule diameter without collision is given by:

$$t = \frac{\delta_{collision}}{z\left[\sigma_v + \sigma_w(h)\right]}$$

where

δ collision = clearance between fairing and planetary vehicle

z = number of standard deviations needed for collision

σ_v = standard deviation for lateral velocity

σ_w = standard deviation for tumble rate

h = height of fairing c.g. above separation plane

Considering no c.g. offset of the fairing and a four-spring separation system (assuming 1^o misalignment and a lateral spring force of 1 percent of axial, per spring) giving the fairing a velocity of 2 ft/sec, t was found to be 2.3 seconds. The quantities used in the above analysis are as follows:

$$\delta_{collision} = 3 \text{ in.}$$

$$\sigma_v = 0.186 \text{ in./sec}$$

$$\sigma_w = 0.0012 \text{ rad/sec}$$

$$h = 187 \text{ in.}$$

Although there is only a 2-inch nominal radial clearance between capsule maximum diameter and the limits of the planetary vehicle dynamic envelope, 3 inches were used in this calculation as being more representative of the physical shroud. The value of h used is equivalent to a fairing length extending to 4.6 feet aft of the capsule maximum diameter.

Thus, it is concluded that such a fairing can clear the capsule without guidance with a probability of collision of 3.4×10^{-6}.

The problem of a guided planetary vehicle will now be considered. The planetary vehicle will be spring ejected, but will be guided out of its shroud hole. It has been assumed that the rollers used to guide the planetary vehicle will be located at the separation plane. The planetary vehicle will be restrained from moving laterally, but will not be rotationally restrained.

Two other variations have been included. They are a c.g. offset of 0.25 inch and a spring position offset of 0.1 inch. The spring position offset will be lumped together with the c.g. offset and a 0.35 inch c.g. offset will be the only variation considered.

The value of z as a function of time was computed for the above situation. The minimum z was found to be approximately 15, which corresponds to a probability of 10^{-50}.

The equation used was

$$z = \frac{\delta_{collision}}{t\sigma_w h}$$

where

$\delta_{collision}$ = clearance between planetary vehicle and shroud

t = time after separation

σ_w = standard deviation of the tumble rate due to 0.35 c.g. offset

k = height from rollers to top of shroud hole

$$k = k_o - v_s t$$

where

k_o = initial height of shroud opening above planetary vehicle separation plane

v_s = velocity of planetary vehicle

The quantities used in the above analysis are as follows:

$\delta_{collision}$ = 3 in.

σ_w = 0.000338 rad/sec

k_o = 163 in.

v_s = 12 in./sec

It is concluded that no rotational control in guiding planetary vehicles is required, and that the collision probabilities are very small with a shroud separation plane as far forward as the capsule maximum diameter.

APPENDIX C

NOSE FAIRING COLLISION PROBABILITY ANALYSIS

The probability that the nose fairing and stage will collide was calculated with the aid of "Description of Design Considerations for the Voyager 1971 Spacecraft Utilizing the Saturn III Launch Vehicle Configuration," JPL Report PD-86, June 1966. The probability of impact (P_i) between the nose fairing and the stage is (see Figure C-1)

$$P_i = \frac{r^2}{2\sigma_R^2} e^{-R^2/2\sigma_R^2}, \quad \text{for } \sigma_R >> r$$

where

r = impact radius

R = normal distance between fairing and launch vehicle

σ_R = position dispersion of the fairing and launch vehicle

The parameter σ_R is the root sum of the squares of the 1σ position uncertainties of the fairing (σ_s) and launch vehicle (σ_v)

$$\sigma_R = \sqrt{\sigma_S^2 + \sigma_V^2}$$

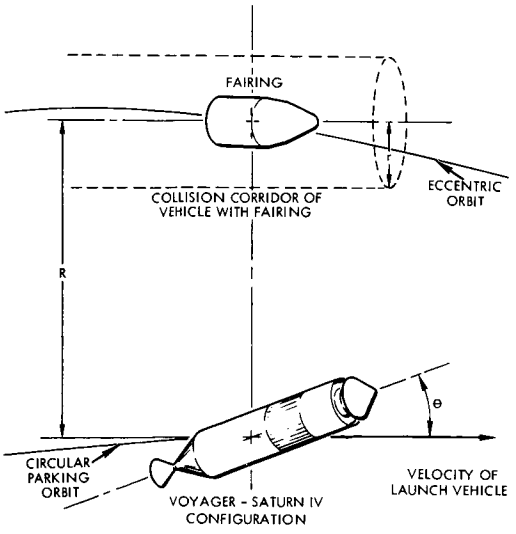

Figure C-1. Geometry of Collision

The impact radius can be expressed as

$$r = \frac{s + \sin\theta \left(\ell + \frac{d}{\tan\theta} \right)}{2}$$

where

s is the diameter of the fairing

ℓ is the length of the launch vehicle

d is the diameter of the launch vehicle

θ is the angle between longitudinal axis of launch vehicle and velocity of launch vehicle with respect to shroud

For maximum r, $\theta = 65.8^{\circ}$. With ℓ, s, and d given, $r_{max} = 9.31 \times 10^{-3}$ mile. Maximum r was used in all probability calculations.

The launch vehicle dispersion (σ_v) was taken to be 10 meter/sec of burning time, where the burning time was calculated from

$$T = \sqrt{\frac{2S}{a}}$$

and the S is the arc distance of the fairing ahead of the stage at reignition.

The dispersion of the fairing (σ_s) can be obtained from

$$\sigma_s = \sigma_E \Delta V T_c$$

where T_c is the coast time from ejection of the fairing to reignition, σ_E is the 1σ execution accuracy which was taken to be 0.01, and ΔV is the separation velocity. In the table below, collision probability is given for the critical coast times from ejection to reignition for various V's.

Table C-1. Collision Probability

T_c (min)	ΔV = 1(ft/sec)	$\Delta V = 2$	$\Delta V = 4$	$\Delta V = 6$	$\Delta V = 8$
14	2.06×10^{-4}	7.38×10^{-10}	1.79×10^{-18}	3.86×10^{-25}	2.21×10^{-36}
15	9.16×10^{-6}	4.82×10^{-14}	4.22×10^{-29}	1.29×10^{-40}	7.33×10^{-59}
16	2.01×10^{-6}	2.91×10^{-22}	5.57×10^{-52}	8.02×10^{-75}	–
17	5.11×10^{-8}	4.30×10^{-43}	–	–	–
18	2.31×10^{-10}	–	–	–	–
21	2.00×10^{-30}	–	–	–	–

Table C-1. Collision Probability

T_c (min)	ΔV = 1(ft/sec)	$\Delta V = 2$	$\Delta V = 4$	$\Delta V = 6$	$\Delta V = 8$
14	2.06×10^{-4}	7.38×10^{-10}	1.79×10^{-18}	3.86×10^{-25}	2.21×10^{-36}
15	9.16×10^{-6}	4.82×10^{-14}	4.22×10^{-29}	1.29×10^{-40}	7.33×10^{-59}
16	2.01×10^{-6}	2.91×10^{-22}	5.57×10^{-52}	8.02×10^{-75}	—
17	5.11×10^{-8}	4.30×10^{-43}	—	—	—
18	2.31×10^{-10}	—	—	—	—
21	2.00×10^{-30}	—	—	—	—

APPENDIX D

POST-INJECTION COLLISION PROBABILITY ANALYSIS

The planetary vehicles are separated by a series of spring systems after insertion into the Mars transfer orbit. The separation sequence will be as follows: upper planetary vehicle, shroud center section, lower planetary vehicle (see Figure D-1).

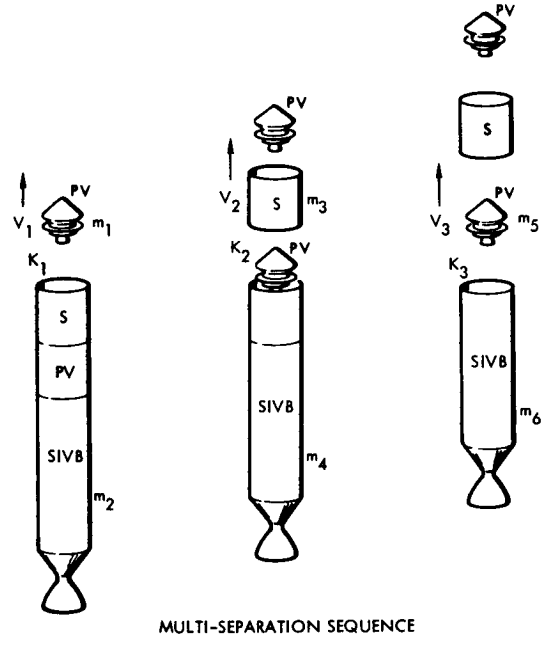

Figure D-1. Post-Separation Collision Probability Model

There are three design criteria for the spring separation system:

1) The spring separation system of each planetary vehicle to be interchangeable.

2) The spring separation system used to separate the nose fairing must be the same as the one used to separate the shroud center section.

3) The spring system should be designed so that the nominal velocity of the shroud center section falls midway between the nominal velocities of the two planetary vehicles. This would yield the same probability of collision between upper planetary vehicle and shroud section as between the shroud section and lower planetary vehicle assuming any variation in each separation does not affect the other separations.

To establish the likelihood of collision* is to establish what the probability (P) is that any one component will have the same velocity as any other component due to variation in the nominal values of separation potential energies. This analysis is conservative by neglecting the time lag between separation events. Covariance, or the effect of one separation on another, was included in the analysis. Lateral and rotational motion during separation was not included. This analysis is clearly conservative then since lateral dispersions are ignored.

The following parameters were used in the analysis: (Figure D-1)

V_1 = velocity of upper planetary vehicle

V_2 = velocity of shroud center section

V_3 = velocity of lower planetary vehicle

K_1 = twice the potential energy of the first separation

K_2 = twice the potential energy of the second separation

K_3 = twice the potential energy of the third separation

m_1 = mass of upper planetary vehicle

m_2 = mass of shroud center section, lower planetary vehicle, and S-IVB

m_3 = mass of shroud center section

m_4 = mass of lower planetary vehicle and S-IVB

m_5 = mass of lower planetary vehicle

m_6 = mass of S-IVB

The velocities above are with respect to a coordinate system that has the velocity of the entire stage after completion of Mars trajectory insertion, but before the first planetary vehicle separation.

*TRW Memo 67-3343.5-19, "Voyager Shroud Separation Studies," 19 September 1967.

Using conservation of energy and momentum the velocity of each component can be determined:

$$V_1 = (K_1/a_1)^{1/2}$$

$$V_2 = (K_2/a_2)^{1/2} - (K_1/a_3)^{1/2}$$

$$V_3 = (K_3/a_4)^{1/2} - (K_2/a_5)^{1/2} - (K_1/a_3)^{1/2}$$

where

$$a_1 = m_1\left(1 + \frac{m_1}{m_2}\right)$$

$$a_2 = m_3\left(1 + \frac{m_3}{m_4}\right)$$

$$a_3 = m_2\left(1 + \frac{m_2}{m_1}\right)$$

$$a_4 = m_5\left(1 + \frac{m_5}{m_6}\right)$$

$$a_5 = m_4\left(1 = \frac{m_4}{m_3}\right)$$

Using design criteria, 1, 2, and 3 which state that

$K_1 = K_3 = cK$ (due to design criterion 1)

$K_2 = K$ (a known quantity due to design criterion 2)

$\frac{V_1 + V_3}{2} = V_2$ (design criterion 3)

the constant c relating the two separation potential energies can be determined as

$$c = \frac{\left(\frac{2}{\sqrt{a_2}} + \frac{1}{\sqrt{a_5}}\right)^2}{\left(\frac{1}{\sqrt{a_3}} + \frac{1}{\sqrt{a_4}} + \frac{1}{\sqrt{a_1}}\right)^2}$$

Given the ΔV of the nose fairing separation and the spring constant K of the separation springs used to attain it, the required spring constants for the remaining separations can be calculated using the above design criteria and equations.

The probability that any section will collide with another can be obtained by dividing the relative velocity between the two sections by the standard deviation (σ) in this quantity and using that number (z) of standard deviations to determine the probability from a table of two-tailed normal distributions. The values of z considered will be as follows:

$$z_1 = \frac{V_1 - V_2}{\sigma_1}$$

$$z_2 = \frac{V_2 - V_3}{\sigma_2}$$

$$z_3 = \frac{V_1 - V_3}{\sigma_3}$$

Where the standard deviations σ_1, σ_2, and σ_3 are given by:

$$\sigma_1 = \sqrt{\text{Var}(V_1) + \text{Var}(V_2) - 2\,\text{Cov}\,(V_1 V_2)}$$

$$\sigma_2 = \sqrt{\text{Var}(V_2) + \text{Var}(V_3) - 2\,\text{Cov}\,(V_2 V_3)}$$

$$\sigma_3 = \sqrt{\text{Var}(V_1) + \text{Var}(V_3) - 2\,\text{Cov}\,(V_1 V_3)}$$

The terms under the radical signs are elements of the covariance matrix:

$$\left[\text{Cov.}\right] = \begin{bmatrix} \text{Var}\,(V_1) & \text{Cov}\,(V_1 V_2) & \text{Cov}\,(V_1 V_3) \\ \text{Cov}\,(V_2 V_1) & \text{Var}\,(V_2) & \text{Cov}\,(V_2 V_3) \\ \text{Cov}\,(V_3 V_1) & \text{Cov}\,(V_3 V_2) & \text{Var}\,(V_3) \end{bmatrix}$$

This matrix is obtained as follows:

$$\left[I\right] \quad \left[\Delta K^2\right] \quad \left[I\right]^T \quad = \quad \left[\text{Cov.}\right]$$

where $\left[I \right]$ is the influence matrix and $\left[\Delta K^2 \right]$ is a diagonal matrix with the variance of the K's (twice the potential energy of separation) on the diagonal.

The influence matrix has the form:

$$\begin{bmatrix} \frac{\partial V_1}{\partial K_1} & & \\ \frac{\partial V_2}{\partial K_1} & \frac{\partial V_2}{\partial K_2} & \\ \frac{\partial V_3}{\partial K_1} & \frac{\partial V_3}{\partial K_2} & \frac{\partial V_3}{\partial K_3} \end{bmatrix}$$

where

$$\frac{\partial V_1}{\partial K_1} = 1/2\ (K_1)^{-1/2}$$

$$\frac{\partial V_2}{\partial K_2} = 1/2\ (K_2)^{-1/2}$$

$$\frac{\partial V_3}{\partial K_3} = 1/2\ (K_3)^{-1/2}$$

$$\frac{\partial V_2}{\partial K_1} = -1/2\ (K_1)^{-1/2}$$

$$\frac{\partial V_3}{\partial K_1} = -1/2\ (K_1)^{-1/2}$$

$$\frac{\partial V_3}{\partial K_2} = -1/2\ (K_2)^{-1/2}$$

The variance matrix has the form:

$$\begin{bmatrix} (\Delta cK)^2 & & \\ & [\Delta K]^2 & \\ & & [\Delta cK]^2 \end{bmatrix}$$

After substitution of the above into the equation for the covariance matrix its terms take the form:

$$\text{Var}(V_1) = \left(\frac{\partial V_1}{\partial K_1} \quad \Delta cK\right)^2$$

$$\text{Var}(V_2) = \left(\frac{\partial V_2}{\partial K_1} \quad \Delta cK\right)^2 + \left(\frac{\partial V_2}{\partial K_2} \quad \Delta K\right)^2$$

$$\text{Var}(V_3) = \left(\frac{\partial V_3}{\partial K_1} \quad \Delta cK\right)^2 + \left(\frac{\partial V_3}{\partial K_2} \quad \Delta K\right)^2 + \left(\frac{\partial V_3}{\partial K_3} \quad \Delta cK\right)^2$$

$$\text{Cov}(V_1V_2) = \text{Cov}(V_2V_1) = \frac{\partial V_2}{\partial K_1} \frac{\partial V_1}{\partial K_1} (\Delta cK)^2$$

$$\text{Cov}(V_2V_3) = \text{Cov}(V_3V_2) = \frac{\partial V_2}{\partial K_1} \frac{\partial V_3}{\partial K_1} (\Delta cK)^2 + \frac{\partial V_3}{\partial K_2} \frac{\partial V_2}{\partial K_2} (\Delta K)^2$$

$$\text{Cov}(V_1V_3) = \text{Cov}(V_3V_1) = \frac{\partial V_3}{\partial K_1} \frac{\partial V_1}{\partial K_1} (\Delta cK)^2$$

Now σ_1, σ_2, and σ_3 can be calculated, and in turn the z_i can be calculated. These values of z_1, z_2, and z_3 now determine, with suitable tables of probability, the probability (P_1, P_2, and P_3) of collision between the first planetary vehicle and the shroud midsection, the shroud midsection and the second planetary vehicle, and, included for completeness, the probability of collision between the first and second planetary vehicles.

Given the component masses, velocities and spring rates and assuming a 2 percent deviation in the spring constant, collision of any two elements would occur in less than one time in one million.

As an example let the nose fairing $\Delta V = 1$ ft/sec and deviations in K and cK be 2 percent (or $\Delta cK = 0.02$ cK and $\Delta K = 0.02$ K) and masses and K's be:

$$m_1 = 69.4 \text{ lb-in./sec}^2$$

$$m_2 = 178.2$$

$$m_3 = 13.7$$

$$m_4 = 164.5$$

$$m_5 = 69.4$$

$$m_6 = 95.1$$

$$K = 1125 \text{ lb-in.}$$

$$cK = 6060$$

The computations were performed on a digital computer giving for the above case $z_1 = 17$, $z_2 = 19.8$, $z_3 = 36.6$, and $c = 5.38$. The probabilities corresponding to the above z's are $P_1 \approx 10^{-64}$, and $P_2 \approx 10^{-88}$ and $P_3 \approx 10^{-283}$.

For the recommended nose fairing separation velocity of 2 ft/sec the collision probabilities will be correspondingly less.

APPENDIX E

SEPARATION SHOCK ENVIRONMENTS

The planetary vehicles will be subjected to shock loads generated by the pyrotechnic separation mechanisms. Experience has shown that separation shocks produced by explosive (or pyrotechnic) devices may cause malfunctions or deterioration of performance in electronics and electromechanical packages located near or in a direct shock transmission path. The severity of the shock environment will be determined by the type of separation methods employed. Specification of shock tests will be based on structural configuration and location of equipment and components. References E-1, E-2, and E-3 describe the types of environments encountered with pyrotechnic devices.

The shroud and planetary vehicle separation concept results in a total of four separate shock events: the nose fairing and upper shroud separation, the forward planetary vehicle's separation from its adapter, the shroud center section, and finally the second planetary vehicle separation. But since the nose fairing separation plane is far from the shroud/adapter interface, structural attenuation of the shock will render it harmless. The only shock loading of concern then, is planetary vehicle separation.

The shock environment for sensitive equipment will be that which is transmitted through a series of structural members and discontinuities. These structural discontinuities (which constitute impedance mismatches) include panel attachment points, the equipment module/propulsion module interface and equipment component attachment brackets on the equipment module.

The wide variation in the severity of the separation shock with type of separation device and amount of intervening structure, combined with the difference in type of shock sensitive equipment and distribution of the equipment locations, results in the requirement for specification of more than one shock level for realistic equipment design and test. The shock test level specified for a component or group of components will be based on structural location (by designated zones) and the most severe anticipated shock from planetary vehicle separation.

The designation of at least three zones may be required. The first zone would include bracket mounted components in the equipment module. Equipment and components on the upper portion of the equipment module structure near the capsule adapter would be in a second zone, and equipment attached to the propulsion module near the separation plane would be in the third zone.

1. SEPARATION DEVICES

The standard types of explosive separation devices employed are electro-explosive/frangible nuts and bolts. The fasteners are fractured or destroyed so that adjacent units are free to separate. Explosive nuts produce the mildest shocks.

When the fasteners are fractured, the peak amplitude accelerations will be confined to a relatively small area around each joint. The structural modes excited in the radial direction are dependent on the number and spacing of the explosive bolts or nuts. The transient accelerations produced by the springs extending and separating the units will be primarily in the longitudinal direction and of insignificant magnitude compared to the explosive shock.

2. EXPLOSIVE SEPARATION SHOCK DESCRIPTION

2.1 Shock Characteristics

The characteristic transient excitation or shock due to explosive separation is a complex wave form consisting of high amplitude, wide frequency range acceleration components. In many instances, the shock pulse can be described as a very short duration random vibration excitation with modulated peak accelerations. The peak accelerations in structures at separation planes typically range from several hundred to several thousand g's, and the frequencies of the acceleration components range up to 10,000 Hz (which is usually the upper frequency limit of measuring systems). Typical pyrotechnic shock data are shown in Figure E-1.

A shock pulse measured at a considerable distance from a Delta fairing separation plane in a recent test where explosive nuts were used

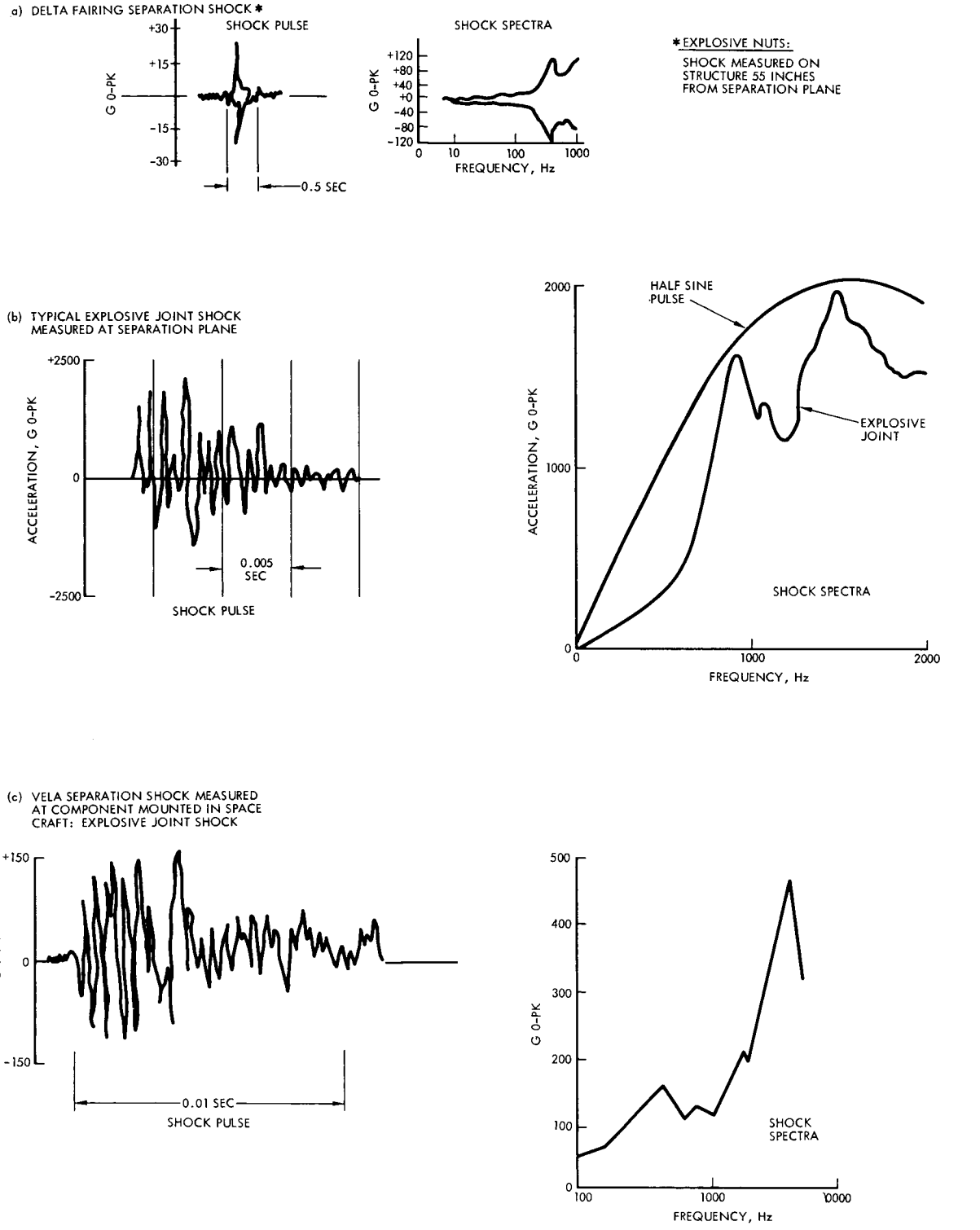

Figure E-1. Pyrotechnic Shock Data: Typical Curves for Release Device Explosions

for separation is shown in Figure E-1(a). The peak accelerations were approximately 25 g. The associated shock response spectra also shown in Figure E-1(a) indicate that elements of a component mounted at the measurement location could experience 60 to 120 g (0-peak) acceleration in the frequency range 300 to 1000 Hz. A typical acceleration record of separation shock on structure adjacent to an explosive joint (skin cutting mechanism) is shown in Figure E-1(b). This represents one of the more severe shock environments encountered by spacecraft components. However, this level of shock excitation would apply only to components attached to the joint structure within a relatively short distance from the separation plane. The response of elements of a component to this type of shock excitation is partially defined by the associated acceleration (or shock) spectra curve shown in Figure E-1(b). For comparison, the response spectra for a half sine shock pulse are also shown.

The type of shock pulse at the base of a component located on spacecraft structure at some distance from a fairing separation joint is illustrated by Vela test data shown in Figure E-1(c). The magnitude of the peak acceleration is of course much less than that measured at the separation joint. The shock response spectra associated with the excitation at a Vela component base are also shown in Figure E-1(c).

2.2 Structural Response

The nature of the damaging transient excitation is such that there is poor repeatability for the response of apparently identical structural samples to the shock, and there is wide variation in response in different parts of the structure. The dynamic response characteristics of equipment support structure involve complex modes of excitation, which are important to consider only in the local region of the equipment.

The localized structural response resulting from the transient excitation is highly dependent on the separation mechanism and the vehicle structural design in the region of separation. The separation shock excites many structural modes, but the damaging portion of the shock excitation will have frequency components associated with the local natural frequencies and the higher modal frequencies of the overall structure.

3. STRUCTURAL ATTENUATION

Pyrotechnic shock measurements have shown that in typical spacecraft payload structure there is a marked decrease in acceleration amplitude with increase in length and complexity of the transmission path. Reduction ratios of as much as 1 to 10 are associated with distance increases of 10 to 1 (the relationship is not necessarily linear). The amount of attenuation of shock magnitude is related more to the number of structural discontinuities (stiffeners, bulkhead and stringer attach points) and mass loading by components along the transmission path rather than to structural (material) damping. The transient acceleration magnitude reduction is 40 or 50 percent across a structural stiffener. The addition of a massive (relative to the weight of local attachment structure) component at a measurement location in the shock transmission path has been observed to reduce the shock magnitude by greater than 50 percent.

4. DETERMINATION OF SHOCK LEVELS

The foregoing sections have presented general descriptions of the proposed Voyager payload configuration and separation devices, and the types of shock excitation associated with pyrotechnic separation. The shock pulses and response spectra shown in Figure E-1 represent the type of excitation and possibly the range of magnitude of shock levels that will be incurred by components in the Voyager payload. However, more specific information about (1) the shock measurements shown in Figure E-1, (2) the structural dimensions and component weights and locations in the Voyager payload, (3) the separation device type, size, amount of charge, and amount of material to be severed, and (4) the separation point locations (relative to the components) and firing sequence is required to extrapolate to or estimate shock pulse magnitudes and response spectra for specifying shock design and test criteria.

5. RECOMMENDATIONS

The Voyager Environmental Predictions Document (Reference E-4) is limited to predictions of actual environments and does not include considerations of factors appropriate to definition of formal test requirements or generation of design criteria. The ignition staging and separation shock environment presented in Reference E-3 is based on Mariner Mars (1964)

spacecraft data in which pretensioned V-bands were released by pyrotechnic bolt cutters to perform shroud and spacecraft separation. The shock pulse estimated as inducing response equivalent to the separation pulse was a 200 g (0-peak) terminal peak sawtooth of approximately 1 millisecond duration. Investigation of available shock data and the proposed Voyager concept configuration and separation devices indicates that lack of specific detail prevented direct determination of estimates for magnitude of shock excitation at components. Therefore, additional empirical and theoretical analyses are recommended to determine realistic design and test criteria for the separation shock environments of the Voyager payload unit components.

An estimate of the range of response spectra for test criteria for the Voyager components is shown in Figure E-2. This estimate was obtained from the data shown in Figure E-1(a) and E-1(b). The lower response curve is applicable to larger components at same distance from the separation point and the upper response curve is for smaller components. It is possible that zoning could be established on the basis of both component size and location relative to the separation point. Both upper and lower limits are shown for each response curve. The width of the limits is based on the range of amplification factors assumed for elements of components and the limitations on test repeatability by the testing equipment.

It should be noted that this type of test specification indicates the required shock response to be obtained at the test specimen rather than giving the shock pulse shape to be used for the test.

The amount of uncertainty associated with the estimates of the range of response spectra has not been determined. If more accurate estimates are required for specifying shock design and test criteria, then the following recommendations must be considered:

a) Search for separation shock measurement data more directly applicable to the Voyager case in regards to type of separation device, charge size, measurement location, etc.

b) Establish strength of shock pulse expected at point(s) of separation in Voyager payload.

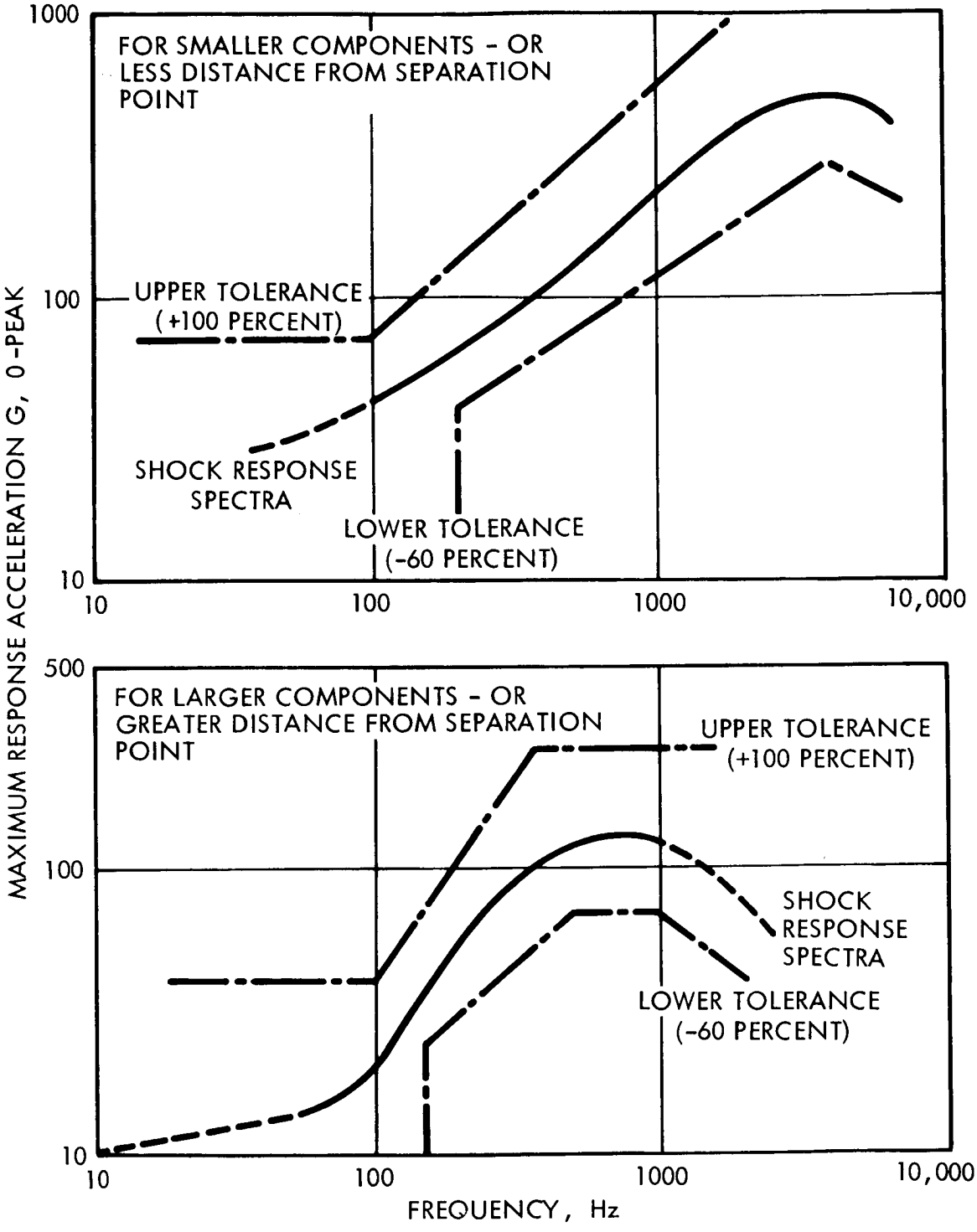

Figure E-2. Spacecraft Components Shock Response Spectra

c) Determine most direct transmission path to components on structural members containing groups of components; dimensional details, number of structural discontinuities, weights of components.

d) Estimate shock acceleration amplitude and duration for various zones or component locations. Establish type of response spectra which best represents the input excitation to the components.

REFERENCES

E-1 D.E. Hines, "Generation and Propagation of Stage Separation Shocks in Missiles and Space Vehicles," Douglas Aircraft Company Paper 1815, presented to Institute of Environmental Sciences, 15 April 1964.

E-2 Shock and Vibration Bulletin #33, Shock, Vibration and Associated Environments, Part IV Department of Defense, Washington, D.C., March 1964.

E-3 Voyager Environmental Predictions Document, JPL SE 003 BB001, 1B28, October 26, 1966.